

# **Analysis of Factors Affecting the Performance of Retinal Prostheses Using Finite Element Modelling of Electric Field Distribution in the Retina**

THÈSE N° 5048 (2011)

PRÉSENTÉE LE 1<sup>ER</sup> JUILLET 2011

À LA FACULTÉ SCIENCES ET TECHNIQUES DE L'INGÉNIEUR

LABORATOIRE DE MICROSYSTÈMES 4

PROGRAMME DOCTORAL EN MICROSYSTÈMES ET MICROÉLECTRONIQUE

ÉCOLE POLYTECHNIQUE FÉDÉRALE DE LAUSANNE

POUR L'OBTENTION DU GRADE DE DOCTEUR ÈS SCIENCES

PAR

**Sri Harsha KASI RAJ**

acceptée sur proposition du jury:

Prof. J. Brugger, président du jury  
Prof. Ph. Renaud, directeur de thèse  
Dr G. Cosendai, rapporteur  
Prof. N. de Rooij, rapporteur  
Prof. M. Giugliano, rapporteur



ÉCOLE POLYTECHNIQUE  
FÉDÉRALE DE LAUSANNE

Suisse  
2011



ॐ असतो मा सद्गमय ।  
तमसो मा ज्योतिर्गमय ॥  
मृत्योर् मा अमृतं गमय ।  
ॐ शान्ति शान्ति शान्ति ॥ - बृहदारण्यक उपनिषद् १.३.२८.

From ignorance, lead me to truth; from darkness, lead me to light;

From death, lead me into immortality; Oh, let there be peace.

- Bruhadaranyak Upanishad 1.3.28

With love

*to amma, daddy, sindhu*

*and eternally beautiful urmila*

In the loving memory of

Elsa Siegrist

1923 – 2010

Henri Riedweg

1920 – 2011





## ABSTRACT

---

This dissertation proposes a computational framework targeted at improving the design of currently employed retinal prostheses. The framework was used for analysing factors impacting the performance of prostheses in terms of electrical stimulation for retinal neurons, which might lead to a perception of pixelated vision. Despite their demonstrated effectiveness, the chronic and safe usage of these retinal prostheses in human and animal trials is jeopardised due to high stimulation thresholds. This is related to the distance between the stimulating electrodes and the retinal neurons resulting from the implantation procedure. The major goal of this dissertation was to evaluate the stimulation efficacy in current implantable planar microelectrode-based retinal prostheses and consequently demonstrate their weakness, thereby providing scope for the development of future implants.

The effect of geometrical factors i.e., electrode-retina distance and electrode size on stimulation applied to the retina by retinal prostheses was studied. To this end, a finite element method based simulation framework to compute electric field distribution in the retina was constructed. An electrical model of the retina was an integral part of the framework, essentially represented by a resistivity profile of the multi-layered retina. The elements of a retinal prosthesis were modelled by incorporating realistic electrode sizes, an anatomical and electrical model of the retina, a precise positioning of stimulation and return electrodes and the location of the implant with respect to the retina representing the epiretinal and subretinal stimulation schemes.

The simulations were carried out both in quasi-static and direct current (DC) modes. It was observed that electrode-electrolyte interface and tissue capacitance could be safely neglected in our model based on the magnitude of the applied voltage stimulus and frequencies under consideration. Therefore, all simulations were conducted in DC mode. Thresholds and lateral extents of the stimulation were computed for electrode sizes corresponding to existing and self-fabricated implants. The values and trends obtained were in agreement with experiments from literature and our collaborators at the les Hôpitaux Universitaires de Genève (HUG). In the subretinal stimulation scheme, the computed variation of impedance with electrode-retina distance correlated well with time varying *in vivo* impedance measurements in rats conducted in collaboration

with the Institut de la Vision, INSERM, Paris. Finally, it was also reiterated that the currently employed retinal prostheses are not very efficient due to a significant distance between the stimulation electrode and the retinal cells.

In addition, I present a new experimental technique for measuring the absolute and local resistivity profile in high-resolution along the retinal depth, based on impedance spectroscopy using a bipolar microprobe. This experiment was devised to extract the resistivity profile of an embryonic chick retina to construct an electrical model for the simulation framework to simulate *in vitro* retinal stimulation experiments conducted by HUG collaborators. We validated the capability of the technique in rat and embryonic chick retinas.

In conclusion, the computational framework presented in this dissertation is more realistic than those found in literature, but represents only a preliminary step towards an accurate model of a real implantation scenario *in vivo*. The simulation results are in agreement with results from clinical trials in humans for epiretinal configuration (literature) and with *in vitro* results for epiretinal and subretinal stimulation applied to chick retinas (HUG).

The developed simulation framework computes quantities that can form a reference for quality control during surgery while inserting implants in the eye and functionality checks by electrophysiologists. Furthermore, this framework is useful in deciding the specifications of stimulation electrodes such as optimal size, shape, material, array density, and the position of the reference electrode to name a few. The work presented here offers to aid in optimising retinal prostheses and implantation procedures for patients and eventually contribute towards improving their quality of life.

Keywords: Simulation Framework, Finite Element Method, Electrode-retina Distance, Retinal Prosthesis, Microelectrodes, Tissue Resistivity Profiling

Ce travail de thèse cherche à améliorer la conception d'implants rétiniens par la modélisation et la vérification des paramètres influant sur l'efficacité de la stimulation électrique nécessaire pour stimuler les neurones de la rétine, et ainsi promouvoir la sensation d'une vision pixellisée. En effet, les implants rétiniens actuellement utilisés lors des tests *in vivo* sur des animaux ainsi que sur l'homme ont pour désavantage de présenter, une fois inséré, une distance entre les électrodes de stimulation et les neurones de la rétine. Ceci entraîne un seuil de stimulation requis élevé et par conséquent une efficacité réduite, ainsi qu'un risque de dégradation des cellules de la rétine liée à ces implants. L'étude d'intégration numérique présentée dans ce travail permet de caractériser l'efficacité d'implants rétiniens, d'en démontrer les points faibles, et ainsi d'améliorer le développement de futurs implants.

Le modèle utilisé dans cette étude évalue l'effet de facteurs géométriques, la distance entre l'électrode et la rétine ainsi que la taille des électrodes, sur la stimulation appliquée à la rétine par les implants. Pour cela, une simulation par éléments finis a été réalisée pour calculer la distribution du champ électrique, suivant un modèle électrique de la rétine établi durant cette étude, qui tient compte du profile de résistivité de la rétine multicouche. Ainsi, les implants ont été modélisés en intégrant une dimension d'électrodes réaliste, un modèle électrique de la rétine anatomiquement correct, un arrangement précis des électrodes de stimulation et de la masse, ainsi que l'emplacement de l'implant par rapport à la rétine dans les cas d'implants épirétiens et sous-rétiens.

Les simulations ont été effectuées en mode quasi statique et courant direct (DC). Il a été observé que, considérant les amplitudes du potentiel de stimulation et les fréquences appliquées, l'interface électrode/électrolyte et la capacité du tissu peuvent être négligés dans notre modèle. De ce fait, toutes les simulations ultérieures ont été effectuées en mode DC. Les valeurs seuils et l'extension latérale de la stimulation ont été calculées pour des tailles d'électrodes correspondant aux implants existants et fabriquée au cours de ce travail. Les valeurs et les tendances obtenues correspondent à celles trouvées dans la littérature et par nos collaborateurs aux Hôpitaux Universitaires de Genève (HUG). En condition de stimulation sous-rétinien, les variations d'impédance calculées selon la distance électrode/rétine correspondent bien aux mesures d'impédance *in vivo* en

fonction du temps effectuées sur des rétines de rats dans le cadre d'une collaboration avec l'Institut de la Vision, INSERM, Paris. Enfin, il a été démontré que les prothèses rétiniennes planes basé sur des microélectrodes actuellement employées sont peu efficace due à une distance significative entre l'électrode de stimulation et les cellules excitable de la rétine.

Une nouvelle technique expérimentale de haute résolution pour mesurer le profil de résistivité en fonction de la profondeur dans la rétine basée sur les mesures de spectroscopie d'impédance bipolaire par une microsonde a été utilisée pour construire le modèle de simulation correspondant aux expériences conduites au HUG. La performance de cette méthode a été validée par des mesures sur des rétines de rat et d'embryon de poussin.

En conclusion, le modèle de simulation de la rétine et de l'implant développé dans ce travail est un modèle plus complet que ceux trouvé généralement dans la littérature, mais représente qu'une étape préliminaire envers un modèle précis du comportement complet d'un implant rétinien *in vivo*. Les résultats de simulation obtenus sont en accord avec des résultats d'essais cliniques chez l'humain dans la configuration épirétinienne (littérature) et avec des résultats *in vitro* pour les configurations épirétinien et sous-rétinien pour le poussin (HUG).

Au niveau de la conception d'implants rétiniens, cette étude permet lors de la phase préliminaire de conception de prendre des décisions quant aux spécifications des électrodes de stimulation telles que la taille optimale, la forme, le matériau, la densité du réseau d'électrodes, la position de l'électrode de référence, etc. Le modèle de simulation développé permet d'obtenir des résultats quantitatifs utilisables en tant que référence pour le contrôle de la qualité de l'insertion des implants rétiniens dans l'œil par chirurgie ainsi que le contrôle du fonctionnement de l'implant par les électrophysiologistes. Ce travail permettra d'optimiser dans le futur l'implantation des implants rétiniens pour les patients et ainsi d'améliorer leur qualité de vie.

Mots-clés: Méthodes de simulation, simulations par éléments finis, distance electrode/rétine, implants rétinienne, microélectrodes, resistivité tissulaire

## PUBLICATIONS

---

Some ideas and figures have appeared previously in the following publications:

*Simulation of epiretinal prostheses – Evaluation of geometrical factors affecting stimulation thresholds* - Kasi H., Hasenkamp W., Cosendai G., Bertsch A., Renaud P., Accepted by *Journal of Neuroengineering and Rehabilitation*, 2011 (provided basis for **Chapter 5**)

*Simulation of spatial extent of stimulation and effect of electrode-tissue gap in subretinal implants* - Kasi H., Bertsch A., Guyomard J.-L., Kolomiets B., Picaud S., Pelizzone M., Renaud P., In Press, *Medical Engineering & Physics*, 2011 (provided basis for **Chapter 6**)

*Direct localised measurement of electrical resistivity profile in rat and embryonic chick retinas using a microprobe* - Kasi H., Meissner R., Babalian A., van Lintel H., Bertsch A., Renaud P., *Journal of Electrical Bioimpedance*, 2010 (provided basis for **Chapter 3**)



## ACKNOWLEDGMENTS

---

I owe my deepest gratitude to a great teacher in all walks of life, Professor Philippe Renaud. He believed and provided me with the opportunity to succeed by offering unlimited expert advice and most appreciated support throughout my stay in his laboratory. I can never forget his informally declared motto: “My students’ success, is my success”.

I sincerely thank Professor Michele Giugliano from University of Antwerp, Prof. Nico de Rooij from EPFL, and Dr. Gregoire Cosendai from Second Sight for accepting to be members of the jury and deeply criticising my work. Their constructive comments and suggestions were invaluable for this dissertation to attain its current form. Undoubtedly, Professor Jürgen Brugger was commendable for his task to preside over the jury and carry out the examination in a fair and pleasant manner.

The impact of any doctoral work can generally be rated by the quality of peer reviewed and published manuscripts. On this account and throughout my thesis, I am grateful to the priceless criticism and the meticulous scientific communication skills of Dr. Arnaud Bertsch towards this achievement. My special token of appreciation to Robert Meissner, Willyan Hasenkamp, Dr. Bogdan Kolomiets, Dr. Alexandre Babalian, Dr. Serge Picaud, Jean-Laurent Guyomard, Harald van Lintel and Dr. Gregoire Cosendai for their guidance and significant contribution to the articles. Not to forget, the informal reviews and excellent suggestions offered by Pontus Linderholm, Prof. Sujit Sikdar, Dr. Robert Wilke, Prof. Michele Giugliano and the very generous Dr. Ashish Ahuja. I wish to warmly thank them one and all.

I am extremely pleased to have shared an unforgettable learning experience with my colleagues at the Microsystems Laboratory, LMIS<sub>4</sub>. Of particular pertinence to this work, my heartfelt thanks to Andre Mercanzini for his advice on experiments with microelectrodes, mentorship and friendship, Thomas Braschler for his brilliance and mind-boggling conversations on just about anything, Sebastien Jiguet for his expert guidance on microfabrication and presentation skills, Marc Heuschkel for sharing his invaluable experience with microelectrodes and the rest of the LMIS<sub>4</sub> team for their creativity.

I truly enjoyed the precious company and friendship that I experienced with my office mates: Lynda Metref for her multidisciplinary conversations, Nicolas Durand for his immaculate sense of punctuality and organisation and Robert Meissner for the relaxing and stimulating discussions on any topic – thank them all so much. I relished sharing an office, as well as many off-work hours together with them.

I feel humble to have a long list of collaborators of highest quality imaginable. In the framework of the artificial retina project, I had the immense pleasure to work with collaborators from Hôpital Universitaire de Genève (HUG). I personally thank Dr. Marzia Lecchi, Dr. Angelica Perez-Fornos, Dr. Jörg Sommerhalder and especially Dr. Joel Salzmann for making the long hours during *in vivo* trials in Geneva, a stimulating and useful learning experience. In addition, I am grateful to Prof. Marco Pelizzone for guiding me on the right path when I was off track. Furthermore, I had the exciting opportunity to be able to work in collaboration with the immensely talented and very competent group of Dr. Serge Picaud at INSERM. A special mention of thanks to the warmth and affectionate nature of Dr. Bogdan Kolomiets who was of great help scientifically and personally motivating. I feel more confident after my interaction of a multidisciplinary nature with you all.

Facilities and resources are key aspects in conducting scientific experiments of highest quality. In this respect, I would like to express my sincere gratitude to:

Jean-Pierre Rougnon, Mechanical Engineering workshop (ATME), EPFL for his kind, patient and hard-working nature. All parts fabricated by him were like masterpieces for me.

Prof. Anne Grapin-Botton, EPFL for her guidance and kindly allowing me to use the excellent incubation facility at her lab.

Dr. J. Patterson for the generous and timely supply of chick eggs complemented by useful tips.

Shruthi Muralidhar and Vincent Delattre for their expert advice on neuroscience, tissue slicing and experimental protocols. Rajnish Ranjan on his expert suggestions and discussions on modelling neuronal dynamics using NEURON in particular. Srikanth Ramaswamy for his constructive criticism on manuscripts, scientific approach and using his flair for scientific writing in reviewing major parts of my dissertation report. All of them were from the Neural Microcircuitry Laboratory (LNMC), EPFL and more than their above-mentioned contribution, was indeed their friendship.



Peter Brühlmeier and Georges Vaucher at ACI (EPFL) for sharing their circuit design expertise and generous supply of basic electric and electronic components for free.

Comsol international support team for patiently and efficiently resolving many of the problems I faced during modelling and simulation.

EPFL library services for their timely and prompt assistance with the literature that I desired.

Centre of MicroNanoTechnology (CMI), EPFL for their cooperation, knowledge and the very helpful nature.

There are so many people who contributed to various parts of this work; if I neglect to mention your name, rest assured that I greatly appreciated your assistance.

I would fail in my endeavour if I forget to convey my special appreciation to Marie Halm, Sylvie Clavel, Rose-Mary Apotheloz, Kathlyn Mayor and Sandra Roux for all their relentless support, a big smile, in all administrative issues. They eased the pressure on me and helped me focus on my research.

“All work and no play makes Jack a dull boy” was always on my mind. I thank my colleagues and friends at the EPFL for the lighter moments and escapades. It really was refreshing and inspirational for a fresh start at work after those events.

I sincerely thank the Indian community in EPFL, Lausanne and Switzerland. I have taken part in numerous social gatherings organised by many of these families, which always helped me to feel home in spite of being away from India.

My wholehearted gratitude to two very important people for hosting and sharing their living space with me during this doctoral thesis: late Mrs. Elsa Siegrist for her motherly care and Venkat Sivagnanam for his motivation and inspiration. I thank them both from the bottom of my heart for bearing with me.

Finally, my heartfelt love and appreciation is due to my mother, father and sister for their invaluable support through all phases of my life. I take this opportunity also to kindly thank all my teachers for the perseverance and effort they put in training me to bring me up to this level. Last but not least, I would like to express my warmest love and earnest gratitude to Urmila for having persisted with me during the most difficult phases of my life. Without her loving support and understanding, I would not have achieved my goals.



# CONTENTS

---

<b>I</b>	<b>DISSERTATION</b>	<b>1</b>
<b>1</b>	<b>INTRODUCTION</b>	<b>3</b>
1.1	Scope	9
1.2	Modelling problem and its significance	10
1.2.1	Positioning of electrodes	11
1.2.2	Geometrical factors	12
1.2.3	Electric model of the retina	13
1.3	Literature review	13
1.3.1	Retinal implants	14
1.3.2	Optogenetics - replacing electrode with light stimulation	21
1.3.3	Modelling strategies	24
1.4	Dissertation position with respect to the state of the art	32
1.5	Research objectives	34
1.6	Limitations	34
1.7	Dissertation layout	35
<b>2</b>	<b>ELECTRICAL STIMULATION OF RETINA: FROM ELECTROPHYSIOLOGY TO MODELLING</b>	<b>39</b>
2.1	Introduction	39
2.2	Physiological basis for neurostimulation	40
2.3	Electric fields in volume conductors	41
2.3.1	Quasi-static formulation	42
2.3.2	Potential from a monopolar disc	42
2.3.3	Inhomogeneous volume conductors	43
2.4	Stimulus characteristics affecting retinal stimulation	43
2.4.1	Cathodic and anodic stimulation	44
2.4.2	Monopolar and dipolar configuration	44
2.4.3	Current-controlled versus voltage-controlled stimulation	45
2.4.4	Strength-duration relationship	46
2.4.5	Selective stimulation of retinal cells	47
2.5	Safe stimulation of neural tissue	47
2.5.1	Mechanism	48

2.5.2	Parameters for safe stimulation	49
2.5.3	Induced retinal injury by stimulation	51
2.6	Direct and indirect stimulation	51
2.7	Modelling retinal stimulation	52
2.8	Summary	53
3	DETERMINING RESISTIVITY PROFILE OF THE RETINA	55
3.1	Introduction	55
3.2	Materials and methods	56
3.2.1	Animals	56
3.2.2	Electrode design and fabrication	56
3.2.3	Measurement method and modelling	57
3.2.4	Measurement apparatus and protocol	60
3.3	Results	62
3.3.1	Electrode characterisation and PRF shift	62
3.3.2	Resistivity profiling in rat and embryonic chick retinas	64
3.4	Discussion	65
3.5	Conclusion and outlook	68
4	FEM-BASED INTEGRATED SIMULATION FRAMEWORK	71
4.1	Introduction	71
4.2	Geometrical factors	71
4.2.1	Electrode-retina gap model	71
4.2.2	Electrode size	72
4.3	Simulation framework	75
4.3.1	Constituents of the framework	75
4.3.2	Hypotheses for RGC activation	79
4.4	Integrated FEM model	81
4.5	Extracted parameters	83
4.5.1	Current	84
4.5.2	Impedance	84
4.5.3	Lateral extent	84
4.6	Conclusion and Outlook	84
5	SIMULATION OF EPIRETINAL PROSTHESES	87
5.1	Background	87
5.2	Methods	89

5.3	Results and Discussion	89
5.3.1	Stimulation thresholds as a function of electrode-retina distance	89
5.3.2	Stimulation thresholds as a function of electrode sizes	91
5.3.3	Impedance variation based on electrode-retina distance	93
5.3.4	Estimation of resolution based on spatial extent of stimulation	94
5.3.5	Simulation vs. <i>in vitro</i> epiretinal stimulation - Our implant	95
5.4	Conclusions	96
6	SIMULATION OF SUBRETINAL PROSTHESES	99
6.1	Introduction	99
6.2	Methods	101
6.2.1	Hypotheses for retinal stimulation	101
6.2.2	FEM modelling	101
6.2.3	Animal model and impedance spectroscopy	101
6.3	Results	102
6.3.1	Spatial extent of the threshold current	102
6.3.2	Effect of a gap between the electrode and the retinal tissue	103
6.4	Discussion	106
6.4.1	Threshold current	106
6.4.2	Spatial extent of stimulation	107
6.4.3	Effect of electrode size	107
6.4.4	Effect of electrode-tissue gap	108
6.4.5	Simulation vs. <i>in vitro</i> subretinal stimulation - Our implant	110
6.5	Conclusion	111
7	CONCLUSION	113
7.1	Summary of main results	113
7.2	Significance of contribution to knowledge	114
7.3	Future outlook	115
7.3.1	Comsol-NEURON integration	115
7.3.2	Electrode array	115
7.3.3	Pulse dependent stimulation	116
7.4	Verdict	116
II	APPENDICES	117
A	MICROFABRICATION PROTOCOL FOR THE MICROPROBE	119
B	SUPPLEMENTARY INFORMATION ON RESISTIVITY PROFILING EXPERIMENT	121

B.1	Electric field penetration depth	121
B.2	Computed cell constant	122
B.3	Impedance stabilisation with time	123
B.4	Simulation on reduction of fringing effects	124
C	MISCELLANEOUS SIMULATIONS AND CALCULATIONS	125
C.1	Validation for neglecting electrode interface	125
C.1.1	Electrode-Electrolyte Interface	125
C.1.2	Calculations	127
C.2	Validation for neglecting capacitive tissue impedance	128
C.2.1	Model	128
C.2.2	Calculations	129
	BIBLIOGRAPHY	131

## LIST OF FIGURES

---

Figure 1.1	Vision simulations for retinal degenerative diseases	4
Figure 1.2	Visual prostheses development worldwide	8
Figure 1.3	Placement scheme for subretinal and epiretinal prostheses	14
Figure 1.4	Subretinal prosthesis placement	15
Figure 1.5	Epiretinal prosthesis system	16
Figure 1.6	Artificial silicon chip (ASR)	17
Figure 1.7	Retina Implant AG subretinal implant	18
Figure 1.8	Boston retinal implant	18
Figure 1.9	Various generations of Argus implants	20
Figure 1.10	Our retinal implant	21
Figure 1.11	Sensors and actuators - Optogenetics	22
Figure 2.1	Cable model for the axon	41
Figure 2.2	Dipolar stimulation of the nerve fibre	45
Figure 2.3	Strength-duration relationship	48
Figure 2.4	Response-stimulus curve	49
Figure 3.1	Electrodes schematic	57
Figure 3.2	Photograph of the microprobe	57
Figure 3.3	Electrical equivalent for measured impedance	58
Figure 3.4	Bode plot and fit at 80 $\mu\text{m}$ depth	59
Figure 3.5	Experimental apparatus	61
Figure 3.6	Bode plot in Ringer's solution	63
Figure 3.7	Bode plot at various depths in a rat retina	63
Figure 3.8	Data comparison between rats and embryonic chicks	69
Figure 4.1	Schematic to exhibit electric field lines in case of electrode-retina gap or no gap	72
Figure 4.2	SEM image of the EPFL implant	74
Figure 4.3	Argus I implant with both electrode variants	75
Figure 4.4	Extrapolated retina model from Heynen and Norren's data on macaque retina	77

Figure 4.5	Simulation model with explanation on placement and RGC depth 79
Figure 4.6	Voltage and electric field plots in subretinal mode 86
Figure 4.7	Graphical representation of the lateral extent 86
Figure 5.1	Threshold current vs. electrode-retina distance (Epiretinal) 90
Figure 5.2	Threshold current vs. electrode diameter/area (Epiretinal) 92
Figure 5.3	Impedance vs. electrode distance (Epiretinal) 94
Figure 5.4	Lateral extent of stimulation (Epiretinal) 95
Figure 5.5	Lateral extent of stimulation for our implant (epiretinal configuration) 96
Figure 6.1	Spatial extent of various threshold stimulation currents (Subretinal) 103
Figure 6.2	Threshold currents vs. Lateral displacement (Subretinal) 104
Figure 6.3	Threshold currents vs. electrode distance (Subretinal) 105
Figure 6.4	Impedance vs. electrode distance (Subretinal) 106
Figure 6.5	Impedance vs. time (Subretinal) 106
Figure 6.6	Threshold vs. impedance (Subretinal) 109
Figure 6.7	Lateral extent of stimulation for our implant (subretinal configuration) 110
Figure B.1	Quasistatic simulation of electric field distribution for bipolar electrodes during recording phase 121
Figure B.2	Determining the duration after which resistivity measurements were stable 123
Figure B.3	Finite element simulations to demonstrate the reduction of fringing effects by rounding electrode corners 124
Figure B.4	A zoomed version of the previous figure to show evidence of reduction in fringing effects by rounding electrode corners 124
Figure C.1	Circuit model and quasistatic equations representing boundary conditions 126
Figure C.2	Overpotential vs. charge transfer current 128
Figure C.3	Tissue voltage and overpotential for all values of applied electrode voltage 128



Figure C.4      Circuit equivalent (Cole model) of the simulation model between the electrode and ground      129

LIST OF TABLES

Table 4.1	Thresholds and lateral extents for different electrode sizes	73
Table 4.2	Positioning of ground electrodes	76
Table 4.3	Boundary conditions and equations in DC	83
Table 4.4	Constants employed for the quasistatic and/or DC simulations	84
Table 4.5	Solver parameters for simulations	85
Table 6.1	Thresholds and lateral extents for different electrode sizes	108
Table C.1	Relation between the overpotential and the charge transfer current	127

ACRONYMS

AAVs	adeno-associated viruses
AMD	Age-related Macular Degeneration
ASR	Artificial Silicone Retina
ChR2	Channelrhodopsin-2
CPE	constant phase element
DC	direct current
eNpHR	enhanced Natronomonas pharaonis Halorhodopsin
FEM	Finite Element Method
FCM	Fohlmeister-Coleman-Miller

PRF Peak Resistance Frequency

PF physiological fluid

RD Retinal Degeneration

RF radio frequency

RGC retinal ganglion cell

RP Retinitis Pigmentosa

RPE Retinal Pigment Epithelium

SSMP Second Sight Medical Products

SD standard deviation

WHO World Health Organisation

Part I

DISSERTATION



## INTRODUCTION

---

Most of the intractable blindness conditions originate from the retina, the most common being the age-related or inherited retinal degenerations. The most vital part in the eye contributing to vision is the retina even though other parts are equally important for perceiving a good image. The retina is basically a piece of brain tissue that receives direct stimulation from the outside world's lights and images. Retinal degenerations form a broad, heterogeneous family of eye diseases that primarily target the retinal photoreceptor cells. They are broadly classified into two groups: (1) degenerations like Retinitis Pigmentosa (RP) that begin by primarily affecting rod photoreceptor cells; and (2) macular degenerations that mainly affect cone photoreceptors. Age-related Macular Degeneration (AMD) constitutes the most common non-avoidable cause of visual disability, affecting approximately 8 million people worldwide (World Health Organisation (WHO), 1997), a number that continues to increase with the ageing population [Congdon *et al.* 2004]. RP is the principal cause of inherited blindness. It has an overall prevalence of 1:3000 to 1:5000 [Haim 2002] and affects approximately 1.5 million people worldwide [Boughman *et al.* 1980, Haim *et al.* 1992, Humphries *et al.* 1992]. Other important unavoidable causes of blindness are glaucoma, diabetic retinopathy, and trauma [Thylefors *et al.* 1992, Congdon *et al.* 2003, Margalit and Sadda 2003]. The prevalence of these diseases, mainly age related, is expected to increase with the current ageing of the population. These diseases generally have a negative impact on the otherwise healthy individuals subjecting them to social and economic hardships bringing down their quality of life drastically. The affected individuals often are in need of substantial specialised attention from governmental agencies for the rest of their lives incurring costs on both the individual and the government.

Treatment for these retinal degenerative diseases can be summarised below:

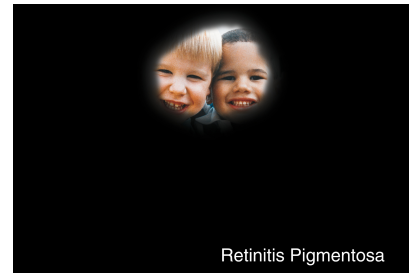
- Medical treatment: AMD can occur in two forms - dry and wet. While there is no effective treatment for dry AMD which comprises 90% of AMD patients, an advancement of the disease may be reduced by frequent supplements of specific vitamins and zinc [AREDS Study Research Group 2001]. Anti-angiogenic therapy



(a) Normal vision.



(b) A scene as it might be viewed by a person with age-related macular degeneration.



(c) A scene as it might be viewed by a person with retinitis pigmentosa.

Figure 1.1: Retinal degenerative disease simulations that demonstrate impaired vision (from wikimedia under public domain).

(injectable drug treatment - ranibizumab [Lucentis®] or bevacizumab [Avastin®]) and laser photocoagulation [Pauleikhoff 2005] are routine therapies available for wet AMD and benefits only a limited number of patients. Other experimental treatments for this disease like photodynamic therapy, pharmacological inhibition, surgical intervention, and radiation therapy are being explored [Ciulla *et al.* 1998]. Periodic screening and early laser treatment have proven to be helpful tools for preventing blindness in patients suffering from diabetic retinopathy, and alternative therapies are currently being studied [Harding 2003]. In hereditary degenerations with known biochemical alterations, research has focused on non-specific “antidegenerative” approaches, including the use of growth factors, apoptosis control, and antioxidants (see e. g. [Dufier 2003, Zeiss *et al.* 2006]).

- Genetic treatment: It is expected to be the best alternative for RP [Hims *et al.* 2003, McFarland *et al.* 2004] in cases where the patient’s retina has some viable photoreceptor cells. The basic principle of these therapies is to introduce normal copies of defective genes into affected retinal neurons. It has been suggested that gene vectors could be injected close to the photoreceptors, because the sub-retinal

space can be easily accessed. The gene transfer into post-mitotic cells appears however to be difficult.

One of the promising gene therapy approaches involves Channelrhodopsin-2 (ChR2). It is derived from the green alga *Chlamydomonas reinhardtii*, and is a microbial-type rhodopsin. Its speciality is that it functions as a light-driven cation-selective channel. It has recently been reported [Doroudchi *et al.* 2011] that the specific and stable expression of ChR2 in light-insensitive retinal neurons called the bipolar cells using a recombinant adeno-associated viral vector (rAAV). Targeted expression led to ChR2-driven electrophysiological ON responses in postsynaptic retinal ganglion cells and significant improvement in visually guided behaviour for multiple mice models of blindness up to 10 months post-injection. Light levels to elicit visually guided behavioural responses were within the physiological range of cone photoreceptors. The *in vivo* results demonstrated that virally delivered ChR2 can provide a viable and efficacious clinical therapy for photoreceptor disease-related blindness.

- Stem cell transplantation: When all photoreceptors are dead or otherwise not functioning, photoreceptor cell transplantation and stem cell therapy would be ideal. Transplantation of Retinal Pigment Epithelium (RPE) has proven to rescue degenerating photoreceptors by phagocytic action and probably also by the release of various trophic factors (see e.g. [Saigo 2004]). Transplantation of normal photoreceptor rods to the Retinal Degeneration (RD) mouse (mutated retinal degeneration species) retina seems to prevent and even reverse cone degeneration [Mohand-Said *et al.* 2000]. Moreover, visual evoked responses have been obtained on dystrophic rodents after transplantation of healthy retina into the subretinal space [Woch *et al.* 2001, Klassen *et al.* 2004]. Stem cell therapy on an animal model of RP resulted in some functional photoreceptor replacement [MacLaren *et al.* 2006] but significant safety and functional difficulties need to be addressed before the technique is used on a large scale. In conclusion, there is no treatment yet that demonstrates long-term improvements in visual function on RP or AMD patients.

Cure for RP or AMD patients through medical and genetic treatment is a far fetched goal. Over the last three decades an alternative approach is creating a niche in an attempt to impart partial vision to such patients: *visual prostheses*. It all started as early as 1755, when LeRoy discovered that electricity applied to a blind patient's eye with cataract resulted in a perception of light [Clausen 1955]. The relation between

electricity and vision were not discussed again until early 20th century when a group of researchers described phosphenes<sup>1</sup> elicited by direct electrical stimulation of the cortex during surgery [Löwenstein and Borchart 1918, Krause 1924, Foerster 1929, Urban 1937, Penfield and Jasper 1954]. These findings led Giles Brindley and his colleagues to the first human trial<sup>2</sup> of a “visual prosthetic implant” [Brindley and Lewin 1968a;b, Brindley 1973]. A few years later, Dobelle followed in Brindley’s footsteps and performed several experiments with acute electrode configurations before implanting permanent devices [Dobelle and Mladejovsky 1974, Dobelle *et al.* 1974, Klomp *et al.* 1977] in human subjects. Several volunteers participated in these trials, and two have kept the implant for more than 20 years [Dobelle 2000]. Thus, both Brindley and Dobelle with their pioneering efforts in demonstrating feasibility of the approach, opened doors to the promising field of visual prostheses.

During last three decades, there has been immense progress in development of electronic visual prostheses. Even though optical [Banghart *et al.* 2004, Bi *et al.* 2006], hybrid [Yagi *et al.* 1999, Wu *et al.* 2003] and chemical or physiological [Peterman *et al.* 2003, Zibek *et al.* 2010] stimulation of retinal neurons are envisioned, electronic prostheses are considered more feasible and promising. This can be associated with the recent progress in microtechnology making it possible to envision extremely small and densely integrated neurostimulators. These small neurostimulators or electrodes can activate well defined volumes in the tissue enabling a resolution sufficient for useful vision. Moreover, the success of cochlear implants influenced the early visual prosthesis researchers to explore stimulation of secondary neurons to pass sensory information and examine proper functioning of retino-cortical connections in profoundly blind people [Dagnelie 2008]. Morphometric results from the studies on eyes from patients with AMD or RP revealed the partial preservation of inner retinal cells [Stone *et al.* 1992] e.g. ganglion cells. Post-mortem studies on profoundly blind people demonstrated that 80% of inner nuclear layer and about 30% of the ganglion cell layer was retained [Stone *et al.* 1992]. Simultaneously, in degenerated retinal models of human and animals, abnormalities in the neuronal network within the retina were observed in the form of neurite sprouting [Fariss *et al.* 2000] and neural remodelling [Marc *et al.* 2003]. Therefore, the numerous pathological changes occurring within the degenerated retina may seem to have serious implications on the ultimate success of visual prostheses. However,

<sup>1</sup> phosphene: a sensation of a ring or spot of light produced by pressure on the eyeball or direct stimulation of the visual system other than by light. (Oxford Reference Online, 2010)

<sup>2</sup> in 1956 an Australian researcher Tassicker [Tassicker 1956] was the first to patent a method of implanting a light-sensitive selenium photodiode behind a blind person’s retina to restore intermittent light sensations.



careful investigations and varied approaches [Humayun *et al.* 1996; 1999, Weiland *et al.* 1999] revealed that the brain can indeed respond to electric retinal stimulation [Chader *et al.* 2009]: (1) even after long years of little or no formed sight or even light perception. (2) in a damaged retina with the inner retinal neurons being the target of stimulation.

Presently, various teams are working towards the development of a visual prosthesis, each of them with an approach to restore visual functionality at different stages of the visual pathway. They can be categorised based on electric stimulation applied at cortex [Schmidt *et al.* 1996, Maynard *et al.* 1999, Dobbelle 2000], optic nerve [Veraart *et al.* 1998, Lambert *et al.* 2003] and retinal stages [Rizzo *et al.* 2003, Hornig *et al.* 2005, Palanker *et al.* 2005, Fujikado *et al.* 2007, Gerding *et al.* 2007, Yanai *et al.* 2007, Zhou *et al.* 2008, Dommel *et al.* 2009, Zrenner *et al.* 2010]. Retinal implants seem to be the most elegant and promising way to approach artificial vision [Perez Fornos 2006]. They could benefit from the natural processing in the still intact key structures of the visual system. Surgery is less invasive in comparison with other stimulation sites, which forms an important clinical advantage. Finally, intuitions and conjectures about which approach might be most suitable will have to be concluded based on the results of chronic implantation in humans. Until sufficient data becomes available to draw concrete conclusions, it is advisable to remain open-minded as to which approach might prove to be the best.

The growing popularity of retinal prostheses has currently influenced more than 20 different groups (see Figure 1.2) examining the evolution of intraocular (subretinal<sup>3</sup>, epiretinal<sup>4</sup> and suprachoroidal<sup>5</sup>) and extraocular (trans- and episcleral<sup>6</sup>) retinal prostheses (for schematic illustration on implant placement refer to paper by Gerding2007 [Gerding 2007]). These retinal prostheses have evolved on two main concepts, one where the viable optic path within the eye is still used to transmit visual information. In the second concept, visual information is obtained by a camera system. This information is then further processed depending on the stage of the visual pathway where the stimulation is intended. However, common features [Ameri *et al.* 2008] of almost all retinal prostheses are: (1) a light-sensitive device for capturing image data, (2) implanted microelectronics for converting image data into a stimulus pattern, and (3) a microelectrode array interface for delivering the stimulus current to the retina. Both

---

3 the implant is located on the outer retinal surface (behind the photoreceptor layer and in front of the RPE).

4 the implant is placed on the inner retinal surface (against the retinal ganglion cell layer)

5 the implant is placed between the choroid and the sclera

6 the implant is placed on the sclera

epiretinal and subretinal implants have undergone chronic testing in humans while the extraocular approaches have been limited to *in vitro*<sup>7</sup> studies and animal models.

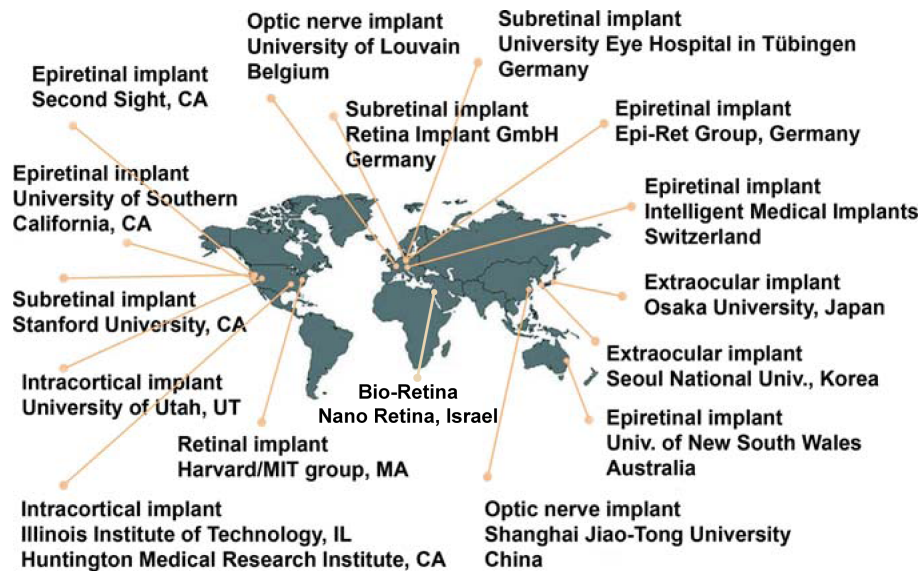


Figure 1.2: Some research teams and industrial groups worldwide that are developing implantable visual prostheses (modified from Figure 5 of Chapter 1 in [Zhou and Greenberg 2009]). Bio-Retina from Nano Retina, Israel is a new initiative included in this map.

Performance and usefulness of retinal prostheses depends on many aspects, primarily categorised into electrical, surgical, biocompatibility and psychophysical<sup>8</sup>. Psychophysical studies suggest that more than 1000 electrodes are needed for subjects to feel safe in unpredictable environments including moving, eventually hazardous objects [Perez Fornos 2006]. The electric current injected by these electrodes flows into the retinal tissue and follows a certain path terminating at the return (ground) electrode located in the eye. The consequent electric field distribution formed within the retina is the major cause of activation in excitable cells [Palanker *et al.* 2005] that eventually contributes to a visual sensation. In a conventional intraocular retinal prosthesis (subretinal and epiretinal only) setup - the stimulation and return electrodes, retina and the vitreous medium surrounding them are arranged in a specific arrangement. In such a complex arrangement, it is experimentally tedious to determine the electric current or field distribution originating from delivered stimulus on the electrodes. Moreover, an essential

<sup>7</sup> *in vitro* (latin: “in glass”), refers to the measurements on cells cultured outside the body, *i.e.* in a test tube or a culture dish.

<sup>8</sup> Psychophysics: the branch of psychology that deals with the relations between physical stimuli and mental phenomena (Oxford Reference Online, 2010). Psychophysical experiments adopting simulated prosthetic vision can provide the minimum specifications of visual prostheses to realise certain tasks.

condition for effective stimulation of the retina is its close proximity with the electrodes. This is based upon the clinical demonstration that close proximity of electrodes to the retina is key to safe and chronic retinal stimulation [de Balthasar *et al.* 2008]. In addition, all clinical trials of retinal implants until now have utilised disc electrodes [Wilke *et al.* 2010b]. This is the major reason as to why either novel electrode geometries (protruding or three-dimensional electrodes) or a way to let the retinal neurons migrate towards the electrodes are being examined [Palanker *et al.* 2005]. An analytic interpretation of such complex electrode-retina bioelectric interface is either tedious or impossible. A computational approach is a promising candidate to investigate the electrical quantities that are in question.

Ultimately, the success of a retinal prosthesis in clinical use relies on its longevity and ability to provide safe and high resolution stimulation. There are various levels of complexity involved before current injected from an electrode results in an image perception [Wilke *et al.* 2010b]. A good understanding of these levels has not yet been established. The initial level of complexity is the electrochemical effects that take place during stimulation, when charge is injected into a sophisticated and anisotropic retinal tissue. Other levels of complexity are related to how the neurophysiological processes within and outside the retinal network in the visual pathway are influenced by the extracellular currents and how the transduced information is eventually perceived. Biophysical modelling in combination with simulation methods, supported with experimental evidence, can be used to bridge the gap in understanding the processes involved in the operation of a retinal prosthesis. In addition, they can contribute in pre-determination of the stimulation efficacy of new electrode designs for retinal prostheses. During the design phase of these electrode arrays, an early knowledge of current densities and potentials in various layers of the retina induced by the electrodes would be beneficial. It is hoped that the models, simulation framework and experiments presented in this work, targeted at understanding important phenomena in *in vitro* retina stimulation experiments and currently implantable retinal prostheses, will be administered as a building block for new retinal prostheses.

## 1.1 SCOPE

This dissertation involves the development of preliminary steps to an integrated simulation framework that can estimate the efficacy of current implantable retinal prostheses for humans. More precisely, a Finite Element Method (FEM) based simulation

framework to estimate the effect of geometrical factors on the stimulation efficacy of clinical epiretinal and subretinal prostheses is presented. The framework was constructed based on a representation of the retinal prosthesis during an implantation scenario with realistic dimensions. The dimensions for the epiretinal case was similar to Argus I clinical trials (Second Sight® Medical Products, Inc.) and for subretinal, it was based on customised implant design meant for *in vitro* retinal stimulation experiments. The retina was purely based on an electric model with its layer inhomogeneity represented as a varying resistivity profile. The electric models of the retina were: (1) extrapolated from *in vivo*<sup>9</sup> resistivity measurements in macaque made by Heynen and Norren [Heynen and van Norren 1985] and applied for simulating current implantable epiretinal and subretinal prostheses; and (2) extrapolated from resistivity profiling in isolated retinal tissue samples and employed for simulating epiretinal and subretinal *in vitro* stimulation in chick retinas. The biological characteristics of the retinal network was not considered as a part of the simulation framework. A hypothesis for stimulation threshold to activate a ganglion cell was constructed from an experimentally validated analytical model recently demonstrated by Boinagrov *et al.* [Boinagrov *et al.* 2010]. The inferences drawn from the simulation framework described the major aspects of currently employed implantable epiretinal and subretinal prostheses' efficacy and safe usage. A less significant but important portion of this dissertation was dedicated to design, characterisation and implementation of electrodes for *in vitro* resistivity profiling, subretinal and epiretinal stimulation experiments in chick retinas. All simulations presented in this dissertation were based on monopolar stimulation<sup>10</sup>. COMSOL MULTIPHYSICS®, Inc.<sup>11</sup> software was used for finite element based computations to solve the electric field distribution in the entire volume conductor<sup>12</sup> and especially in the retina.

## 1.2 MODELLING PROBLEM AND ITS SIGNIFICANCE

Currently implantable retinal prostheses will need to be upgraded with more stimulating electrodes to improve spatial resolution. The development of such high density planar electrode arrays are faced with a serious problem of not being able

<sup>9</sup> *in vivo* (latin: "within the living"), refers to experiments on a whole, living organism.

<sup>10</sup> an electrode of an array serves as a current source with a current sink in the form of a distant large return electrode

<sup>11</sup> Comsol Multiphysics is a partial differential equation software to create 1D, 2D and 3D spatial models and to simulate their static or time-dependent behaviour. It is possible to couple multiple problems based on different physical models.

<sup>12</sup> Trivial definition suggests a *volume conductor* to be the contiguous passive conducting medium that surrounds the region occupied by the excitable tissue (retina here) itself.

to stimulate the retina safely and efficiently [Dowling 2009]. This can be primarily attributed to the distance between the target cells in the retina and the stimulating electrodes themselves [Palanker *et al.* 2005]. The threshold current needed to activate target retinal neurons depends on physical, electrical and biological aspects influencing them. Physical aspects involve the electrode geometries, position of these electrodes, natural curvature of the retina, etc. Electrical aspects consist of stimulus parameters (width, duration, polarity of the pulse), conductivity and permittivity parameters defining the volume conductor, retina, etc. Biological aspects are related to the electrophysiological properties of the retinal neurons, neuronal cell density, neuronal shape, retinal network behaviour, etc.

In order to understand functioning of current implantable retinal prostheses and build new designs optimised for enabling a good degree of vision in affected patients - a complete, integrated simulation framework addressing all above mentioned aspects is indispensable. The significance of such a framework includes estimation and evaluation of factors affecting performance of retinal prostheses such as stimulation thresholds, spatial resolution, electrical (electroporation) and thermal (heat generated by the implant) damage to the retina, power consumption, mechanical damage to the retina and information on retinal network processing. As early modelling steps, taking into account some of the critical physical and electrical aspects influencing activation of retinal neurons, the simulation framework computes the electric fields in the electrode-retina interface. Furthermore, knowledge of current densities in the retinal tissue can resolve significant questions which include: design of implantable electrode arrays, a proper location for the implant to be placed, optimal electrode geometry and ground position, efficiency of different shapes and sizes of electrodes, optimal inter-electrode spacing, maximum amount of current injected safely for a given configuration, efficiency of current injection and current circulation in a tissue for a particular scenario (epiretinal or subretinal). The following sections describe the model parameters that were included in the simulation framework described in this dissertation.

### 1.2.1 *Positioning of electrodes*

Extracellular stimulation of the retina is employed by retinal prostheses through their electrode arrays. This stimulation results in an application of electric field to the medium surrounding the excitable retinal neurons. A retinal neuron is activated when a change in the cross-membrane potential reaches a threshold value. The electric

field distribution and current spread within the retina is strongly dependent on the position of the stimulation and the return electrodes. Depending on the positioning of these two electrodes, stimulation schemes can be classified as three types: monopolar, dipolar and multipolar<sup>13</sup>. Electrode arrays used in current clinical trials are designed for monopolar stimulation [Wilke *et al.* 2010b]. A monopolar design is the most effective in terms of number of electrodes needed to create a single phosphene ignoring time multiplexing occurring in high electrode density arrays. Moreover, in large number electrode arrays, the number of electrodes that can be activated without temporal overlap is based on the stimulus pulse duration. Thus, monopolar schemes does not support sequential activation in high resolution implants [Palanker *et al.* 2007]. Dipolar or multipolar electrode configurations, while being less economic in terms of space and power consumption, can deliver localised and closely confined stimulation to a certain target volume. This is made possible because there exists a current source and sink for each pixel of the retinal prosthesis and is consequently believed to decrease cross-talk between electrodes. Hence, it is essential to consider the physical location of electrodes in the model contributing to the correctness of retinal prosthesis simulation.

### 1.2.2 Geometrical factors

The proximity of the retina to the stimulation electrodes is crucial for safe and efficient retina stimulation. Any distance between electrodes and the target neurons will increase charge density, power and the spatial extent of supra-threshold electric fields necessary for retinal stimulation [Palanker *et al.* 2005]. The higher charge injection, in turn, causes increased cross-talk between electrodes, electrochemical erosion of stimulating electrodes and probably even damage to the retina due to excessive heating. Further, variation in distance between electrodes across the implant surface and the retina leads to associated fluctuations in stimulation thresholds. These uncertainties in the stimulation thresholds have been observed in basic clinical studies on functioning of an epiretinal implant in patients receiving the Argus I (16 electrode) device [de Balthasar *et al.* 2008]. Interestingly, these researchers found a strong correlation between stimulation thresholds and implant-retina distance but not with other parameters. Therefore, proximity of electrodes to the target cells along with the volume (occupied by interstitial medium) between the retina and implant are important issues to consider in modelling and design of high-resolution retinal prosthetic devices.

<sup>13</sup> two (dipolar) or more (multipolar) electrodes in close proximity forming one functional unit of stimulation and return electrodes to generate a phosphene



### 1.2.3 *Electric model of the retina*

The retina contains various layers comprising different types of neuronal cells (e. g. horizontal, on- and off- bipolar, amacrine, and ganglion cells) with a complex array of interneurons forming synapses between the photoreceptors and optic nerve [Kolb 1994]. Each of these multiple layers, characterised by different cell types and densities [Rodieck 1973], render the retina electrically inhomogeneous in a transverse (radial) direction. Neural tissue inhomogeneity is an important parameter affecting neural stimulation [Lee and Grill 2005, Miranda *et al.* 2007]. By constructing an electric model based on inhomogeneity, it is feasible to compute the electric field distribution in the retina and consequently estimate parameters such as stimulation extents and threshold for a retinal prosthesis. For a successful simulation, the framework should include anatomically correct retina model describing electrical characteristics of the retinal layers [Schmidt *et al.* 2008] with due attention to the size of the retina corresponding to an actual implantation scenario. Recent modelling results [Minnikanti *et al.* 2010] indicate that electric fields of high intensities (formed close to the electrode) are also formed deep in the tissue when modelled as an anisotropic resistivity model. The significance and relevance of an anisotropic electric model of a retina is justified in modelling and simulation of a retinal prosthesis.

## 1.3 LITERATURE REVIEW

A brief record of retinal implants employed in ongoing clinical trials is presented in the first part of this section. Subsequently, a short description of a parallel but rapidly advancing field of Optogenetics<sup>14</sup> is presented and its potential to replace electric stimulation as a tool for retinal prostheses and in general neuroprostheses is explored. In the last part, a review of the modelling strategies proposed by various researchers which can act as building blocks for an integrated simulation framework is discussed. With these two separate sections, it is hoped that the reader will appreciate the need for formulating an integrated simulation framework that can estimate useful parameters necessary for understanding and predicting the behaviour of implantable retinal prostheses.

---

<sup>14</sup> Optogenetics is the combination of genetic and optical methods to control specific events in targeted cells of living tissue, even within freely moving mammals and other animals, with the temporal precision (millisecond-timescale) needed to keep pace with functioning intact biological systems. Source: Wikipedia

### 1.3.1 Retinal implants

Current retinal implants used in clinical trials consist of conventional planar electrodes placed directly in contact with the retina using either a subretinal or epiretinal approach. In the subretinal approach, the implant is placed in the subretinal space between the pigment epithelial cells and the dead/dying photoreceptors. In the epiretinal approach, the implant is placed on the surface of the retina that is in contact with the vitreous, *i. e.*, the ganglion cell layer. Both approaches are illustrated in Figure 1.3.

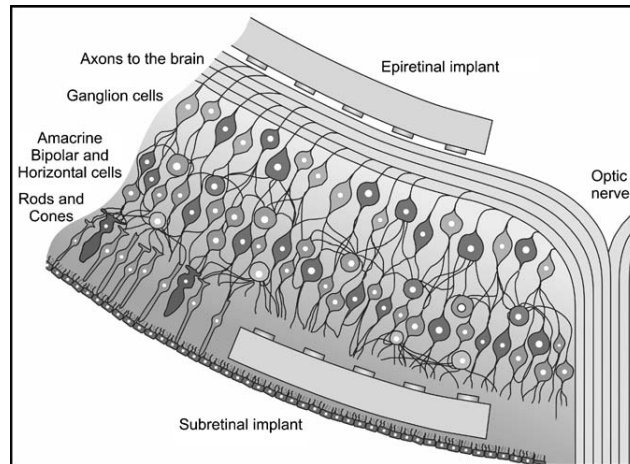


Figure 1.3: Schematic of the retina with two possible types of implants. An epiretinal implant device consists of a photodiode array that receives signals from a camera, and sends preprocessed information to the electrode array sitting directly on the retina. The subretinal implant uses similar signal processing with the advantage of being close to the natural situation, that is, the network of retina cells is directly involved (from [Resatz and Rattay 2004]).

The subretinal implant is a single device implanted in the subretinal space [Chow *et al.* 2004, Besch *et al.* 2008], between the outer retina and the RPE, activated by ambient light incident on an array of photodiodes integrated in the device. An illustration of a subretinal prosthesis system is presented in Figure 1.4. Hypothetically, the device activates remaining intact neurons of the degenerate retina (predominantly bipolar cells) present in the middle layers of the retina, utilising its inherent ability to encode information. The whole implantation of a single device would use the eye's existing optics and its motility, and deter the need for externally supported electronic equipment. These are some factors which may render the subretinal approach advantageous over epiretinal prostheses.



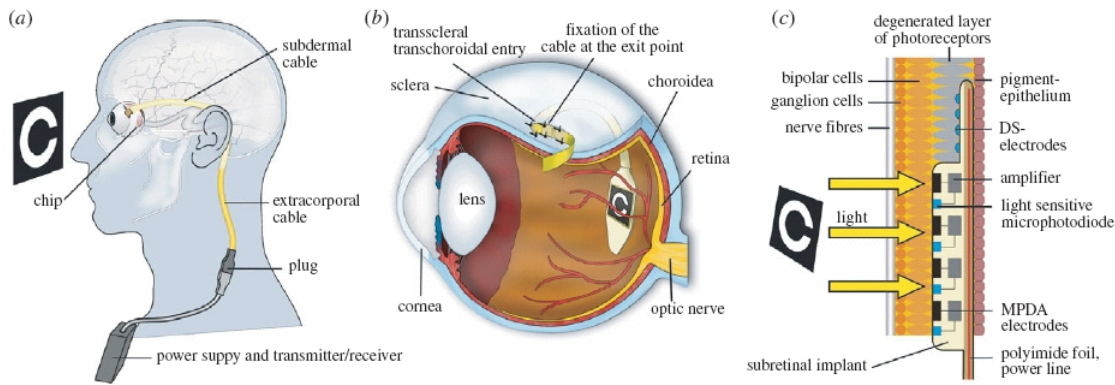


Figure 1.4: Components of an example electronic subretinal prosthesis system. (a) The cable from the implanted chip in the eye leads under the temporal muscle to the exit behind the ear, and connects with a wirelessly operated power control unit. (b) Position of the implant under the transparent retina. (c) Microphotodiode array (MPDA), amplifiers and electrodes in relation to retinal neurons and RPE. (from [Zrenner *et al.* 2010])

The epiretinal approach generally consists of a two-unit device [Majji *et al.* 1999, Rizzo *et al.* 2003, Roessler *et al.* 2009] wherein an extraocular and intraocular device communicate either through transcutaneous radio frequency (RF) telemetry or transcorneal laser. The extraocular device comprises a camera and microelectronic circuitry for encoding and transmitting stimulation patterns. The intraocular device receives the transmission and provides controllable charge injection to intact neurons at the inner retina by means of an electrode array placed in the vitreoretinal interface. An epiretinal prosthesis system is shown in Figure 1.5. While the subretinal approach offers the advantage of light transduction followed by retinal stimulation in situ (achieved by a photodiode and a stimulating electrode located at each site), the epiretinal approach offers control on stimulation algorithms. Electronics that lie between the image capture and the stimulating electrodes mean that optimal stimulation parameters may be devised and subsequently implemented without any further surgical intervention on the patient (for further discussion, refer [Eckmiller *et al.* 1999]).

Both these approaches have captured commercial and academic interests around the world. A detailed listing of visual prosthetic initiatives in research laboratories and medical institutions around the world has been summarised by Rizzo *et al.* [Rizzo *et al.* 2007]. A brief review of the intraocular (subretinal and epiretinal) implants used in clinical human trials is presented subsequently.

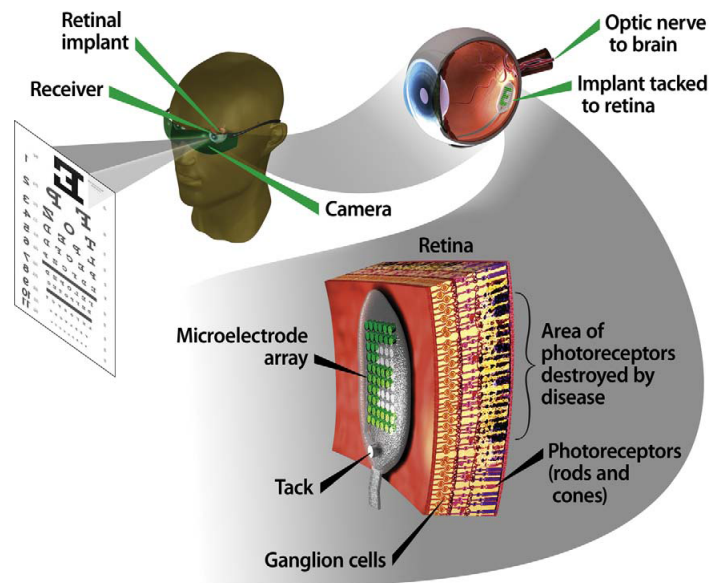


Figure 1.5: Components of an example electronic epiretinal prosthesis system. (Left top) A miniature camera mounted behind the eyeglasses of the patient captures external images such as from an eye chart. (Right top) These signals are sent to a microprocessor that converts the data into an electronic signal, then to a receiver in the eye, and finally to a microelectrode implant tacked to the retina. The array stimulates underlying retinal cells and this biological signal is sent through the optic nerve to the brain for the creation of a visual image. (Bottom) The enlarged area of the retina shows a theoretical microelectrode array tacked to the front, vitreal (ganglion cell) side of the retina (from [Chader *et al.* 2009]).

Optobionics was the first company to attempt a clinical trial in the USA using a subretinal implantation approach with a semiconductor-based microphotodiode array [Peachey and Chow 1999] presented in Figure 1.6. Their device apart from surgical complications suffered from the fact that it generated current only from light energy, i. e., it is passive without any external power supply. In spite of these problems, initial results of their Artificial Silicone Retina (ASR) indicated that it was both safe and efficacious [Chow *et al.* 2004]. In fact, the implanted six RP patients demonstrated unexpected improvements in visual function. Interestingly, this improvement included areas relatively far from the implants, suggesting a “possible generalised neurotrophic-like rescue effect on the damaged retina caused by the presence of the ASR” [Chow *et al.* 2004]. Since Optobionics did not meet the endpoints in the human trial, the company is now inoperative.

A more successful hybrid subretinal device with integrated microphotodiodes and microelectrodes has been developed by Retina Implant AG (Reutlingen, Germany) and a team headed by Dr. E. Zrenner, Eye Clinic, University of Tuebingen [40]. The

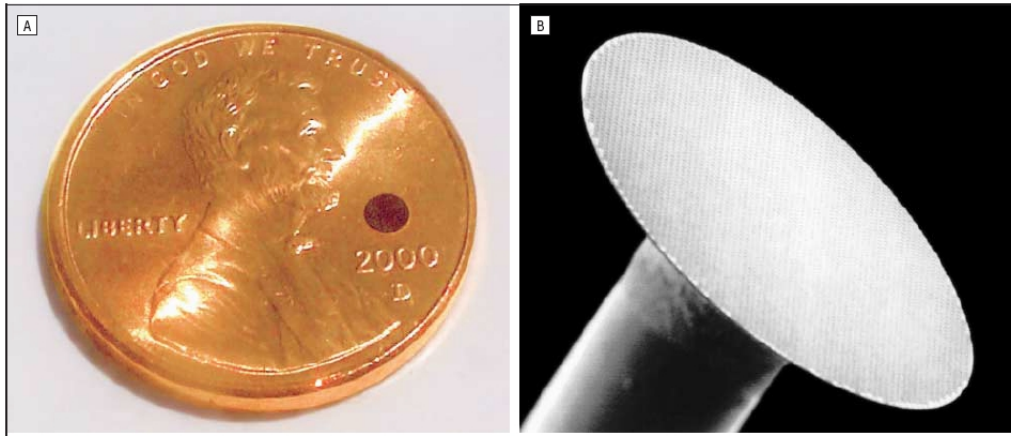


Figure 1.6: Artificial silicon retina (ASR). The model used here is 2 mm in diameter and 25  $\mu\text{m}$  thick and contains approximately 5000 negative intrinsic layer-positive microphotodiode pixels electrically isolated from each other and separated by 5  $\mu\text{m}$ . Each pixel is 20 $\times$ 20  $\mu\text{m}$  square and is fabricated with a 99  $\mu\text{m}$  iridium oxide electrode deposited and electrically bonded to each pixel. Pixel current was 8 to 12 nA with approximately 800 foot-candles of illumination. The ASR microchip was placed within a fabricated Teflon sleeve and secured intra-operatively to a saline-filled syringe injector; it was then deposited within the retina by fluid flow. (a) The ASR's size relative to a penny. (b) The ASR microchip with at 36X original (from [Chow *et al.* 2004]).

device consists of an active chip (3 $\times$ 3.1 $\times$ 0.1 mm) with 1500 microphotodiodes and an additional 16 Titanium Nitride electrode (diameter 50  $\mu\text{m}$ ) array of 4 $\times$ 4 layout with a 280  $\mu\text{m}$  intra-electrode space for direct stimulation powered externally. Each microphotodiode cell has an area of 72 $\times$ 72  $\mu\text{m}$ . Unlike the Optobionics device, it has an external power source. A photograph of the implant with description is shown in Figure 1.7. With a pilot study involving three subjects, they recently demonstrated for the first time that subretinal microelectrode arrays with 1500 photodiodes can create detailed meaningful visual perception in previously blind individuals allowing localisation and recognition of objects up to reading capability [Zrenner *et al.* 2010]. Follow-up studies are on-going to improve the capability of the implant and the wireless transmission of power between the implant and the external power supplying unit.

A long-time leader in implant science has also been the Boston Retinal Implant Project, a prototype presented in Figure 1.8, led by Drs. Joseph Rizzo and John Wyatt Jr. They have developed novel strategies in engineering, surgical approaches, functional neuroimaging and human testing, for example, studying the perceptual efficacy of array stimulation in short-term surgical trials in humans [Rizzo *et al.* 2003].

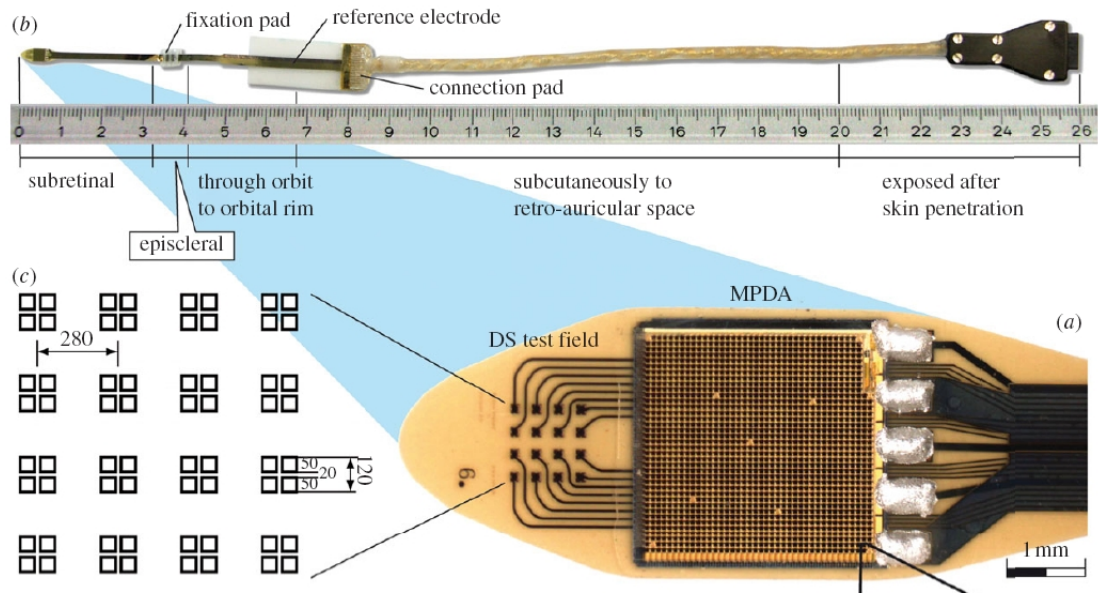


Figure 1.7: Subretinal implant jointly fabricated by Retinal Implant AG and Zrenner's group. (a) The microphotodiode array (MPDA) is a light sensitive  $3.0 \times 3.1$  mm CMOS-chip with 1500 pixel-generating elements on a  $20 \mu\text{m}$  thick polyimide foil carrying an additional test field with 16 electrodes for direct electrical stimulation (DS test field). (b) The foil exits approximately 25 mm away from the tip at the equator of the eyeball and is attached to the sclera by means of a small fixation pad looping through the orbit to a subcutaneous silicone cable that connects via a plug behind the ear to a power control unit. (c) Magnification of the DS electrode array showing the 16 quadruple electrodes and their dimensions. (from [Zrenner *et al.* 2010]).

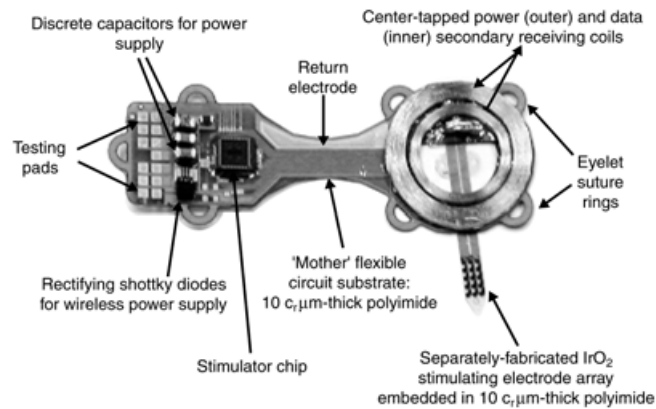


Figure 1.8: Photograph of a recent design of the animal retinal prosthesis. The secondary coils for power and data transmission and the integrated circuit and discrete electronic components are all mounted on a flexible, polyimide substrate. Only the stimulating electrode array enters the eye, where it is positioned within the subretinal space. (from Rizzo *et al.* [Rizzo *et al.* 2007])

Arguably, the most advanced prosthesis project is led by Dr. Mark Humayun at the Doheny Eye Institute, University of Southern California Medical School in conjunction with Second Sight Medical Products (SSMP). This is an effort initiated originally by Dr. Humayun with Dr. Eugene de Juan Jr. about two decades ago. In 2002, Second Sight

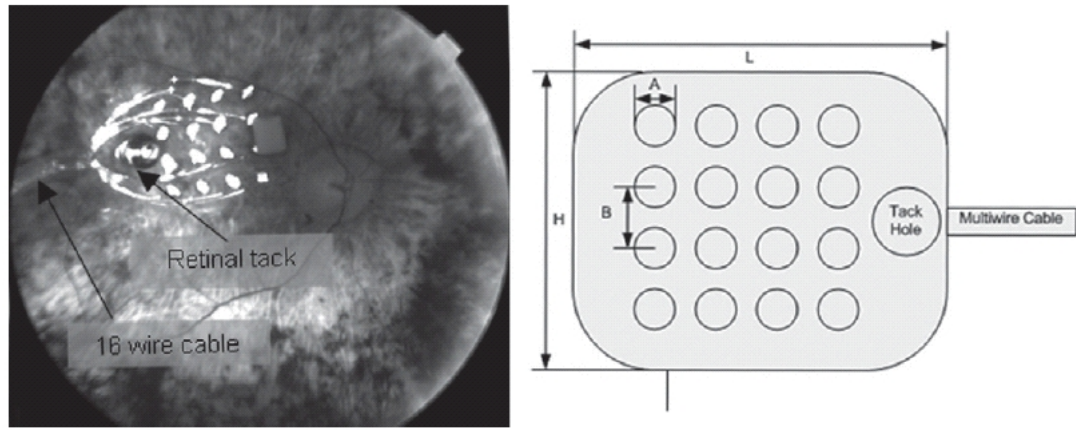
launched its first trial involving the first generation epiretinal prosthesis called Argus I. This 16-electrode device was implanted in six patients with RP between 2002 and 2004. The electrode array consisted of a combination of 260  $\mu\text{m}$  and 520  $\mu\text{m}$  diameter disc electrodes. The prosthesis enabled these patients to detect when lights were on or off, describe an object's motion, count discrete items, and locate and differentiate basic objects in an environment. Five of the six patients carried on to use the retinal prosthesis at home. In 2006, Second Sight began a study of the Argus II, a second-generation retinal prosthesis with 60 electrodes. The electrode array comprised 200  $\mu\text{m}$  diameter disc electrodes. Thirty-two patients, including 14 in the United States, have been enrolled at 11 sites in five countries (France, Mexico, Switzerland, and the United Kingdom). The Argus II group has recently claimed the first report of a visual prosthesis improving the performance of 27 blind subjects, including those with a measurable amount of native vision, in a spatial-motor task over a large cohort [Ahuja *et al.* 2010]. It is the only clinical study of a chronically implanted active prosthesis in humans that is used routinely, even out of the clinic and in the homes or business places of the users. Other such studies so far have been only of short duration with relatively infrequent use outside and limited to clinical trials alone [Kreatsoulas 2010]. SSMP has already launched their Argus III implant having 200+ electrodes for the third phase that will expand the number of patients, the quality of vision provided, and ease in which the device is implanted [Saenz 2010]. This latest variant is currently undergoing animal trials. The three generations of the Argus implants are presented in Figure 1.9.

Two other major efforts on epiretinal implants that have progressed to the point of clinical testing is worth mentioning:

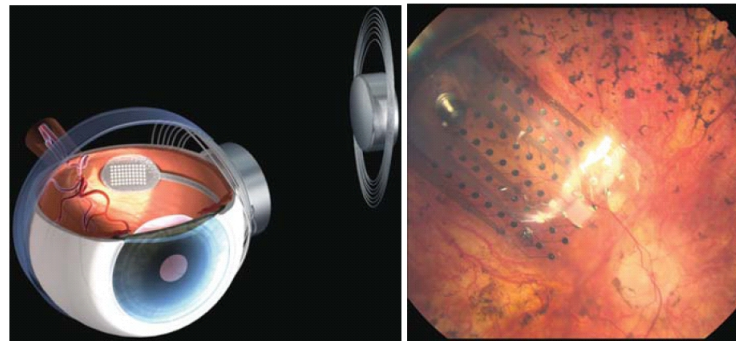
1. IIP Technologies GmbH<sup>15</sup>, who publicised an implant called the Learning Retina Implant which has been designed such that the patients can optimise their visual perceptions operated by dialog with a computer. Implantation studies on legally blind patients were successfully carried out [Feucht *et al.* 2005].
2. Another effort is called the EPI-RET project. This implant has a “learning neural computer” called a Retina Encoder, that works interactively with the user to achieve the best image possible. After implantation in two rabbits, Gerding *et al.* [Gerding *et al.* 2007] stated that “Retinal implant areas in contact to implanted devices presented a severe structural damage and disorganisation.” A prospective clinical trial report [Roessler *et al.* 2009] shows that six subjects have been

<sup>15</sup> now called IMI Intelligent Medical Implants GmbH)

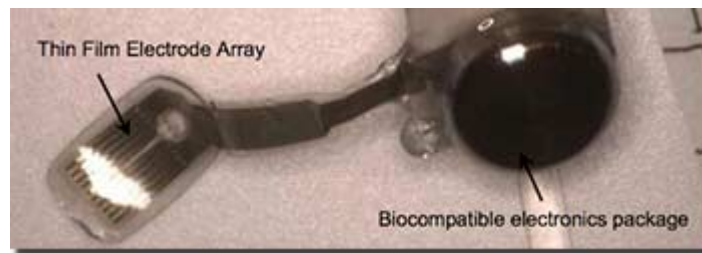




(a) Argus I device with 16 electrodes. Left: Fundus photograph of an electrode array in S3. Right: Diagram of the epiretinal electrode array with 16 platinum electrodes arranged in a  $4 \times 4$  distribution. All arrays were: H-5.5 mm, L-6 mm, and B-0.8 mm (from [Yanai *et al.* 2007]).



(b) Argus II device with 60 electrodes. Left: Schematic of its placement. Right: array in the eye of an RP subject. (from Figure 10 of Chapter 1 in [Zhou and Greenberg 2009])



(c) Argus III device. An overview of the 200+ artificial retina implant including the array and its implantable electronics package (from [Johnston 2010]).

Figure 1.9: The three generations of the epiretinal implant from SSMP.

implanted with the 25-electrode device that is relatively large and includes a part that replaces the ocular lens as well. The implants from all subjects were removed successfully after a 4-week acute study.

Alternatively, we have fabricated passive electrodes (*i.e.* without CMOS electronics) for *in vitro* electrophysiology experiments and for in-vivo experiments with rats. This flexible implant is presented in Figure 1.10. The *in vitro* stimulation experiments were conducted on isolated retinal slices of embryonic chick in both epiretinal and subretinal schemes of stimulation by our collaborators at the Geneva University Hospital (HUG). A total of more than 100 rats have been implanted with our chips in collaboration with INSERM Paris. A reliable surgical procedure has been set-up and good implantation results obtained. A quantitative assessment of the electrode-retina interaction was made by monitoring the electrical impedance for more than two months.

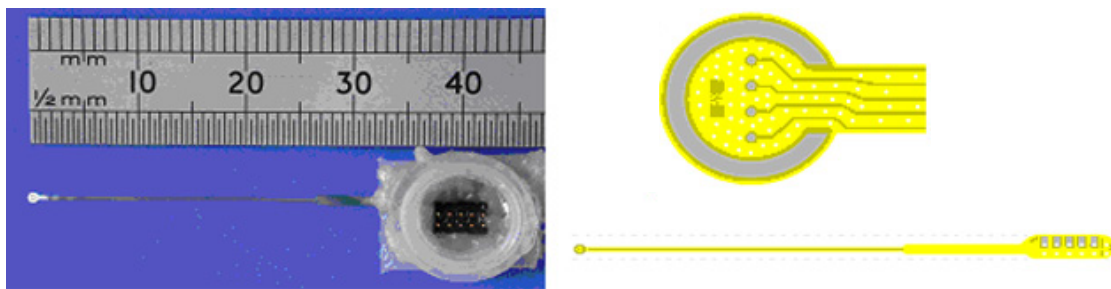


Figure 1.10: (Left) Photo of a passive flexible microelectrode array and its connector box designed for implantation in rats. (Right) Layout of the flex and the tip of the probe.

### 1.3.2 Optogenetics - replacing electrode with light stimulation

Before discussing the state-of-the-art modelling strategies, we digress slightly to discuss a relatively new technique known as Optogenetics that has the prospect of developing into next generation neurostimulation technology where neurons would be activated by light. The general information in this section is based primarily on review articles by Miesenböck [Miesenböck 2009] and Scanziani *et al.* Häusser [Scanziani and Häusser 2009].

Optogenetics, as a term, appeared in literature only in 2006 [Miller 2006]. Purists have remarked that “optogenetics” is a misnomer: similar coinages, such as optoacoustics or optoelectronics, refer respectively to interactions of light with sound and electrons. Optogenetics, by contrast, has nothing to do with interactions between light and genes; it is the effects of light on the protein products of genes that matters. There are two classes of optogenetic devices (Figure 1.11): sensors and actuators. Sensors translate cell physiological signals into optical signals, making themselves indicators of cellular function. Actuators transduce optical signals into physiological signals taking the role of controlling cellular function. The nice symmetry between sensing and actuation

is practically important because sensors and actuators together make up a complete experimental package: Actuators deliver controlled perturbations, and sensors report system responses back.

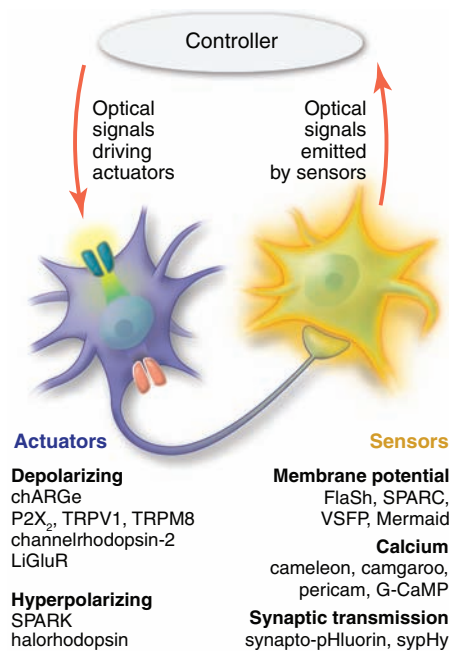


Figure 1.11: Sensors and actuators. Light-driven actuator proteins are used to control genetically targeted cells in a neural circuit. The actuators transduce optical commands into de- or hyperpolarising currents. Light-emitting sensor proteins report changes in membrane potential, intracellular calcium concentration, or synaptic transmission (from [Miesenböck 2009]).

The two main mechanisms which trigger activity in the nervous system are by sensory and electrical stimulation. The former is the method opted by sensory physiologists, because by engaging the nervous system in an ethologically relevant manner, representation of the various features of the physical world can be studied through neuronal activity. In contrast, electrical stimulation is used to study mechanisms, such as synaptic transmission, because by bypassing sensory interfaces it can be applied to isolated preparations; furthermore, the activity generated by electrical stimuli is temporally precise and reproducible.

Electrical stimulation involves the use of metal or glass electrodes to trigger action potentials in individual neurons or groups of neurons. This approach has three key limitations: it lacks specificity (except when stimulating single neurons or single synapses); inhibiting neurons is difficult; and it is invasive, causing damage at high stimulation intensities. These problems can be overcome by using two complementary



optical approaches. The first is the use of caged compounds, which involves a pharmacologically active substance that excites or inhibits neurons, delivered in an inert ('caged') form and activated ('uncaged') by breaking a photolabile bond, generally with ultraviolet radiation. The second is the use of optogenetic tools, a new class of light-sensitive proteins that, when expressed in neurons, allow their activity to be modulated by light. These proteins are either intrinsically coupled to ionic conductances or pumps, or affect neuronal excitability through second-messenger pathways [Nagel *et al.* 2003, Airan *et al.* 2009].

Optogenetic tools represent another valid alternative to the stimulation electrodes, and substantially surpass it in specificity and versatility [Nagel *et al.* 2003, Airan *et al.* 2009]. Targeted expression of light-activated molecules such as channelrhodopsin [Boyden *et al.* 2005], light-gated ionotropic glutamate receptor [Szobota *et al.* 2007] or halorhodopsin [Han and Boyden 2007, Zhang *et al.* 2007] allows neurons or their subcellular compartments to be stimulated with precise spatial, temporal and genetic specificity. These new optical tools can perform tasks well beyond the capabilities of conventional stimulation electrodes, such as independent stimulation of multiple blended populations [Zhang *et al.* 2008], bistable activation of neurons [Berndt *et al.* 2009] and stimulation of defined second-messenger pathways (for example to mimic modulatory neurotransmitter pathways [Airan *et al.* 2009]). These approaches can be harnessed to map functional connectivity [Petreanu *et al.* 2009], to influence the dynamics of neuronal circuits [Boyden *et al.* 2005, Zhang *et al.* 2007, Cardin *et al.* 2009] and finally, to control behaviour [Szobota *et al.* 2007, Tsai *et al.* 2009b].

One of the most recent uses of an optogenetic tool as a cure for retinal degeneration has been in restoring visual responses in mice models or human *ex vivo* retinas affected by RP [Busskamp *et al.* 2010]. As a common pathology in RP, rod photoreceptors die early, whereas light-insensitive, morphologically altered cone photoreceptors persist longer in both humans and animals [Lin *et al.* 2009]. In order to restore light-evoked activity in these light-insensitive cone photoreceptors, Busskamp *et al.* [Busskamp *et al.* 2010] genetically targeted a light-activated chloride pump, enhanced *Natronomonas pharaonis* Halorhodopsin (eNpHR) [Gradinaru *et al.* 2008], to photoreceptors by means of adeno-associated viruses (AAVs) [Lebherz *et al.* 2008]. Light-activated chloride pumps were chosen as the rational candidates for reactivating vertebrate photoreceptors, as both eNpHR-expressing cells [Zhang *et al.* 2007] and healthy photoreceptors hyperpolarise in response to increases in light intensity.

Busskamp *et al.* showed that a microbial gene introduced to surviving cone cell bodies reactivated retinal ON and OFF pathways and the retinal circuitry for lateral inhibition and directional selective responses. Moreover, the reactivated cones enabled retinally degenerated mice to perform visually guided behaviours. The tested time window of intervention was up to ~260 days in both fast and slow retinally degenerated mice models, suggesting that persisting cone cell bodies (~25%) are enough to induce ganglion cell activity, even during later stages of degeneration. Their finding that AAVs with a cell-specific promoter specifically transduced human photoreceptors and the identification of patients with little measurable visual function and no outer segments but surviving cone cell bodies suggest a potential for translating eNpHR-based rescue of visual function to humans.

In the future, eNpHR-based restoration may be combined with other approaches that increase the survival of altered photoreceptors [Chen and Cepko 2009, Yang *et al.* 2009, Léveillard and Sahel 2010]. More studies need to be conducted to bring the potential halorhodopsin-based therapy to blind human patients and most importantly be analysed for reliable and sustainable cure to their visual impairment.

### 1.3.3 Modelling strategies

Modelling and simulation offer a method of evaluating more experimental conditions than would be possible through direct experimentation. The need for better models for simulating electric stimulation of the retina was recognised and initiated by Weiland and Humayun [Weiland and Humayun 2005] when only few simulation studies [Greenberg *et al.* 1999, Resatz and Rattay 2004] were performed despite the existence of models on retina biophysics and retinal circuitry. There has been a substantial contribution in the field of modelling studies for more than a decade since then. An attempt is made in this section to cover the multitude of aspects documented in literature that is relevant for construction of an integrated simulation framework. This simulation framework can be employed in understanding and predicting various factors affecting retinal stimulation. The work cited in this section are in a chronological order of their original publication.

One of the first studies in models for retinal stimulation were presented by Greenberg and his team. They used cell tracing methods to accurately model a retinal ganglion cell (RGC) [Greenberg *et al.* 1999]. Their goal was to determine whether the RGC was preferentially stimulated at its soma or the passing fibres distant from the soma. Using NEURON [Hines 1993], a multicompartamental simulation package, they tested three

cell membrane models: a linear passive model, a Hodgkin–Huxley model with passive dendrites (HH) and an all active compartmental Fohlmeister-Coleman-Miller (FCM) model with five nonlinear ion channels. These models for epiretinal stimulation of retinal ganglion cells predicted almost equivalent thresholds for axons and soma. Their model, simulated as extracellular monopolar stimulation, did not consider the effect of resistive retinal layers and precise location of the return electrode. The contribution of RPE, choroid and sclera were not considered, as in an actual implant, the return electrode is placed on the sclera (external to the eye) on the opposite side of the retina from the stimulating electrode array [Greenberg *et al.* 2008].

Rattay and Resatz developed a model that predicted stimulus thresholds for electrical pulses applied between two strip electrodes running parallel to the retinal ganglion cell axons [Rattay and Resatz 2004]. The aim was to analyse the possible influence of electrode geometry on selective stimulation of a target RGC by avoiding co-activation of passing axons. Using COMSOL<sup>16</sup> and compartmental models (FCM) of RGC and bipolar cells, the estimated excitation thresholds were calculated with the help of an activating function. The thresholds were higher than those found experimentally. However, the model does predict an increase in neurotransmitter release in the bipolar cells with increased pulse duration and electrode size. The drawbacks however were similar to those of Greenberg’s approach as the retina was treated electrically as vitreous humour having resistivity of  $57 \Omega \cdot \text{cm}$ . The location of the return electrode and the electric influence of the anatomical features of the eye wall behind the retina were not considered.

Computational modelling has been used to estimate the temperature increase in the eye and head due to heat generation in the retinal prosthesis system. Gosalia *et al.* [Gosalia *et al.* 2004] obtained thermal elevation results for a 3-D model using the explicit finite difference method to implement the bio-heat equation. The spatial resolution of the model used was discretised to 0.25 mm by 3-D interpolation from an original 1 mm cross-sectional slice obtained from the National Library of Medicine (NLM) “Visible Man Project”. An analysis of different locations (in the centre of the vitreous cavity and at the anterior of the eye between the ciliary muscles) and sizes ( $4 \times 4 \times 0.5 \text{ mm}$  and  $6 \times 6 \times 1 \text{ mm}$ ) were considered. The chip was covered by an insulating encapsulation with a uniform thickness of 0.5 mm, and was allowed to dissipate 12.4 mW over its entire volume (excluding the insulation). The thermal conductivities of the chip and the

<sup>16</sup> COMSOL was previously known as FEMLAB®

insulation were assumed to be constant and uniform over their volume and equal to  $60 \text{ J}/(\text{m}\cdot\text{s}\cdot^\circ\text{C})$  and  $30 \text{ J}/(\text{m}\cdot\text{s}\cdot^\circ\text{C})$ , respectively. As those simulations showed, placing the chip in the anterior region, or increasing its size, reduced the computed temperature increase in the vitreous humour and the retina. Their study disregarded the power dissipated in the retina due to the stimulating array and also neglected the electrical properties of the multilayered retina. This was later taken into account by Schmidt and his team [Schmidt *et al.* 2008] mentioned later in this section.

The signals of ganglion cells are the indications of the complex retinal network activity, which is transmitted by the ganglion cell axons to the brain [Zrenner 2002]. Appropriately, Eckmiller *et al.* [Eckmiller *et al.* 1999] devised a “retinal encoder” to stimulate ganglion cells with a pattern similar to the ganglion cell output generated by a native retina. The encoder approximates the typical primate ganglion cell-receptive field properties of primate RGCs by means of individually tuneable spatiotemporal receptive field filters. The encoder maps visual patterns onto spike trains for a number of contacted ganglion cells. Clinical results on the success of this retinal encoder are not available. The framework of that simulated visual system was later exploited by another team [Cai *et al.* 2007] to investigate the encoding mechanism of the RGC. In addition, Hornig and Eckmiller used FEMs to demonstrate that control of the maximum voltage field increases with the orthogonal distance to the electrode (z-direction) [Hornig and Eckmiller 2001]. Hornig modelled layers of retina neurons and used a training algorithm to selectively stimulate individual model cells distal to a flat simulating grid. With this approach, Hornig was able to discriminate between two adjacent model cells: one cell was set into a sub-threshold refractory period while the other was stimulated.

Cottaris and Elfar developed a retina model that includes all major retinal cell types and the corresponding interconnections among them to characterise the spatiotemporal activation<sup>17</sup> of the retina circuitry during the electrical stimulation period [Cottaris and Elfar 2005]. Their simulation results show that during the period of electrical stimulation, the activation of RGCs is governed mainly by the electric field imposed by the stimulating electrode. This electric field causes the indiscriminate excitation of

<sup>17</sup> Selective stimulation requires spatial and temporal coordination of voltage fields in conductive cellular media. Some control over the spatial contour of the fields is afforded by the shape of the current-induced voltage fields, where the spatial decay of the field is given by the resistivity of the solution, electrode shape and material [McIntyre and Grill 2001]. Unfortunately, temporal control over the propagation of signals in cellular media is virtually impossible to achieve [Ross 2008]. While, it is not feasible to temporally sum signals at the neuron, the temporal component of voltage fields in the retina-vitreous medium are still very relevant.

ON and OFF retinal ganglion cells. This finding helps to design the image encoding strategies for the retinal prosthesis.

In order to investigate retinal activation patterns resulting from dipolar current stimulation, Dokos *et al.* [Dokos *et al.* 2005] formulated a simplified bidomain model of bulk retinal tissue, epiretinally stimulated by one or two pairs of hemispherical electrodes providing biphasic currents. To the best of our knowledge, this is the first report of electrode-retina gap inclusion in a model for studying retinal stimulation. They used the bidomain theory which states that extracellular currents are able to stimulate excitable cells only if the anisotropic ratios of intracellular and extracellular conductivities are unequal [Roth 1992]. They assumed an unequal anisotropy ratio in both domains of a retina such that RGC and bipolar cells are intracellularly coupled preferentially in the vertical direction normal to the retinal surface, with minimal synaptic coupling in the lateral directions. A modified RGC model and Poisson equation within the epiretinal vitreous were used for the computations. Calculations were carried out in time domain using a custom predictor-corrector algorithm. Results from these simulations suggested that a biphasic cathodic-anodic stimulus sequence is effective in providing targeted focal activation of retinal tissue.

An improvement over Dokos's previous model was recently reported by his team [Yin *et al.* 2010] to include an active implementation of the retinal ganglion cell tissue layer and passive implementation of deeper cell layers. The retinal ganglion cell layer receives excitatory presynaptic inputs from the bipolar layer and inhibitory presynaptic inputs from the amacrine layer. Simulations were performed to investigate the behaviour of retinal tissue activation with epiretinal and suprachoroidal electrode stimulation. The results indicated the presence of both early and late onset action potentials consistent with experimental findings.

Another very important factor to consider in modelling studies is the depth of an excitable neuron within the retina and at various eccentricities from the stimulating electrode. Ziv *et al.* investigated the target cell location using threshold data from the stimulation of RGCs in rabbit to build a mathematical model of the excitation field around a conical-tipped electrode [Ziv *et al.* 2005]. The experiments had reported that the threshold had a  $1/r^{0.84} - 1/r^{3.19}$  dependence on distance from the stimulation tip, in slight contrast with the strict  $1/r^2$  dependence predicted by Coulomb's law [Jensen *et al.* 2003]. To explain this discrepancy, they proposed a modified model that takes into account the location of the return electrode and the non-infinite dimensions of

the experimental environments often used for *in vitro* electrophysiology and some retinal prosthetic designs. The horizontal displacement of the neuron with respect to the electrode was also considered in the model. Their analytical model did not yield predictions for neuronal depth that were statistically superior to those of the square law. Instead, it did provide more realistic median values for cell depth than the square law when these models were tested with threshold data points that were obtained from more widely distributed areas on and above the retina. In conclusion, they stated that a larger threshold data pool would be needed to make more definitive statements about the relative value of their model versus the traditional square law model.

A series of interesting analytical models to predict the effect of distance between the stimulation electrode and the target retinal cells over the threshold currents, cross-talk between electrodes, electrochemical limitations, tissue heating were discussed by Palanker and his team [Palanker *et al.* 2005]. They also predicted the resolution of a retinal prosthesis based on considerations for some parameters mentioned above (e.g. electric field interference between electrodes and intraocular heating). These simulations were based on a hemispherical electrodes considering the return electrode to be at infinity. Subsequently, they also studied a configuration involving closer return electrodes (targeted for a high-resolution retinal prosthesis) and disc electrodes (Chapter 14 of [Humayun *et al.* 2007]). These models were studied in a homogeneous medium disregarding the electrical anisotropy of the retina.

Schiefer and Grill [Schiefer and Grill 2006] studied the retinal sites of excitation after epiretinal electrical stimulation. Computer-based, compartmental models of a simplified, isolated RGC were simulated in NEURON to study the effects of cellular geometry, electrode to neuron distance and stimulus duration and polarity on activation of a RGC produced by extracellular stimulation. They found that stimulation was highly dependent on the physical geometry between the electrode and the underlying ganglion cells. Thresholds were lowest when the electrode was placed close to the characteristic 90° bend<sup>18</sup> in the ganglion cell axon, perhaps explaining why epiretinal stimulation “results in the production of punctuate rather than diffuse or streaky phosphenes” [Humayun *et al.* 1996].

One of the most complete studies in modelling and simulation of an epiretinal prosthesis was demonstrated by Schmidt and his colleagues [Schmidt *et al.* 2008]. This work was published while the present thesis work was being carried out, and will be

<sup>18</sup> The bend is naturally due to the anatomical layout of ganglion cells with axons leading to the optic fibre relaying signals to the visual cortex.

treated as the state of the art for modelling and simulation framework presented in this dissertation. Although the computation tool and representation of various building blocks forming the simulation framework were different in this thesis - the general idea of including features like realistic geometries, electrode placement and inclusion of retinal inhomogeneity were identical.

In their work, a Partial Inductance Method was used for the computation of the electrical coupling parameters of the radiating and receiving telemetry coils of a dual-unit<sup>19</sup> retinal prosthesis. Results for the inductive coil coupling were presented and different coil geometries were compared. Further, a Finite-Difference Time-Domain (FDTD) method for the solution of a bio-heat equation was used to compute the temperature increase caused by the implanted electronics and the electromagnetic absorption due to the external power and data telemetry link [Singh 2009]. Temperature increases due to the implanted microchip, coils, and stimulating electrode array were presented.

In addition, they computed current spread in a human retinal tissue based on a refined electric model of a retina using multi-resolution impedance method. Results showed variations of current spread in the retina and eye due to different electrode array geometries and placement configurations. As an advancement over studies conducted by Gosalia *et al.* mentioned earlier, Schmidt *et al.* found that complexity of the relation between temperature increase and physical characteristics of the implanted electronics is not only limited to their position or size; for e.g., it may also involve the power distribution characteristics and material properties of biocompatible materials used for insulating the chip. The drawback of an electric retina model used by Schmidt and his team was refined from existing resistivity measurements in a frog Karwoski *et al.* [1985] and not a human. Moreover, their model did not include the effect of the electrode-retina gap and its effect on retinal stimulation.

In order to study the effects of monopolar, dual monopolar and dipolar stimulation schemes over the threshold currents necessary to epiretinally stimulate the RGCs, the electric field distribution between the electrode and the retina was analysed by Ahuja *et al.* Ahuja *et al.* [2008]. Simple direct current (DC) simulations using COMSOL were conducted to conclude in support of their experimental results which showed 212% higher thresholds for a dual monopolar in comparison to a monopolar stimulation scheme. The simulations were made in physiological saline once again

---

<sup>19</sup> external camera and wireless transmitter integrated in a single device



without considering the anisotropic retina. The details of the geometry were ignored too as this was more of a validation study to support their experimental results.

A simulation study targeted at modelling electrophysiological properties of RGCs during epiretinal stimulation was presented by Kameneva *et al.* [Kameneva *et al.* 2010]. A model of the electrophysiological properties of ON and OFF retinal ganglion cells (RGCs) was constrained and validated using experimental data from the literature. Their simulations supported the experimental findings that differ in the magnitude of the T-type  $Ca^{2+}$  current explaining differences in the intrinsic electrophysiology of ON and OFF RGCs. These models can be used to investigate the potential for differential stimulation of ON and OFF RGCs during retinal stimulation with sinusoidal current. The model predicts that OFF cells fire preferentially over ON cells in a frequency band around 10 Hz. The suggested low frequency raises questions on the temporal resolution and assurance against electrode corrosion. These kinds of studies are out of scope for this dissertation and hence not commented upon.

To our best knowledge, the first modelling studies on subretinal stimulation of retina was only demonstrated recently by Gerhardt *et al.* [Gerhardt *et al.* 2010]. They investigated the spatial characteristic of retinal polarisation obtained by electric field simulation through a subretinally placed monopolar and dipolar electrode array. They combined electric potential simulation through a boundary element method with a segmented bipolar cell model. They used this to compute the membrane voltage at the axon terminal of the bipolar cells as a function of the axon length and the electrode diameter. They found that dipolar arrays offer a promising approach when simultaneous stimulation is necessary at multiple retinal sites. The limitations of their study includes the negligence of retinal inhomogeneity and distance between the electrode array and the soma-dendritic terminal of the bipolar cells.

The group of Wilke [Wilke *et al.* 2010b] investigated the electric cross-talk between the electrodes in a monopolar high resolution (up to 1500 electrodes) retinal prosthesis when driven simultaneously. The electric field distribution was calculated with the help of COMSOL, essentially by solving the Poisson equation in physiological saline with 25 to 1681 electrodes activated all together. The limit of spatial frequency of visual patterns that could be resolved by such arrays can be assessed to be 4.5; 1.2; and 0.7 cycles/mm, for an anticipated distance of target neurons of 20  $\mu\text{m}$ , 200  $\mu\text{m}$  and 400  $\mu\text{m}$ , respectively. This relates to a best achievable theoretical visual acuity of 2%, 0.6%, and 0.3% of normal vision, respectively. Their studies reiterated the importance of electrodes



being closer to the target cells or even creating more confined stimulating fields within the retina to guarantee high resolution retinal stimulation and good visual acuity. They neglected the electrical properties of the retina.

An important reference for the simulation framework presented in this dissertation which validates our assumption on the implemented threshold criterion, is an analytical study from the group of Palanker [Boinagrov *et al.* 2010]. They modelled extracellular neural stimulation numerically and analytically for several cell shapes and types bearing active membrane properties. The strength-duration<sup>20</sup> relationship was found to differ significantly from classical intracellular models. It was demonstrated that extracellular stimulation can have not only lower but also upper thresholds and may be impossible below certain pulse durations. It was inferred that in some regimes the extracellular current can hyperpolarise cells, suppressing rather than stimulating spiking behaviour. It was demonstrated that thresholds for burst stimuli can be either higher or lower than that of a single pulse, depending on pulse duration. The modelled thresholds from their study were found to be comparable to published experimental data. It was also found that the electroporation thresholds, limiting the range of safe stimulation, were exceeding the stimulation thresholds by two orders of magnitude. Their results provide a biophysical basis for understanding stimulation dynamics and guidance for optimising the neural stimulation efficacy and safety.

Finally, the most recent of all modelling studies that justifies and proves the relevance of using an electrically anisotropic model of the retina for simulation studies was conducted by Minnikanti *et al.* [Minnikanti *et al.* 2010]. This work complements the usage of a electric laminar model of a retina for simulation of retinal stimulation as mentioned in the study conducted by Schmidt *et al.* [Schmidt *et al.* 2008] described earlier. They developed a compartmentalised FEM of the electric field generated in the rabbit retina caused by a biphasic stimulus pulse. The model included the different resistivities and capacitances of the retina, RPE, and sclera. Axisymmetric 2-D FEMs were created for monopolar stimulation electrodes using COMSOL. Electrodes of 250  $\mu\text{m}$  diameter with 10  $\mu\text{m}$  thick insulation were placed in three configurations with respect to the retina: epiretinal, subretinal and suprachoroidal. A broad return electrode was located at the back of the eye on the sclera. The relative dielectric constants of each eye-wall layer with linearly varying resistivity for the retina layers were also incorporated into the model. Simulations using biphasic  $1 \text{ mA}/\text{cm}^2$  current pulses with pulse widths

---

<sup>20</sup> A graph relating the intensity of an electrical stimulus to the length of time it must flow to be effective.

of either 0.5 ms ( $0.5 \mu\text{C}/\text{cm}^2$ ), 1 ms ( $1 \mu\text{C}/\text{cm}^2$ ), and 5 ms ( $5 \mu\text{C}/\text{cm}^2$ ) indicated high electric fields in the RPE for all three configurations. They claim that RPE needs to be taken into consideration for determining safe levels of stimulation. In conclusion, they demonstrate the differences in using a retina model of constant resistivity ( $4k \Omega \cdot \text{cm}$ ) in comparison to that of a Gaussian resistivity model ( $3k - 7k \Omega \cdot \text{cm}$ ).

#### 1.4 DISSERTATION POSITION WITH RESPECT TO THE STATE OF THE ART

There has been extensive previous work in modelling and simulation to better understand retinal stimulation and appropriately aid in designing efficient retinal prostheses. But none of the previous modelling studies on modelling retinal stimulation dealt with the elements of an implantable retinal prosthesis in an integrated simulation framework. The contribution this dissertation makes to the field of modelling retinal stimulation are the preliminary experimental and modelling steps taken in constructing a complete framework for simulating the behaviour of retinal prostheses under various clinical and experimental conditions.

The primary goal of this dissertation was to study the effects of geometrical factors affecting stimulation thresholds of a retina. One of the major contributions made in achieving this was the utilisation of FEM-based simulation framework to evaluate these effects for different retinal stimulation schemes. The simulation results described in Chapters 5 and 6 were intended to explain the effects of these factors for epiretinal and subretinal stimulation schemes respectively. The parameters included were: (1) the location and dimensions of stimulation and ground electrodes adapted to real *in vitro* or implantation scenarios; (2) a realistic representation of the electrical properties of the retina; (3) choice of a simplified, yet realistic activation threshold criterion based on a recent analytical study [Boinagrov *et al.* 2010] that incorporates the critical stimulation parameters such as stimulus type (monophasic/biphasic), shape (cathodic/anodic) and duration under a single unified model (4) Estimation and prediction on threshold currents and impedance with varying electrode-retina distances for different electrode dimensions. Using our simulation framework, variation of threshold currents and impedances were computed using different electrode-retina distances and disc electrode sizes. In order to demonstrate the relevance of our framework, the frame of reference for the computed results was the most recent *in vitro* and clinical data drawn from our collaborators and literature. These data allowed us to demonstrate the role of geometrical factors affecting stimulation thresholds. We estimated lateral extents of

stimulation for the electrodes which provides an indication to the resolution of the retinal prostheses used currently. Subsequently, parameters within our simulation framework can be easily modified to predict the efficiency of novel electrode geometries for future retinal prostheses.

As mentioned before, previous theoretical studies [Lee and Grill 2005, Miranda *et al.* 2007] associate importance to neural tissue inhomogeneity in relation to neural stimulation. This fact was illustrated for retinal stimulation in recent modelling studies [Schmidt *et al.* 2008, Minnikanti *et al.* 2010] as electric models of retina having a resistivity profile. These resistivity profiles were extrapolated from previous resistivity measurements in frogs [Karwoski *et al.* 1985, Xu and Karwoski 1994] for the purpose of their simulations. In order to explain the *in vitro* retinal stimulation results from embryonic chick retinas obtained by our collaborators using our simulation framework, it was necessary to know the retina resistivity profile to draw realistic and appropriate comparisons between experiments and simulations. To the best of our knowledge, until today, there exists no resistivity profile measurements in an embryonic chick retina.

A secondary goal of this work was to establish a convenient and accurate method for determining the resistivity profiles in a retina. Another significant contribution of this dissertation therefore was the experimental determination of resistivities in isolated retinal slices from rats and embryonic chicks. A direct localised measurement of resistivities in these retinal slices using bipolar<sup>21</sup> electrodes was demonstrated in Chapter 3 of this dissertation. For the first time, a flexible microprobe was employed to measure local resistivity with bipolar impedance spectroscopy at various depths in isolated rat and chick embryo retinas. Small interelectrode spacing permitted high resolution measurements and the probe flexibility contributed to stable resistivity profiling. The resistivity was directly calculated based on the resistive part of the impedance measured with the Peak Resistance Frequency (PRF) methodology developed by our group previously. The resistivity-depth profiles for both rat and chick embryo models are in accordance with previous mammalian and avian studies in literature. We demonstrated that the measured resistivity at each depth has its own PRF signature. Resistivity profiles obtained with our setup provided the basis for the construction of an electric model of the retina required for making predictions on stimulation parameters.

<sup>21</sup> The word bipolar should not be confused with dipolar. Following the convention by Grimnes and Martinsen (Page 165 of their book [Grimnes and Martinsen 2008]), the terms monopolar–dipolar are of Greek origin, and are preferably used for current carrying systems (stimulation). The terms unipolar and bipolar are of Latin origin and are used for signal pick-up electrode systems (recording).

These predictions were in good agreement with *in vitro* experiments conducted on isolated embryonic chick retinas.

### 1.5 RESEARCH OBJECTIVES

The main objectives for the investigations done as a part of this dissertation can be summarised as follows:

- To establish preliminary steps in forming an integrated simulation framework that accommodates some of the most critical geometrical parameters affecting quality of retinal stimulation significantly
- Devise a high resolution technique for resistivity profiling of the retina. Use the extracted resistivity profiles from isolated slices of embryonic chick retina to construct an electric model of retina. This model is incorporated as an input to the computational framework modelled based on the scenario as in *in vitro* stimulation experiments conducted by our HUG collaborators. A demonstration of relevance of the measured resistivity profile would be proven by an agreement of the computed and experimental values of stimulation parameters obtained during the *in vitro* experiments.
- Evaluate the effect of geometrical parameters on both epiretinal/subretinal stimulation schemes and consequently demonstrate the weaknesses in current clinically deployed retinal prostheses
- Using the simulation framework, predict significant parameters that affect the efficiency of retinal stimulation and demonstrate prospects of a useful tool for new retinal prosthetic designs

### 1.6 LIMITATIONS

Our simulation framework is a preliminary step to build an integrated framework for studying retinal stimulation. The geometrical and electrical parameters in a conventional implantable retinal prosthesis were taken into consideration. But, in order to represent a more accurate and responsive model for extracellular stimulation of the retina, it is imperative to consider the following factors or phenomena:

- Spatiotemporal properties of retinal stimulation [Cottaris and Elfar 2005, Horsager *et al.* 2009; 2011]

- Properties of the retinal network including intercellular connections [Resatz and Rattay 2004, Cottaris and Elfar 2005]
- Degeneration and rewiring [Marc *et al.* 2003] in the retina to be modelled
- Local oedema<sup>22</sup> to be modelled, instead a finite distance between the electrode array and retina was considered
- Ganglion cell density
- Surface (porosity, etc.) and material properties of electrodes; Although, electrochemical effects at the electrode interface were considered as a part of the model
- Depending on the electrode size, close to a planar electrode surface, the field is not anymore uniform [Palanker *et al.* 2005]. In this dissertation, during simulation of epiretinal stimulation, the RGCs are within a distance in the order of the electrode size. Under these circumstances, the assumption on the threshold criterion is questionable and needs to be re-considered.
- Location of the implant with respect to distance from the macula (personal communication with Ashish Ahuja<sup>23</sup>)
- Impact of the electronics, for e. g. in computations for heat dissipation [Schmidt *et al.* 2008]
- Agonist and antagonist effect on depolarisation and hyperpolarisation of excitable retinal cells (Chapter 20 by Hetling from [Humayun *et al.* 2007])

While these factors or phenomena are listed as limitations, some or all of these may form the basis for further research and refinement of the integrated simulation framework proposed in this study.

## 1.7 DISSERTATION LAYOUT

In the present chapter, the scope and the modelling problem were first introduced. An exhaustive review of literature was presented to understand the state-of-the-art retinal implants and the existing modelling strategies for retinal stimulation. After a brief mention of the position of this dissertation with respect to the existing knowledge in

<sup>22</sup> an abnormal accumulation of fluid beneath the electrode array and the retina after retinal prosthesis implantation

<sup>23</sup> Executive Director of Operations of The California Project to cure blindness at USC's Keck School of Medicine. Also a Research Scientist for Second Sight Medical Products

modelling retinal stimulation, the research objectives and limitations of our simulation framework were stated.

A thorough understanding of theoretical concepts, relating to modelling neural stimulation, is necessary for building a simulation framework. Chapter 2 takes a detour presenting theory on the physiological basis for neural stimulation, electric fields in biological volume conductors, stimulus characteristics affecting neural stimulation, safe neural stimulation and direct-indirect retinal stimulation. The chapter also provides a preview to modelling retinal stimulation by stating examples from literature.

The inhomogeneous nature of the retina is a key element in our simulation framework. An accurate and simple method for determining the electrical anisotropy in different layers of the retina is instrumental. In this respect, a detailed description of a direct and local measurement technique to measure retina resistivity profiles in rats and embryonic chicks was given in Chapter 3. A bipolar impedance spectroscopy technique with extraction of tissue resistance at PRF was used for calculating the resistivity profile in the vertical cross-section of the retina.

A computational basis needs to be established in order to evaluate factors affecting the performance of retinal prostheses. Chapter 4 describes these factors in detail and gives an account of the model variations employed for epiretinal and subretinal stimulation schemes resulting in an integrated simulation framework. Corresponding electric models of retina were used for clinical and *in vitro* scenarios. For example, the chick data determined by the resistivity profiling experiment was utilised to construct an electric model of a chick retina. The retinal model is an element of the framework which computes quantities that can then be compared to *in vitro* stimulation experiments using embryonic chick retina slices by our collaborators. In conclusion, the framework was used to estimate and predict performance parameters of retinal stimulation for both clinical and *in vitro* experiments by appropriate scenario-based adjustments.

In order to validate the built simulation framework, we compare the computations with clinical and *in vitro* findings from the literature and experiments conducted by our collaborators for both epiretinal and subretinal schemes. In Chapter 5, we describe the results of the influence of geometrical factors on the stimulation thresholds of a clinically employed epiretinal prosthesis, using our simulation framework. Threshold currents and impedances for planar disc microelectrodes were estimated for different electrode-retina distances. The profiles and the values for thresholds and impedances obtained from our simulation framework are within the range of measured values in clinical

trials (Argus I). An estimation of resolution for the electrodes used in these trials was provided. The relevance of the retina resistivity profile obtained from embryonic chick was demonstrated using valid comparisons with *in vitro* experimental data obtained from our collaborators. Our results reiterate the importance of close proximity between electrodes and retina for safe and efficient retinal stimulation.

After having demonstrated the relevance of the simulation framework for epiretinal scheme, we describe the effects of electrode-retina interactions on subretinal prostheses for *in vitro* and *in vivo* applications in Chapter 6. Threshold stimulation currents and the lateral extent of the stimulation zone were computed for planar disc microelectrodes again. Recent evidence indicates a decrease in threshold charge with time following subretinal implantation [Wilke *et al.* 2010a]. A hypothesis based on an electrode-retina gap was proposed to explain the variation in threshold stimulation currents. Threshold stimulation currents and impedances for different electrode-retina gaps were computed. We validate the hypothesis with our simulation results that the changes in impedance observed with time *in vivo* can be mainly attributed to the varying distance of the ganglion cells from electrodes due to changes in electrode-tissue gap. In addition, through valid comparisons with *in vitro* experimental data obtained from our collaborators in subretinal mode, it was also confirmed that the measured resistivity profile of an embryonic chick retina is relevant for simulation studies.

The dissertation concludes with a discussion on the significance of an integrated simulation framework employed to study the significant factors affecting the safe and efficient stimulation by retinal prostheses in Chapter 7. A brief mention of the future directions to improvements in the simulation framework is also provided.





## ELECTRICAL STIMULATION OF RETINA: FROM ELECTROPHYSIOLOGY TO MODELLING

---

### 2.1 INTRODUCTION

Retinal prostheses in the form of electrode arrays impart extracellular electric stimulation to the retina. There are three possible mechanisms by which this stimulation can activate pathways in the retina to elicit phosphenes in blind patients [Cohen 2007]. First, electrodes can depolarise and form action potentials in ganglion cell axons. Second, electrical currents can depolarise and form action potentials in local ganglion cells directly. Finally electrical currents can depolarise cells in the retinal network such as bipolar or amacrine cells which propagate the visual signal to ganglion cells indirectly. To better understand the activation of a RGC by retinal prostheses, it is necessary to review the fundamental principles of the interaction of electric fields and neurons.

In this chapter, rationales behind neurostimulation are solely discussed as it is assumed that the reader is well versed with the theory on electrode-electrolyte interface and the basic mechanism of charge injection at the interface (electrode double layer<sup>1</sup>). Moreover, the reader is expected to have a fundamental knowledge on anatomical properties of a neuron. Commencing from the physiological basis for activation of neural tissue, the distribution of currents inside the volume conductor and the interaction between a neuronal axon and applied electric fields is described. In addition, the stimulus characteristics affecting neural stimulation such as cathodic and anodic stimulation on activation threshold, mono- and dipolar stimulation, choice of current/voltage controlled stimulation, strength-duration curves and selective stimulation of retina is presented. A brief discussion on safety considerations for both the electrode and retina during extracellular retinal stimulation is also presented. The chapter terminates with a brief account on direct and indirect stimulation of retina and a mention of few models explaining different phenomenon associated with retinal stimulation.

---

<sup>1</sup> the curious reader is referred to: Electric double layer theory - [McAdams *et al.* 1995, Linderholm 2006] and application to neurostimulation - [Merrill *et al.* 2005]

## 2.2 PHYSIOLOGICAL BASIS FOR NEUROSTIMULATION

During extracellular stimulation, electron flow within the stimulation electrode is converted into a current flow of ions within the volume conductor and the tissue. By injecting this ionic current in the extracellular medium, the neural tissue undergoes stimulation at a multicellular level, manipulating the kinetics of the voltage-gated channels on those neural cells.

A neuron is characterised by a bilipid layer membrane that separates the intracellular region from the extracellular medium and acts as a barrier to the movement of ions between these two regions. The channels on the membrane are specific and selective in permitting ion exchange. All neurons have a resting transmembrane potential with the interior being negative with respect to the exterior of the neuron. A typical value of the resting membrane potential is -60 mV measured inside the cell with reference to the outside. This membrane potential is dependent on the concentration of the ionic species such that the equilibrium potential of each ion differs from the membrane potential. In general, the ions of interest are  $K^+$  (potassium),  $Na^+$  (sodium) and  $Cl^-$  (chloride). The electrochemical balance of the neuron is well described by the Nernst potential and Goldman's equation and in turn are sufficient to interpret the physiological activation of neural tissue [Leanne Chan 2009].

The primary effect of an electric stimulation pulse on a neuron is a change of its transmembrane voltage, being either a depolarisation or a hyperpolarisation. When the axon membrane is depolarised up to its threshold voltage, based on its electrical membrane properties, an action potential will be generated by the excitation mechanism first described by Hodgkin and Huxley [Hodgkin and Huxley 1952]. While an action potential generated under normal physiological conditions (at the initial segment of the axon [Fried *et al.* 2009]) propagates orthodromically (away from the soma), a stimulation-induced action potential propagates both orthodromically and antidromically (opposite to the normal, orthodromic direction) along the fibre. A cable network, as shown in Figure 2.1, was proposed by McNeal to calculate how nodal transmembrane voltages are affected by a stimulation induced extracellular field.  $V_e$  represents the nodal field potential.  $R_a$  represents the intra-axonal resistance.  $R_m$  represents the nodal membrane resistance and  $C_m$  represents the nodal membrane capacitance. When a negative electrode (cathode) is placed near to the nerve fibre, the node closest to the cathode will have the most negative  $V_e$  and it will be depolarised the most, described by the activating function  $AF$  by using equation 2.1.  $AF$  is the driving force of the change

of nodal transmembrane voltages. For node  $n$ , the value of  $AF_n$  is calculated as the difference of two potential differences:

$$AF_n = (V_{e,n-1} - V_{e,n}) - (V_{e,n} - V_{e,n+1}) = (V_{e,n-1} - 2V_{e,n} + V_{e,n+1}) \quad (2.1)$$

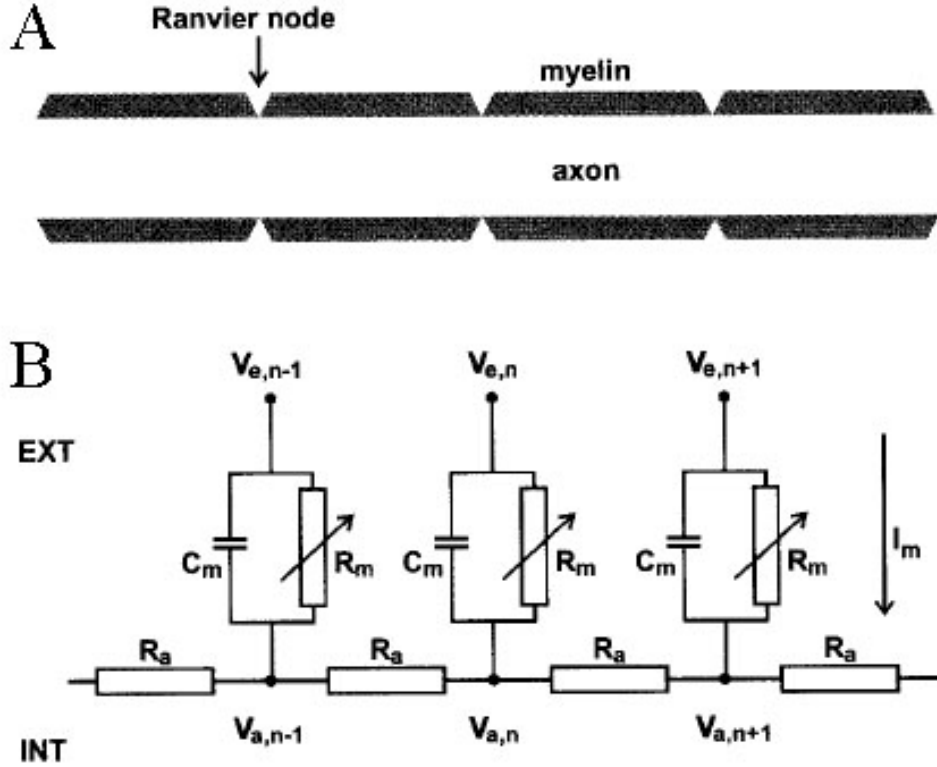


Figure 2.1: Schematic drawings of electrical cable model (A) and myelinated nerve fibre (B). (from [Leanne Chan 2009], originally adopted from [Holsheimer 2003])

Ranck [Ranck 1975] observed that the threshold stimulus of nerve fibre excitation is smallest in the vicinity of a cathode and rises with increasing distance. This observation was explained by the theoretical approach of the activating function. The node closest to the cathode will be excited first when the stimulation current is sufficiently high. As the field potential gradients on both sides of this node get steeper (the field potential gradient near the stimulation site is the steepest),  $AF$  will rise and the stimulus needed for excitation will be reduced. The same situation (obtaining steeper field potential gradient) also occurs when the nerve fibre gets closer to the cathode.

### 2.3 ELECTRIC FIELDS IN VOLUME CONDUCTORS

The retina to be stimulated is in all possibilities surrounded by an extracellular fluid with relatively high conductivity (0.5 to 1 S/m). The electrodes used for electric stimulation are always placed in this “volume conductor” and it is essential to understand how the

currents and the electric fields are distributed. The calculation of current density and electric fields can be convenient in simple cases such as a homogeneous<sup>2</sup> and isotropic<sup>3</sup> medium.

### 2.3.1 Quasi-static formulation

The electric fields generated by an electrode located in a volume conductor can be calculated by solving Maxwell equations. A simplified set of equations known as the quasi-static formulation can be used owing to the fact that the stimulus pulse frequencies are generally under 10 kHz [Plonsey and Heppner 1967]:

Conservation of charge:

$$\nabla \cdot \mathbf{J} = 0 \quad (2.2)$$

Gauss law:

$$\nabla \cdot \mathbf{E} = \frac{\rho}{\epsilon} \quad (2.3)$$

Ohm's law:

$$\mathbf{J} = \sigma \mathbf{E} \quad (2.4)$$

Electric field:

$$\mathbf{E} = -\nabla \phi \quad (2.5)$$

where  $\mathbf{E}$  is the electric field (V/m) defined as gradient of the scalar potential  $\phi$ ;  $\mathbf{J}$  is the current density (defined as the current crossing a given surface, in  $A/m^2$ );  $\sigma$  is the conductivity (inverse of resistivity), in  $S/m$ ;  $\rho$  is the charge density, in  $C/m^3$ ;  $\epsilon$  is the permittivity of the medium; and  $\nabla \cdot \mathbf{A}$  is the divergence of vector  $\mathbf{A}$ .

### 2.3.2 Potential from a monopolar disc

In this dissertation, studies were conducted on disc stimulation electrodes. Under the above mentioned quasi-static conditions, a disc electrode positioned in a semi-infinite homogeneous medium with a return electrode at infinity (monopolar configuration) can be modelled. In this case, the three-dimensional distribution of the extracellular potential,  $V_e$ , is given by [Wiley and Webster 1982]:

$$V_e(x, y, z) = \frac{2V_0}{\pi} \arcsin \left[ \frac{2\alpha}{\sqrt{(r+\alpha)^2 + d^2} + \sqrt{(r-\alpha)^2 + d^2}} \right] \quad (2.6)$$

<sup>2</sup> the same conductivity everywhere

<sup>3</sup> the same conductivity in all directions

where  $\alpha$  is the electrode diameter and

$$r = \sqrt{(x - x_{electrode})^2 + (y - y_{electrode})^2}$$

$$d = z - z_{electrode}$$

$$V_0 = I_{electrode} R_{tissue}$$

with  $x_{electrode}$ ,  $y_{electrode}$ ,  $z_{electrode}$  being the coordinates of the centre of the disc electrode,  $I_{electrode}$  the current injected by the electrode and  $R_{tissue}$  the resistive impedance of the retinal tissue (assuming a linear purely resistive electrode-retinal interface). The derivation is out of the scope of this dissertation.

### 2.3.3 Inhomogeneous volume conductors

In the retina, the volume conductor is clearly not homogeneous due to variation in the intracellular densities. A valid question at this stage is how do those different conductivities affect the potentials generated by the electrode? This can only be answered numerically by computer models that take into consideration these various compartments such as finite-differences, finite-elements, or boundary-elements methods. A simple solution, however, can be obtained in the case of a semi-infinite homogeneous volume conductor using the method of images. Consider two volume conductors with conductivities  $\sigma_1$  and  $\sigma_2$  separated by an infinite plane. A monopolar stimulating electrode is placed in region 1. Potential recordings are made in that same region. It can be shown that the inhomogeneous volume conductor can be replaced by a homogeneous volume by adding another current source located on the other side of the plane with an amplitude equal to [Nunez 1981]:

$$I' = \frac{\sigma_1 - \sigma_2}{\sigma_1 + \sigma_2} \cdot I \quad (2.7)$$

The mirror-image theory is only applicable in simple cases but can be useful to obtain approximations when the distance between the recording electrode and the surface of discontinuity is small, thereby approximating an infinite surface [Durand 2000].

## 2.4 STIMULUS CHARACTERISTICS AFFECTING RETINAL STIMULATION

The variations in stimulus specifications alters the stimulation of a neuron. Following is a brief discussion on the effects triggered by these variations with relevant results from literature. Many of these effects have been previously discussed [Leanne Chan 2009] and are re-visited here:

#### 2.4.1 *Cathodic and anodic stimulation*

There are different stimulation schemes, apart from cathodic and anodic excitation, namely cathodic block and anodic block. These are well known from experimental research [Ranck 1975]. In cathodic excitation, the cathodic current will propagate in each direction from the excitation node. The electric field pattern results in slight hyperpolarisation of the membrane on segments (virtual anodic) just lateral to the area of depolarisation, but under typical circumstances these hyperpolarised segments do not stop action potential propagation. Cathodic block occurs when the virtual anodic hyperpolarisations are sufficient to compensate for the depolarisation induced by the action potential in between the nodes. Hence, action potential propagation will be blocked by these *virtual anodic*<sup>4</sup> nodes. Anodic excitation occurs when the anodic current is so large that the *virtual cathodic* depolarisation on either side of the hyperpolarisation will generate an action potential. These action potentials will propagate in opposite directions, as in cathodic stimulation. Finally, anodic block occurs when an anodic current is applied to a fibre propagating an action potential. A few nodes closest to the anode are hyperpolarised and will block the propagation when the anodic current is large enough.

It has been reported that the anodic excitation is 3-7 times their cathodic excitation threshold [Rijkhoff *et al.* 1994]. The cathodic block threshold is more than 8 times the cathodic excitation threshold [Ranck 1975]. The high thresholds for both anodic excitation and anodic block as compared to cathodic excitation have also been reported elsewhere [Wee *et al.* 2000, Wee 2001]. Hence, cathodic excitation is commonly used in neurostimulation due to its relatively low excitation threshold.

#### 2.4.2 *Monopolar and dipolar configuration*

The injection of current solicits the use of two electrodes, an active electrode and a return electrode. These can be placed in a monopolar configuration where the return electrode is far away and the current radiates outwards from the active electrode, or in a dipolar configuration where the return electrode is relatively close to the active electrode and current is steered towards the return electrode. In monopolar configuration, the current injected by the active electrode is distributed more or less evenly in all directions. The threshold current is reduced when the return electrode gets closer to the active electrode

---

<sup>4</sup> Virtual anode and virtual cathode are the side effects of cathodic and anodic stimulation respectively.

(dipolar configuration) and when the nerve fibre axis is parallel to the active-return electrode axis, and has been shown empirically in Figure 2.2.

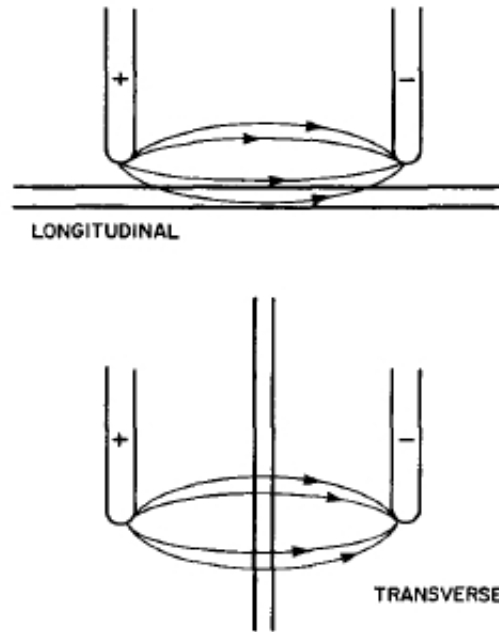


Figure 2.2: Dipolar stimulation of the nerve fibre. More current is needed if the electrodes have a transverse orientation to the fibres versus a longitudinal orientation. (adapted from [Ranck 1975]).

#### 2.4.3 Current-controlled versus voltage-controlled stimulation

Previously, clinical implantable neurostimulation devices have generally been voltage-controlled, such as cardiac pacemakers. In recent times, current-controlled stimulation is commonly used. Current-control means that the output current  $I$  is kept constant, thus creating a rectangular current pulse (current source). The related voltage  $V$  is automatically adjusted based on the load impedance  $Z$ . Current-controlled stimulation is more regularly used than voltage-controlled stimulation because of the following reasons: (1) the kinetics of charge redistribution during change of phase at the interface is better controlled. It is essential for stimulation pulse to be charge-balanced so as to minimise net charges left at the interface, failing which it may increase the electrode potential to the point where harmful quantities of gaseous oxygen or hydrogen are produced (bubbling). (2) a constant electric field is ensured. Excitability of the tissue depends on the electric field applied. The electric field applied is directly related to the injected current. The pulse amplitude needed to activate neural activities with current-controlled pulses is not influenced by the value of  $Z$  which allows the voltage excursion

to stay within the compliance voltage of the stimulator. However, in voltage-controlled stimulation, the voltage needed is influenced by the value of  $Z$  and may thus vary over time. The advantage of using a voltage-controlled stimulation is that it offers high power efficiency, at the expense of safety due to lack of control over the injected charge into the tissue (described above) [Simpson and Ghovanloo 2007]. Voltage-controlled stimulation is beneficial provided that a blocking capacitor is used in the circuit, a compromise on space efficiency. Recently, a voltage-controlled stimulation for safe neural stimulation has been studied [Schuettler *et al.* 2008].

#### 2.4.4 *Strength-duration relationship*

It has been known for a long time that it is the time change in the applied current and not the continuous application of the external stimulus that excites a neuron. Direct current DC cannot excite and even small amplitudes can cause significant tissue damage. It also has been observed experimentally that the relationship between the pulse width and the amplitude suggests that it is the total charge injected that contributes to the neural stimulation.

This relationship between the amplitude and the width of a pulse required to bring an excitable tissue to threshold is known as strength-duration relationship. Strength-duration relationship measures the sensitivity of neuronal elements to stimulation.

When the duration of the stimulus duration  $d$  increases, the stimulus amplitude  $I$  required to elicit a response becomes less. This inverse, non-linear relationship is shown in Figure 2.3 A. The shape of a strength-duration curve is generally characterised by two parameters, the rheobase current  $b$  (mA) and the time constant  $c$  (ms). This curve is described by the LaPicque's equation [Lapicque 1907]:

$$I = b \cdot \left(1 + \frac{c}{d}\right) \quad (2.8)$$

The rheobase current  $b$ , the asymptote of the strength-duration curve, is the minimum stimulus amplitude required to elicit a response with an infinitely long stimulation duration (a theoretical concept). According to this equation,  $c = d$  when  $I = 2b$ , which defines the chronaxie value  $c$  as the pulse duration at twice the rheobase current. Rheobase current is defined by the coupling between the tissue and the stimulating electrode. By increasing the distance from the stimulating electrode to the tissue will increase the rheobase current and therefore increase the necessary stimulus amplitude



for eliciting a response at all pulse durations. Chronaxie is defined by the membrane properties as:

$$\tau_m = R_m \cdot C_m \quad (2.9)$$

with  $R_m$  being the membrane resistance and  $C_m$  being the membrane capacitance of the target neuron. With both sides of equation 2.8 are multiplied by  $d$ , the Weiss' Law [Weiss 1901] is obtained,

$$I \cdot d = b \cdot (d + c) \quad (2.10)$$

with  $I \cdot d$  being the threshold charge ( $\mu\text{C}$ ) required for stimulation. This linear charge duration curve is also shown in Figure 2.3 A. This curve shows that the charged needed for a threshold pulse rises when  $d$  increases. The electrical energy required  $U$  equals to the amount of charge  $I \cdot d$  multiplied by the electrical potential  $I \cdot r$ , where  $r$  represents the tissue resistance. Solving equations 2.8 and 2.10 for the electrical energy and demonstrating in 2.3 B indicates that the most electrically efficient stimulation duration  $d$  equal to the chronaxie  $c$  of the neuron being activated.

Another way to define the relationship between stimulus strength and excitation is through amplitude-intensity function, as shown in Figure 2.4. This is typically used where the response is an evoked potential and generates a plot of the stimulus strength at fixed pulse duration against the amplitude of the evoked response. It helps in determination of true threshold by simply extrapolating the curve to intersect the x-axis. Amplitude-intensity functions are useful because neural prostheses typically operate above threshold to provide a range of sensation or activation.

#### 2.4.5 Selective stimulation of retinal cells

Electrical current pulses are used to activate neurons and replace lost visual functions due to retinal diseases. When a neural system is stimulated, different cells respond in different ways. The duration of the current pulse can be manipulated to target specific neurons. Short current pulses have been demonstrated to target retinal ganglion cells, the neurons closest to the electrode in epiretinal approach [Greenberg 1998, Fried *et al.* 2006, Sekirnjak *et al.* 2006] while long current pulses target bipolar cells.

## 2.5 SAFE STIMULATION OF NEURAL TISSUE

A system for neural stimulation if improperly designed can cause damage to the tissue or to the electrode itself. For any neural stimulation system to be successful, it must elicit

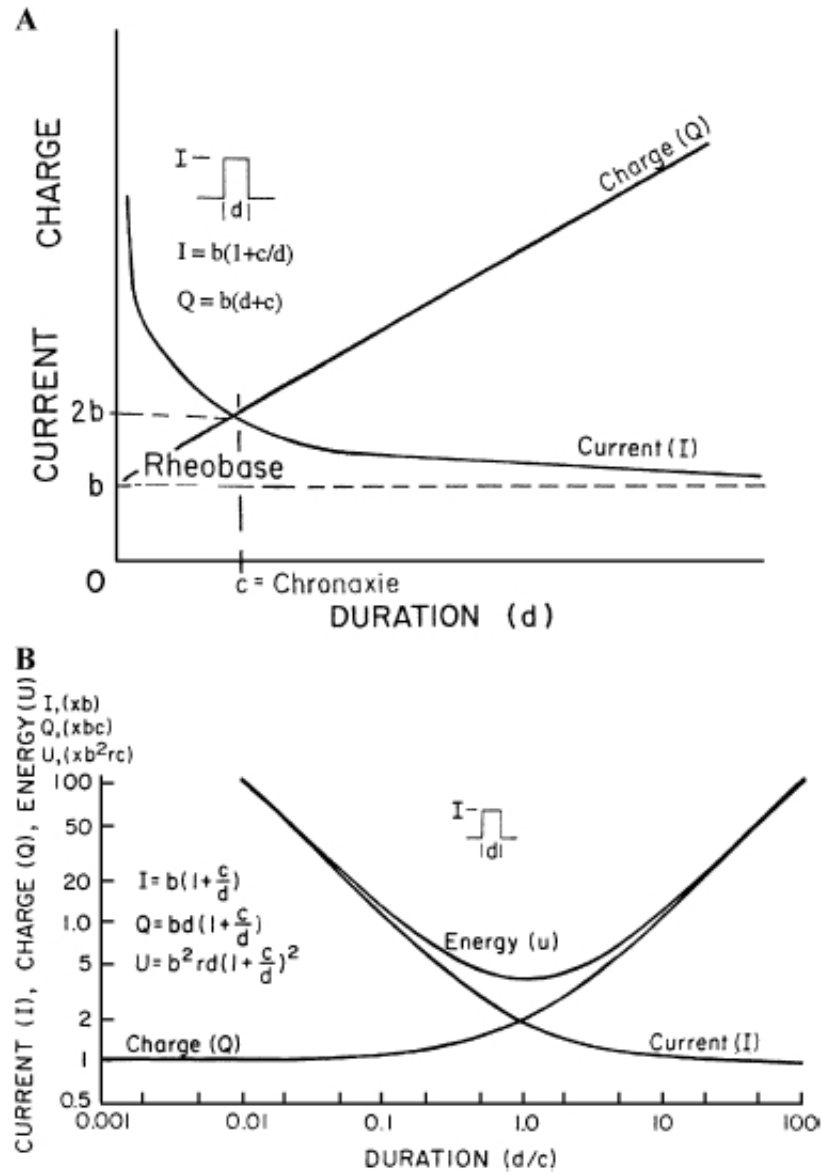


Figure 2.3: Strength-duration curve for current ( $I$ ), charge-duration curve for charge ( $Q$ ) and energy-duration curve for energy ( $U$ ) are plotted in (A) linear and (B) logarithmic scales. (from [Geddes 2004]).

the required neuronal excitation without causing any damage to the biological system. Electrode shape, size and material along with stimulus pulse parameters need to be judiciously chosen to meet the requirements of the system. A representative description of the extensive work carried out in defining the role of different parameters determining the safety limit of the tissue and electrode is given in this section.

### 2.5.1 Mechanism

There are several mechanisms that may cause neural injury and can be broadly categorised into two main classes:

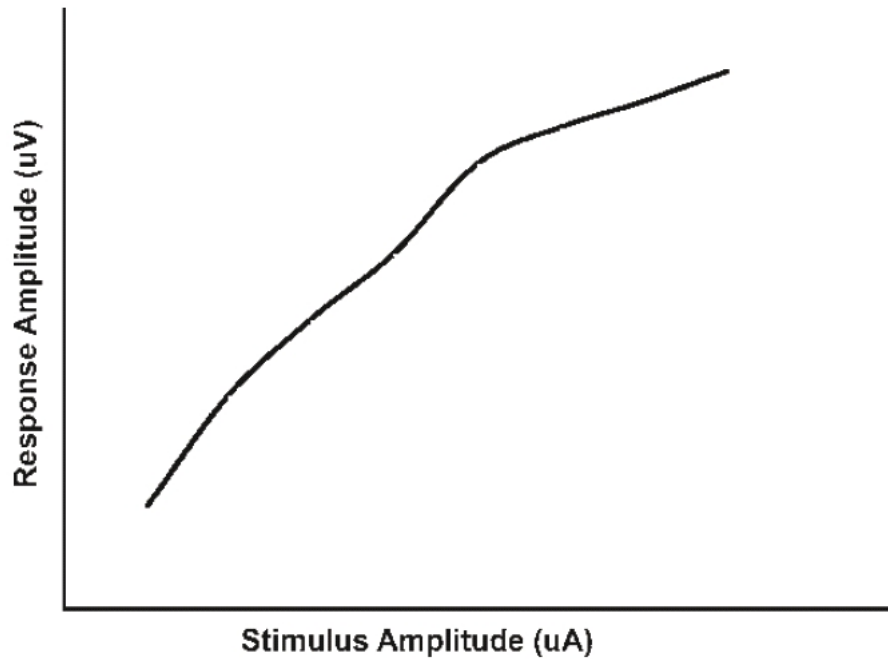


Figure 2.4: Representative graph illustrating the gradual increase in response amplitude as the stimulus strength is increased. The amplitude of response is usually measured in microvolts (mV) while the applied stimulus amplitude is usually in microamps ( $\mu\text{A}$ ). (from Chapter 6 of [Dagnelie 2011])

1. The electrochemical processes through which the stimulus current is injected into the target tissue. Damage is induced due to formation of toxic electrochemical reaction products during stimulation at a rate greater than what can be tolerated by the physiological system. The discussion of these effects is beyond the scope of this dissertation<sup>5</sup>.
2. A second mechanism of neural injury is associated with the flow of current through the target tissue [McCreery 2004]. This involves the metabolic stresses induced on the tissue causing a transient or permanent elevation of neurotransmitter release (excitotoxic effect). It may also include large depolarizations and hyperpolarisations induced by the voltage gradient (membrane electroporation). This second mechanism is dependent on many factors and is complex to understand.

### 2.5.2 Parameters for safe stimulation

A well known principal in neural stimulation is to achieve charge balanced stimulation. As mentioned earlier, charge-balancing ensures that there is no net accumulation of charge, but does not guarantee safety for all kind of waveforms (e. g. monophasic pulse

<sup>5</sup> The reader is encouraged to refer to a review article on related topics [Merrill *et al.* 2005].

with a blocking capacitor). Conventionally, safety limits for neural stimulation have been divided into two broad categories:

1. Neural damage limits - ability of the biological tissue to withstand electric current without any degradation
2. Electrochemical limits - ability of the electrode to store or dissipate electric charge without exceeding the electrolysis limit, outside of which formation of harmful products start

While neural injury limits are defined in terms of both charge density and charge per phase, electrochemical limits are defined in terms of charge density only.

Charge density is simply the total charge per unit area of electrode and determines the magnitude of the depolarisation or hyperpolarisation induced in the neurons and axons close to the electrode. Charge per phase is the amount of charge injected during each phase of the stimulus pulse and determines the distance over which the applied stimulation can activate the neurons, *i. e.* the number of neurons activated. McCreery *et al.* [McCreery *et al.* 1990] have shown that charge density and charge per phase act synergistically to determine the safe or unsafe levels of stimulation. They showed that neural damage is induced with low charge per phase but high charge density, as is often the case for microelectrodes. Based on these data, Shannon *et al.* [Shannon 1992] developed an empirical relationship delineating the boundary between safe and unsafe charge injection for different charge and charge density levels:

$$\log(D) = k - \log(Q) \quad (2.11)$$

where,  $D$  is the charge density in  $mC/cm^2/phase$  and  $Q$  is the charge per phase in  $mC/phase$ . The equation describes a family of lines for different values of  $k$ .

Along with charge density and charge per phase, other stimulus parameters such as frequency of stimulation, duration, etc. play an important role in determining the presence or absence of neural damage. McCreery *et al.* [McCreery *et al.* 1995] demonstrated the effect of stimulus frequency as a parameter in causing injury during peripheral nerve stimulation. Their study showed that continuous stimulation of the cat sciatic nerve for 8 hours over 3 days causes the myelin sheath to collapse into the axonal space leading to early axonal degeneration. The threshold of neural injury decreased with increasing stimulus pulse frequency.

### 2.5.3 *Induced retinal injury by stimulation*

In spite of the large scale studies on developing novel retinal implants and understanding response of the visual system to artificial stimuli, only a few studies so far have been dedicated towards understanding the consequences of long-term stimulation. Güven *et al.* [Güven *et al.* 2005] carried out chronic stimulation studies in dogs and found that the retina is able to tolerate chronic stimulation at  $0.1 \text{ mC/cm}^2$  without any histological detectable damage or change in the electroretinograms (ERGs). Another study investigated chronic stimulation effects through suprachoroidal-transretinal stimulation [Nakauchi *et al.* 2007]. The results of the study showed that threshold for safe charge increased logarithmically or almost linearly with increasing stimulus duration but the threshold for safe current decreased logarithmically with increasing stimulus duration. There was severe damage in the inner layers when the applied current exceeded this threshold. Colodetti *et al.* [Colodetti *et al.* 2007] found that the retina is sensitive to pressure exerted by the electrode. They studied the type of damage due to pressure exerted by the electrode with and without accompanying high charge stimulation in the rodent retina. Although the type of damage exhibited in both cases was roughly similar, the extent of damaged area was significantly larger in the case of accompanying high charge stimulation. In the race to move on to the next generation high resolution retinal prostheses, it is imperative to study the possible consequences of high level stimulation on both the retina and associated cortical structures. The groups led by Palanker [Butterwick *et al.* 2007] and Jensen (Chapter 12 of [Dagnelie 2011]) have made commendable progress in these areas recently.

## 2.6 DIRECT AND INDIRECT STIMULATION

In order to determine a reliable stimulation protocol, it is necessary to establish the fidelity of RGC activation by direct and indirect mechanisms. Several groups have targeted deeper retinal neurons (bipolar cells and photoreceptors) for epiretinal stimulation, which activates ganglion cells through the retinal neural network and thus stimulates them indirectly [Jensen and Rizzo 2007]. Such stimulation attempts use much larger electrodes ( $125\text{--}500 \mu\text{m}$ ) and/or long-duration stimulation pulses (1 ms), and result in multiple evoked spikes at long latencies (10 ms). With these stimulation configurations, spike thresholds are typically much higher than the direct activation values reported in literature [Jensen *et al.* 2003, Suzuki *et al.* 2004, Güven *et al.* 2005, Jensen and Rizzo 2007, Ye and Goo 2007]. There are published reports of epiretinal

stimulation that demonstrate direct activation of ganglion cells by using small electrodes and short pulses [Kuras *et al.* 2004, Fried *et al.* 2004, Sekirnjak *et al.* 2007]. There is a unique study on subretinal stimulation [Tsai *et al.* 2009a] indicating that direct activation is a more robust mechanism to stimulate RGCs. In the simulation framework presented in this dissertation, a direct activation of RGC is considered due to its established potency.

## 2.7 MODELLING RETINAL STIMULATION

A detailed literature review on strategies for modelling various aspects related to retinal stimulation has already been provided in Chapter 1. The methodologies that concern the concepts discussed in this chapter are re-visited here.

There have been many modelling strategies [Greenberg *et al.* 1999, Resatz and Rattay 2004, Schiefer and Grill 2006] supported by experimental studies [Sekirnjak *et al.* 2008, Fried *et al.* 2009, Behrend *et al.* 2009] in order to understand the excitation of a RGC by retinal stimulation; for instance, knowledge of RGC excitation thresholds, exact location of the originating action potential in the RGC, dependence on nature of stimulus pulses used, etc. Cottaris and Elfar [Cottaris and Elfar 2005] developed a sophisticated retina model by integrating the activating function along with all major retinal cell types and the corresponding network connections to characterise spatiotemporal activation within the retina. Effects of monopolar or dipolar stimulation schemes over threshold currents during epiretinal stimulation was studied by Ahuja *et al.* [Ahuja *et al.* 2008]. The differential epiretinal stimulation of ON and OFF RGCs during retinal stimulation with sinusoidal currents by incorporating the electrophysiological properties of both RGC types was investigated by Kameneva *et al.* [Kameneva *et al.* 2010].

Modelling studies in relation to subretinal stimulation were limited to the teams of Rattay and Stett. Resatz and Rattay [Resatz and Rattay 2003] used different electrode geometries with a finite element representative models of two bipolar and a single ganglion cell connected with each other. The activation function was based on models based on compartmental cable equations as seen earlier in the chapter. The main findings indicated that disc electrodes have smaller threshold currents than spherical ones; and long rectangular electrodes parallel to the axons at the retinal surface seemed to be good candidates for local selective stimulation. On the other hand, Gerhardt *et al.* [Gerhardt *et al.* 2010] used a computational method with segmented cable model

for bipolar cells and determined that dipolar electrode scheme is a better approach compared to the monopolar during simultaneous stimulation at multiple retinal sites.

## 2.8 SUMMARY

The concepts and the phenomenon relevant to electric stimulation of neural tissue presented in this chapter provides basis for a simulation framework to study retinal prostheses. During the operation of a prosthesis, at the interface between the electrode and tissue, the shape of the waveform can influence the threshold for activation as well as the corrosion of the electrode and the tissue damage generated. The biological processes and behaviour of retinal neurons are specific and selective to the stimulation parameters used. A meticulous experimental protocol needs to be setup to determine all parameters affecting retinal stimulation which in turn can be used to construct an accurate model of a retinal prosthesis.





## DETERMINING RESISTIVITY PROFILE OF THE RETINA

---

### 3.1 INTRODUCTION

Neural tissue inhomogeneity is an important parameter affecting neural stimulation [Lee and Grill 2005, Miranda *et al.* 2007]. The vertebrate retina is a dense neural tissue composed of multiple layers each characterised by different cell types and densities [Rodieck 1973] rendering it electrically inhomogeneous. By constructing an electric model based on inhomogeneity, it is feasible to compute the electric field distribution in the retina and consequently predict parameters such as threshold and resolution of stimulation for a safe and efficient retinal prosthesis. In order to construct a realistic, passive electric model of a retina, it is necessary to measure layer resistivity locally and precisely.

The resistivity of the retinal layers has been measured for various applications until now such as local electroretinograms [Heynen and van Norren 1985] and current source density analysis [Karwoski and Xu 1999]. Researchers mainly used the four-terminal (tetrapolar) method to measure the resistivity profiles in the depth of the retina. Double-barrelled [Karwoski and Xu 1999] and concentric [Heynen and van Norren 1985] glass micropipettes have been employed as the pick-up electrodes previously. Tetrapolar measurements require a complicated setup due to additional electronics (such as front-end amplifier, current injection electrodes, etc.) and retina sealing issues (in ex vivo eyecup based experiments). These experimental setups operated in constant current injection mode creating an approximately constant current density in the measured retinal area [Ogden and Ito 1971, Karwoski *et al.* 1996]. During measurements, the rigid micropipettes cause a local damage to the retina allowing the perfusion solution to flow into the cleft. This could result in a local redistribution of current around the inserted micropipette that could lead to a change in measured voltage drop. This would result in an inaccurate resistivity measurement due to an increase in the current flow through the cleft leading to a higher voltage drop. In this situation, a constant current supposition results in an artificial increase in measured resistivity. Furthermore, the frequency used in previous experiments was not based on knowledge of the entire impedance spectrum.

Neglecting the practical bandwidth might lead to interference of other parameters (for e. g., interface and parasitic components) on the measured signal [Linderholm 2006]. Lesser reproducibility of glass micropipettes may lead to variability in measurements (a relatively large range of 12-16  $\mu\text{m}$  for electrode spacing was presented by Xu and Karwoski [Xu and Karwoski 1994]).

In this chapter, an alternative and direct approach to measure local resistivities in the various layers of an isolated retina is presented. The approach uses a thin, flexible microfabricated probe of two electrodes to record impedance by an easy to setup bipolar impedance spectroscopy technique. Bipolar measurement is more suitable if one wants to measure a change at a specific position in an otherwise homogeneous sample (Pg. 140 of [Linderholm 2006]). Considering each retinal layer to be homogeneous, the changes in resistivity occurring at various layer interfaces can be well detected by bipolar measurements. Our electrodes with close spacing allow high resolution resistivity profiling in relatively thin isolated rat and chick retina samples.

### 3.2 MATERIALS AND METHODS

#### 3.2.1 *Animals*

Wistar (*Rattus norvegicus*) rats (Charles River or Janvier, France) in their postnatal period between 14 and 16 days and Lohmann race chicks (Animalco AG, Switzerland) in their embryonic stages of 12 and 18 days (E12/E18) were employed animal models in this study.

#### 3.2.2 *Electrode design and fabrication*

Rectangular electrodes with rounded corners were used to reduce fringing effects. The dimensions and design of the microprobe used in this study is presented in Figure 3.1.

The rectangular electrodes are spaced 10  $\mu\text{m}$  apart. The spacing between electrodes is based on a compromise between a localised measurement (high resolution) and maximum current penetration in the retina (sensitivity). Average retinal thickness for rat is 150  $\mu\text{m}$  [Thomas *et al.* 2006] and chicken is 175  $\mu\text{m}$  [Huang *et al.* 1998]. High resolution measurements are required to probe the different layers within the rat and embryonic chick retinas. An electrode spacing of 10  $\mu\text{m}$  is sufficient to obtain an elaborate resistivity profile of the retina addressing typical retinal cell sizes ranging from 10  $\mu\text{m}$ . Both, an analytical (Pg. 203 of [Linderholm 2006]) and finite element method based computation (Comsol Multiphysics 4.0a) of electric field penetration depth in saline ( $\rho = 1.5 \Omega \cdot \text{m}$ )

for a  $10\mu\text{m}$  spacing between electrodes revealed an approximate depth of  $8.3\mu\text{m}$  (see Appendix B). The large enough penetration depth ensures probing retinal cells making an electrode spacing of  $10\mu\text{m}$  appropriate for the application under consideration.

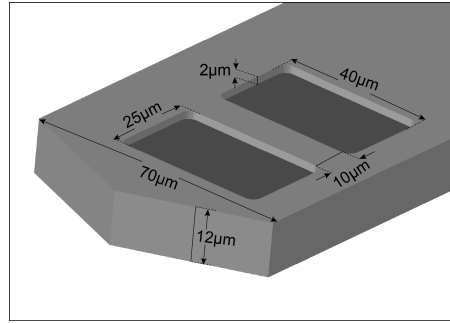


Figure 3.1: A schematic of the electrodes on a flexible substrate with dimensions to scale.

The polyimide-based flexible microprobe  $10\text{--}12\mu\text{m}$  thick consisted of two recessed Platinum electrodes ( $40\mu\text{m}\times 25\mu\text{m}$ ), separated by  $10\mu\text{m}$  was fabricated based on an established process [Metz *et al.* 2004] - refer Appendix A. A photograph of the complete microprobe assembled on a plastic base for easy manipulation is shown in Figure 3.2.

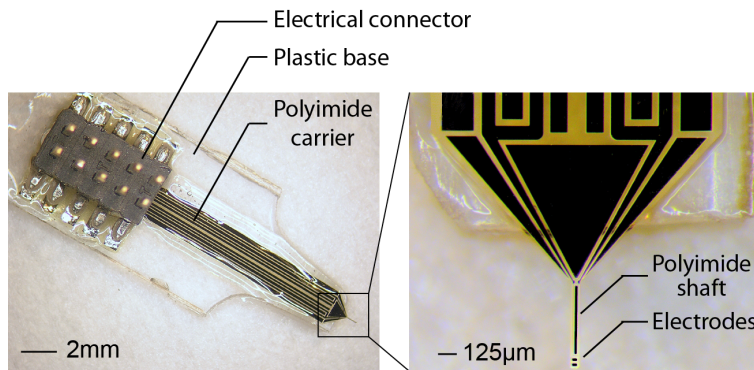


Figure 3.2: Photograph of the device used. (Left) The plastic base is used to facilitate attachment to a micromanipulator (not shown) for assisting in precise insertion of the electrodes into the retina. (Right) The narrow polyimide shaft consisting of the electrodes is the part that is inserted in the retina preparation.

### 3.2.3 Measurement method and modelling

The choice of measurement method depends on the degree of sample homogeneity and the measurement hardware (i.e. whether the measurement hardware is better at detecting absolute or relative changes) [Linderholm 2006]. By virtue of the similarity of

cells within a retinal layer, we can consider each layer to be homogeneous. Owing to their high sensitivity to small changes near the electrodes, bipolar measurements record the resistivity of the layer. Bipolar impedance measurement method is used in this study as it requires a simpler experimental setup compared to multielectrode schemes.

In order to measure a resistivity profile of the retina, it is essential to extract the resistance in each layer. For the extraction of the tissue resistance from the measured impedance, one of the approaches is to consider the impedance of an electrode-retina configuration represented by an equivalent passive electrical circuit model as shown in Figure 3.3. The model consists of contributions due to the electrodes-electrolyte interface and the complex tissue impedance in series with it. The constant phase element (CPE),  $Z_{CPE\_E}$  addresses the non-ideal capacitive behaviour observed in solid metal electrodes [McAdams *et al.* 1995]. The complex tissue impedance is represented by a Cole model [Cole 1940, Grimnes and Martinsen 2008] of a resistance ( $R_{tissue}$ ) in parallel with a series combination of an intracellular resistance ( $R_{intra}$ ) and a CPE ( $Z_{CPE\_T}$ ). The model is suitable for AC analysis alone.

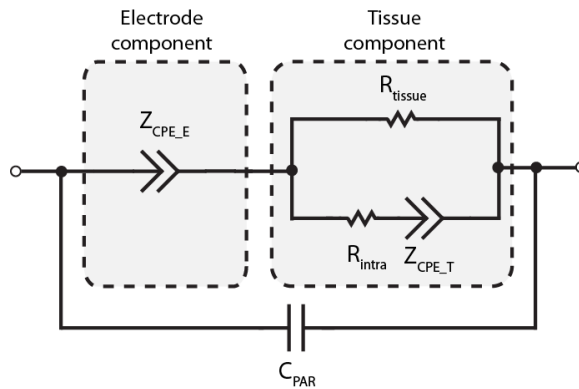


Figure 3.3: An electrical equivalent representing the electrode and tissue components based on Cole model for measured tissue impedance.  $Z_{CPE\_E}$  is the CPE representation of the electrodes.  $R_{intra}$  is the effective resistance offered by the intracellular fluid.  $Z_{CPE\_T}$  is the CPE part of the tissue impedance.  $R_{tissue}$  is the resistive part of the tissue impedance.  $C_{PAR}$  is the parasitic capacitance between the electrodes through the polyimide passivation.

A typical impedance/phase spectrum along with its model fit at a depth in the retinal tissue is presented in Figure 3.4. Tissue resistance can be extracted from experimental data involving impedance/phase spectra by using fitting algorithms applied on the equivalent circuit model. Alternatively, tissue resistance has been extracted using the peak resistance frequency (PRF) method in brain tissue impedance measurements [Mercanzini *et al.* 2009].

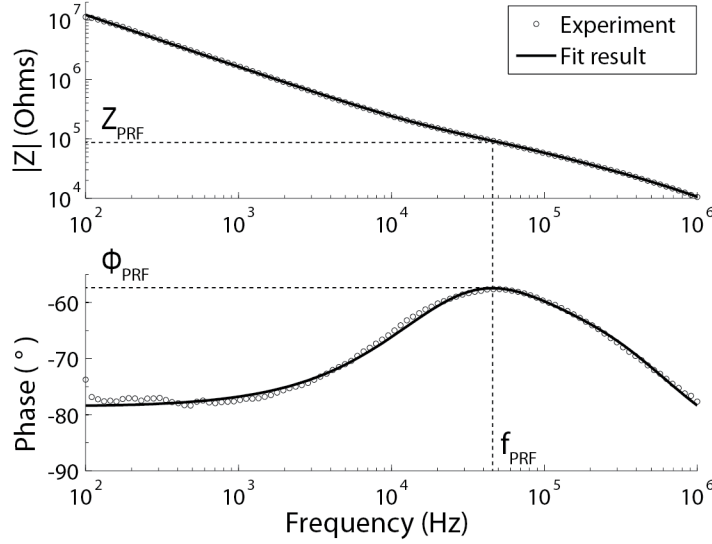


Figure 3.4: Bode plot at a certain depth in the retina and the corresponding fit using the electrical equivalent. The tissue resistance is identified at the peak resistance frequency (PRF), the point at which the phase is closest to  $0^\circ$ .

The PRF method involves finding the frequency at which the measured impedance is least capacitive (or closest to resistive behaviour). Below this frequency, electrode CPE increases the measured impedance; above this frequency, the tissue CPE and  $C_{PAR}$  each separately or jointly decrease the measured impedance. A single choice of frequency to determine tissue resistance is usually defined by the cut-off frequency calculated from the electrode capacitance and tissue resistance itself. The PRF approach helps to define the best measurement frequency for identifying tissue resistance from a typical tissue impedance spectrum. Although, the tissue resistance can be extracted using fitting methods on the electrical equivalent (Figure 3.3), its reliability is limited to uncertainties in the various fitting parameters ( $Z_{CPE\_E}$ ,  $Z_{CPE\_T}$ ,  $R_{tissue}$ ,  $C_{PAR}$ ).

The tissue resistance is extracted from the impedance magnitude at the PRF. At three different depths in the retina, magnitudes at PRFs ( $Z_{PRF}$ ) associated with raw experimental data compared within 10% of their corresponding fitted tissue resistance ( $R_{tissue}$ ) values. We do not observe tissue relaxation as a result of the dominating electrode interface impedance (owing to the small electrode size). In view of possible misinterpretation (curbed tissue relaxation) and algorithmic errors in the fitting method using equivalent circuits, it was proposed to apply the PRF method to extract tissue resistance from impedance spectra recorded at different depths in the retina.

The resistivity ( $\rho$ ) at any depth in the retina can be determined from the measured tissue resistance ( $R$ ) using a simple direct relationship given by  $\rho = R/k$  [Zahn 2003], where  $k$  is the cell constant. The cell constant of the geometry used in this study was analytically calculated as  $232.75 \text{ cm}^{-1}$  according to the method described by Jacobs *et al.* [Jacobs *et al.* 1995]. A 3D finite element simulation revealed a cell constant value of  $232.2 \text{ cm}^{-1}$  indicating a good agreement with the analytical value (see Appendix B). The theoretical and simulated values will be used later to verify the proper functioning of fabricated electrodes. Conversion of measured advancement of electrode to percentage of retinal depth corrects the resistivity profiles for deviation of the microelectrodes from a plane perpendicular to the retina and addresses tissue shrinkage problems due to dehydration during sample preparation.

### 3.2.4 Measurement apparatus and protocol

#### *Experimental apparatus*

The experimental apparatus consisted of a three-axe Eppendorf micromanipulator 5171 used for positioning the microprobe with respect to the retina sample as shown in Figure 3.5. The micromanipulator enables a uniform advancement of the electrodes into the tissue leading to a reliable impedance measurement. The extracted retina slices from a rat or embryonic chick were placed on a 3-5 mm thick Agar (Sigma Aldrich, Switzerland) gel (1% in Ringer's solution) inside a plastic petri-dish. The dual purpose served by Agar gel as a base for the retina is – (i) an indication for the termination of impedance measurement (low resistance of Agar gel) and (ii) a protection cushion for the penetrating electrodes preventing them from breaking by coming in contact with the petri-dish base. The petri-dish is filled with Ringer's solution submerging the retina-gel structure. All complex impedance data were acquired using an Agilent 4294A (Agilent Technologies, USA) precision impedance analyser connected to a PC via a GPIB controller (National Instruments, USA). Signal frequency sweep was made from 100 Hz to 1 MHz for each impedance/phase spectrum, sufficiently covering the bandwidth of electrophysiological interest and ensuring the PRF is easily identified and consequently the tissue resistance. Signal amplitude of 25 mV without dc offset was used as it was a good compromise between generated noise in the recorded signal and preventing possible extreme electric field effects. Moreover, it was supposed that applied signal was small enough to avoid any significant activation of retinal neurons and associated resistivity changes during measurements.

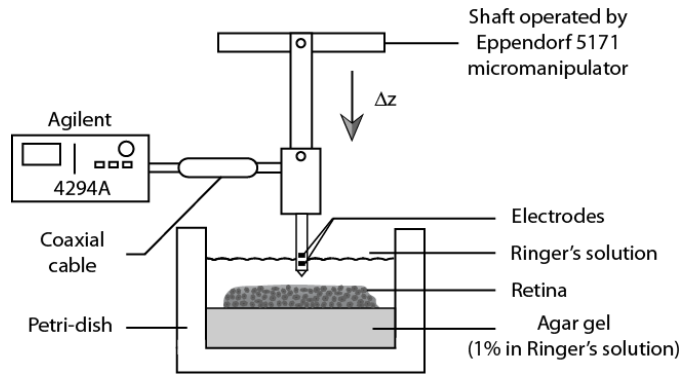


Figure 3.5: Experimental apparatus consisted of (i) an Eppendorf 5171 micromanipulator that displaces the microprobe vertically (z-axis) in steps of  $10\mu\text{m}$ , (ii) an Agilent 4294A impedance analyser for recording impedance/phase spectra for each probed retinal depth. (iii) a plastic petri-dish containing the isolated retinal slice placed on a block of Agar gel (1% in Ringer's solution) submerged in Ringer's solution.

#### *Electrode cleaning and validation*

Before every new experiment, the electrodes were either cleaned with 2% mild soap solution (rat trials) or chemically treated with the RCA-1 [Kern 1993] cleaning process (chick embryo trials) for removing any organic contaminants. They were subsequently treated under a nitrogen gun to dry and blow away dust particles. The impedance spectrum of electrodes was obtained in standard Ringer's solution to validate their proper functioning.

#### *Slice preparation*

A common protocol for retinal slice extraction was followed for both wild-type juvenile rats and embryonic chicks. Eye balls were extracted from decapitated animals. Under low light conditions, the cornea, iris, and lens were removed from the eye ball followed by transection of the eyecup to float pieces of retina into a dish of Ringer's solution to obtain isolated retinal slices without the retinal pigment epithelium. The slices were then perfused in Ringer's solution continuously bubbled in 95%  $\text{O}_2$ /5%  $\text{CO}_2$  until it was placed on the Agar gel. The surface on the Agar gel was pre-treated with a solution of cellulose nitrate (0.14 mg/ml in methanol) and dried. This acted as an adhesion promoter for the retina to stay on the gel preventing it from being washed away when in contact with the Ringer's solution. A few moments before the experiment was conducted, the retinal slice was taken out from the perfusion and was placed on the treated area of the gel with the retinal ganglion cell side facing upwards and the

photoreceptor cells in contact with the gel. The Ringer's solution was then added to fill the petri-dish to a certain level submerging the retina-gel structure.

#### *Impedance measurement*

In every trial, at least three impedance measurements at different depths (every  $10\mu\text{m}$ ) in the bath (Ringer's solution) before entering the retina were performed. The first considerable change in impedance magnitude at PRF indicated the entry into the retina. Visual control using a pair of binoculars confirmed this first electrode-retina contact. Subsequent impedance measurements at every  $10\mu\text{m}$  depth were recorded until an impedance value similar to the one observed in the bath was encountered. Each measurement was recorded with a wait time of 30 seconds for the signal to stabilise after the micromanipulator made the  $10\mu\text{m}$  vertical movement into the retina. This time was determined based on measurement of time taken for the impedance value to stabilise at a random depth in the retina (see Appendix B). Three more recordings at  $10\mu\text{m}$  intervals were made to ensure the electrodes contact with the Agar gel before terminating the experiment and retracting the electrodes to the initial position. The system was under ambient laboratory conditions of  $21^{\circ}\text{C}$  during the impedance measurements.

### 3.3 RESULTS

#### 3.3.1 *Electrode characterisation and PRF shift*

To be able to compute the resistivity from the measured tissue resistance at PRF, the cell constant needs to be experimentally determined. The cell constant of the bipolar electrodes used in this study was calculated using the impedance/phase spectrum of Ringer's solution of predetermined conductivity. The spectrum is as shown in Figure 3.6. Based on an average of such measurements with different batches of electrodes, an average experimental cell constant was found to be  $225\text{ cm}^{-1}$  (less than 5% error). This value is within 3.5% of the theoretical and simulated values of cell constant for the electrode configuration used in this study. The close agreement of the cell constant with previously calculated values validates the proper working of the electrodes for an experiment.



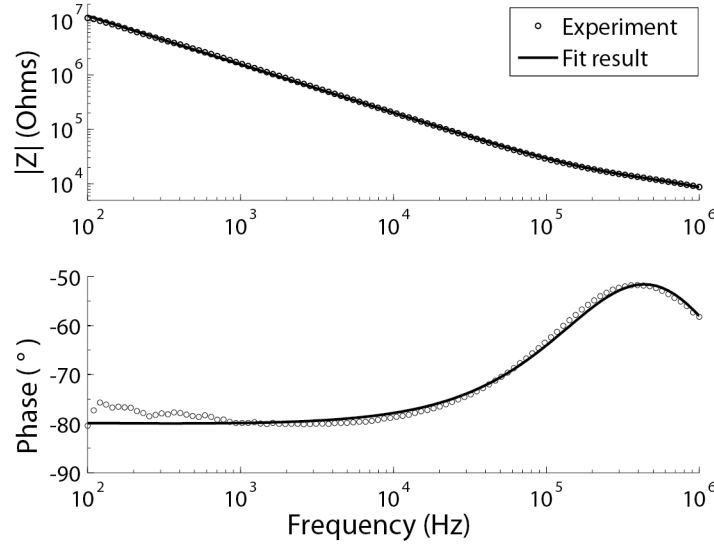


Figure 3.6: Bode plot in Ringer's solution and the corresponding fit using the electrical equivalent replacing the tissue component by a simple resistor representing the solution resistance. The solution resistance is extracted from the modified model fit. Knowing the resistivity of the medium, an experimental cell constant of  $225 \text{ cm}^{-1}$  was calculated. From fitting, the magnitude of  $Z_{CPE\_T}$  was found to be  $3.2 \times 10^{-10} \Omega^{\alpha-1} \cdot F^{\alpha}$ , where  $\alpha=0.85$ .

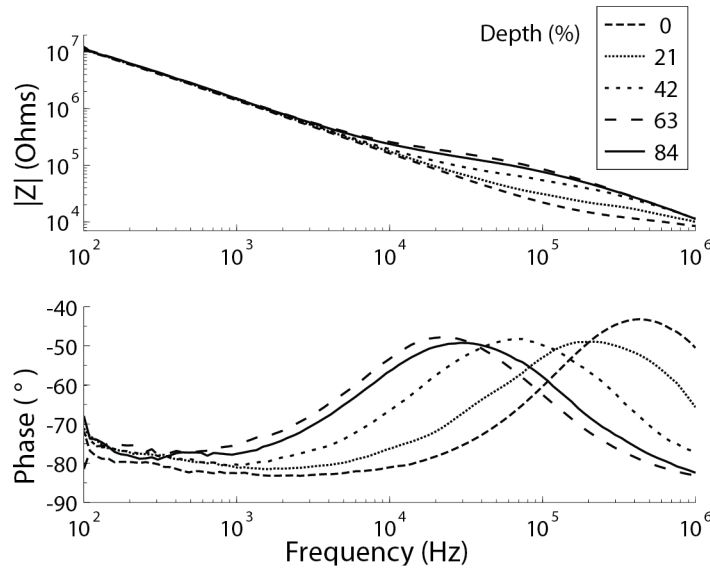


Figure 3.7: PRF shift observed at various depths in a rat retina. As the PRF shifts from the right to left, the impedance increases with increasing depth into the retina (from the retinal ganglion cell towards photoreceptor layer). Depth is normalised to 100% retinal depth. A 10% retinal depth corresponded to an approximate microprobe displacement of  $14 \mu\text{m}$  in the retina.

Following the functional validation of electrodes, they can be employed for impedance measurements at different depths in the retina of the chosen animal model. During these experiments, a shift in the PRF was observed at each depth in the retina as presented in Figure 3.7. Starting from the retinal ganglion cell layer as we go deeper

into retina towards the photoreceptor layer, the PRF moved to lower frequencies and the impedance magnitude rose from a low to a high value between 80-85% of retinal depth spanned during the experiment. With reference to Figure 3.7, a 10% retinal depth corresponded to an approximate microprobe displacement of  $14\mu\text{m}$  in the rat retina.

### 3.3.2 Resistivity profiling in rat and embryonic chick retinas

Impedance spectroscopic measurements at different depths of isolated retinal slices from three rat (14-16 days postnatal) and five chick (three E18 and two E12 embryos) samples were performed. Resistivity values were calculated from the extracted impedance value at the PRF using the direct relation between both for each depth in the retina sample. A resistivity depth of 100% was denoted as the last measurement in the retina before an identical value of resistivity obtained in Ringer's solution is reached (electrodes in Agar gel). Point zero represented the last measurement in the Ringer's solution before there is a significant change in the resistivity, i.e., an appreciable shift in the PRF is observed. Resistivity versus retinal depth profiles for both rats and embryonic chicks are presented in Figure 3.8a and Figure 3.8b respectively.

In both rat Figure 3.8a and embryonic chick Figure 3.8b measurements, an increasing resistivity-depth profile is observed rising gradually from the retinal ganglion cell layer towards the photoreceptor layer. At an approximate depth of 65%, the resistivity reaches a maximum value and then gradually decreases to attain a value obtained in Agar gel. There is a close interspecies resemblance in the studied resistivity profile shapes.

The maximum mean resistivity reached in rat retina samples is  $4.2 \pm 0.9 \Omega \cdot \text{m}$  and for E12 chick is  $4.5 \pm 0.2 \Omega \cdot \text{m}$  occurring between 65-70% retinal depths. On the other hand, the maximum mean resistivity in E18 chick retina samples is  $7.9 \pm 0.6 \Omega \cdot \text{m}$  which is approximately double the value measured in rats and E12 chicks at the same retinal depth. In rat and E18 chick resistivity profile measurements, at around 80% depth into the retina, there is a definite dip in the resistivity profile gradually decreasing into a low value similar to a measurement in Ringer's solution.

The standard deviation (SD) of resistivity from the mean resistivity value at each depth was examined. For the embryonic chick resistivity profiles, it is determined that the SD is low in the Ringer's solution and the Agar gel. In contrast, the rat data demonstrates large SD in these two regions of the resistivity profile.

It is known that there is a PRF shift with a resistivity change in different retinal layers. A representation of the relationship between PRF and resistivity based on the

experiments on rat and embryonic chick retinal slices is depicted in Figure 3.8c and Figure 3.8d respectively. The log resistivity is linearly dependent on the log PRF for both the species. For embryonic chicks, owing to similarity in the data across various trials, it can be observed that there is a unique PRF for each resistivity. On the contrary, the three rat trials suggest multiple PRFs for each resistivity.

### 3.4 DISCUSSION

To the best of our knowledge, planar, bipolar microelectrodes on a flexible substrate were used for the first time in this study to measure resistivity-depth profiles in rat and embryonic chick retinas. We first demonstrated the functionality of the microfabricated device. The electrode cell constant extracted from the measured solution resistance in Ringer's solution compares well with the value obtained by equivalent circuit fitting. The resistivity values at different depths in the retina established by the PRF method are within 10% of the fitted values. This is a confirmation of the electrode interface impedance not interfering with the measurements. There was a close agreement between the experimental and the theoretical/simulated bipolar cell constant values. The experimental value of  $225 \text{ cm}^{-1}$  is low compared to the combined average of both theoretical and simulated value of  $232.5 \text{ cm}^{-1}$ . This low difference of 3.5% is within the experimental variations. Hence, the rounded corners of the electrodes instead of sharp perpendicular shapes may have contributed to reduction in fringing effects of electric field originating from the electrode edges. The resistivity-depth profiles, in both rat and embryonic chick experiments, indicate the inhomogeneous nature of the retina and the trend they follow are in accordance with the results obtained for various species in previous studies [Heynen and van Norren 1985, Karwoski and Xu 1999]. This confirms that our method is valid for retina resistivity profiling studies.

We found the maximum local resistivity occurred in all experiments between 65-70% retinal depths. This can be explained by greater retinal resistivity in regions like the inner nuclear layer (INL) where neurons are packed more tightly than the inner plexiform layer (IPL) [Ogden and Ito 1971]. Our observations are in close agreement with the local maxima occurring at retinal depths of ~80% in monkey (Heynen and van Norren 1985), ~75-80% in rat [Hagins *et al.* 1970] and ~70% in chicken [Ogden and Ito 1971]. The shape of the resistivity profile of the chick embryo was similar to that of the chicken [Ogden and Ito 1971] and the rat resembled mammalian species [Heynen and van Norren 1985] to a large extent. This was particularly true in the region

between the proximal retina and down to the junction of inner and outer photoreceptor segments. We observed an appreciable dip in the resistivity values from a retinal depth of 80% onwards until electrodes come in contact with the Agar gel. This decrease in resistivity in the photoreceptor layer was also found in previous studies using isolated slice models of avian [Ogden and Ito 1971] and rat [Hagins *et al.* 1970] retinas. The local decrease in resistivity might be caused by the relatively large interstitial spaces among the outer and inner receptor segments [Hagins *et al.* 1970]. Resistivity profiles are affected by the type of retinal preparation used (isolated retinal slices and eyecup preparations). For comparing profiles, the anatomical difference between an isolated slice and an eyecup preparation of retina needs to be considered owing to the absence of the retinal pigment epithelium. In an isolated slice preparation, considering that photoreceptors offer low resistance, the effective resistivity profiling is made between the inner and outer limiting membrane [Karwoski *et al.* 1985].

We observed higher resistivity values in E18 compared to E12 chicks. This can be attributed to the ongoing retinogenesis which terminates only at E18 [Doh *et al.* 2010]. Cell differentiation between E12 and E18 is accompanied by cell polarisation, laminar stratification and changes in cell numbers [Livesey and Cepko 2001, Doh *et al.* 2010] potentially explaining resistivity changes within the retina. Further exploration of this subject can be interesting for future studies.

The absolute resistivities found in this study are lower compared to previous findings in rats [Hagins *et al.* 1970] and chicken [Ogden and Ito 1971]. The values may be difficult to compare with former investigations as the measurements are influenced by various factors like the interracial difference, age difference, measurement technique, electrodes used, etc. A majority of previous studies used the tetrapolar method with a constant current injection. The local damage caused by the pick-up micropipettes in the retina may cause a local current increase due to inflow of the perfusion solution. This could lead to an increased voltage drop resulting in a false increase of measured resistivity. In addition, most of the studies were conducted in the low frequency region (ranging between 1 Hz and 100 Hz) with very small electrodes ( $\sim 2\text{--}20\text{ }\mu\text{m}$ ) [Heynen and van Norren 1985, Sieving and Steinberg 1987, Karwoski and Xu 1999]. Regardless of the method used, i. e. bipolar or tetrapolar, it is critical to observe the whole impedance spectrum to identify the practical measurement bandwidth (Linderholm 2006).

The maximum SDs from the mean resistivity at certain retinal depths in our study was found to be high. A large variability between trials was also observed in previous

studies of rat and chicken [Hagins *et al.* 1970, Ogden and Ito 1971] that were used for comparison to our findings. All measurement techniques until now including ours have the following inherent drawbacks that affect the resistivity-depth profiling of the retina – (i) the movement of the electrode relative to the tissue not being accurate due to chip-tissue slippages, (ii) pressure causing damage to the tissue (iii) damage to the tissue by electrodes causing a high-current shunting between them resulting in an erroneous measurement of resistivity in the retinal layers and (iv) unpredictability of resistivity values at the retinal layer boundaries. Apart from these factors, the location on the retinal slice where the electrodes penetrate is a significant reason for the variability in resistivity measurements. A solution, even though it contributes to the experimental complexity, may be to locally stain the retina as a visual aid for electrodes insertion to produce reproducible resistivity profiles of the retina.

The small electrode spacing of the bipolar electrodes permitted high resolution measurements in rat and embryonic chick retinas. The high resolution profiling consisted of 25 depths in embryonic chicks and 15 depths in rats. Assuming a 10  $\mu\text{m}$  microprobe displacement into the retina, the 10  $\mu\text{m}$  spacing between the electrodes used in our study is more sensitive to capture the subtle changes in resistivity between the layers. Previous investigations employed larger electrode spacing of  $\sim 25 \mu\text{m}$  [Heynen and van Norren 1985] and  $\sim 12\text{-}16 \mu\text{m}$  [Karwoski and Xu 1999]. Our electrodes design is an improvement in terms of measurement resolution compared to literature.

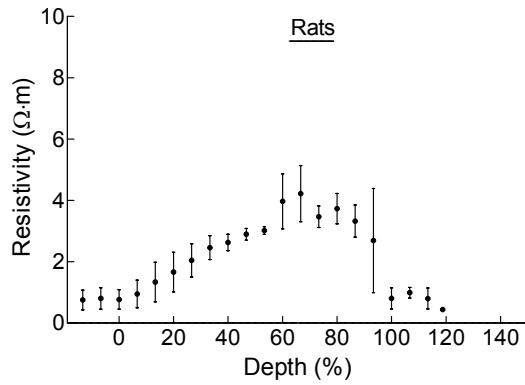
An important result of our study is that the resistivity at a certain depth within the retina is identified by a unique PRF in embryonic chick experiments. Conversely, distinct profiles (refer Figure 3.8c) were obtained in the PRF versus resistivity plots for rats. These profiles can be understood based on the large SDs observed in the Ringer's solution before entering the retina and in the Agar gel (refer Figure 3.8a). Although the PRF is the frequency at which the measured impedance is most resistive, representing the tissue resistance, it is influenced by interface and parasitic capacitances. The large differences in resistivities observed for calibrated mediums could be attributed to changes in electrode capacitance. This may be perceived as the electrodes not being sufficiently clean before the experiment. There could be a thin layer of adsorbed proteins from the retinal tissue cells or damaged limiting membrane residues that may add to the overall measured impedance. Electrodes were cleaned with mild soap solution for rat experiments whereas with RCA-1 cleaning procedure for the embryonic chick experiments. Thus, we conclude that quality of an electrode surface is crucial for good

resistivity profiling in a retina and RCA-1 cleaning process is more effective compared to soap for electrodes used in this study.

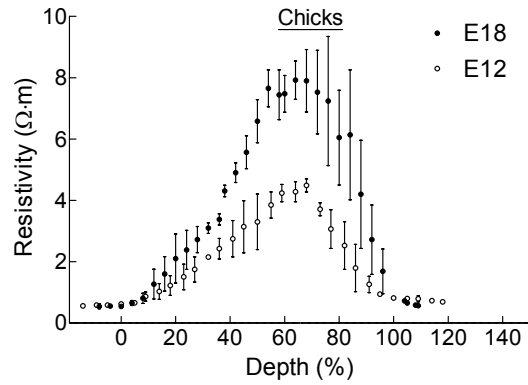
### 3.5 CONCLUSION AND OUTLOOK

An alternative method for high resolution resistivity profiling along the depth in a retina based on bipolar impedance spectroscopy was established. We validated our device by profiling rat and embryonic chick retinas. The resistivity at each retinal depth was calculated based on tissue resistance extracted by peak resistance frequency methodology. Qualitatively, we found the resistivity-depth profiles to be in accordance with earlier studies and that resistivity at any arbitrary retinal depth is characterised by a unique peak resistance frequency. We have shown the potential of planar bipolar microelectrodes as a new technique to probe absolute local resistivity within a retina and multi-layered tissues, in general. We have used the measured chick resistivity profile in constructing a retina model for analysing *in vitro* stimulation data obtained by our collaborators. Relevance and validity of the chick resistivity profile obtained here will be shown in chapters 5 and 6.

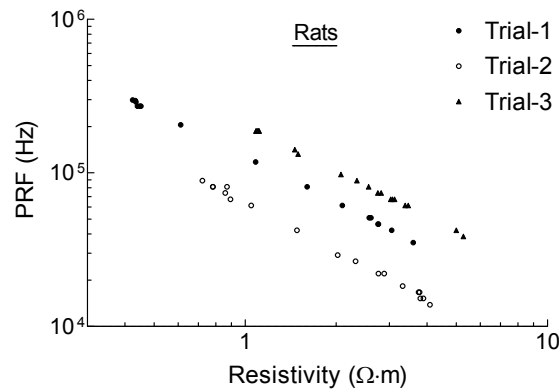
Determining absolute values of resistivities in retina contributes to improved understanding of retinal stimulation by means of modelling studies. The generated resistivity profiles can form the basis for construction of a realistic electric model of a retina. Finite element modelling may be used for estimating and optimising critical parameters such as stimulation thresholds, heat dissipation, resolution, etc. for a given electrode geometry, that are instrumental for the safety and efficacy of a retinal prosthesis. A future improvement of our two-electrode system would be a linear array of electrodes on a single strip. An array of electrodes is capable of probing different layer resistivities with a single insertion into the retina which is expected to cause less damage and provide more reliable measurements.



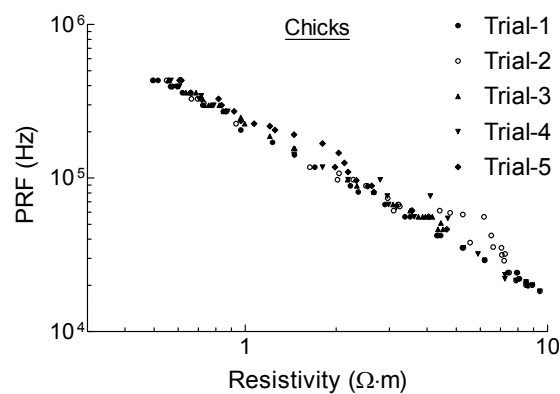
(a) Mean resistivity ( $\pm$ SD) vs. percentage depth profile of three rat retina samples which are extracted from 14-16 day old postnatal wild-type juvenile rats.



(b) Mean resistivity ( $\pm$ SD) vs. percentage depth profile of five chick embryo retina samples of which three are extracted from E18 and two from E12. E18 have a higher peak mean resistivity than the E12 chick trials.



(c) PRF vs. resistivity plots for the three rat experiment trials. A large deviation for resistivity at a particular PRF between the trials was observed.



(d) PRF vs. resistivity plots for the five embryonic chick trials. In general, a good reproducibility of resistivities at a particular PRF in the trials was observed.

Figure 3.8: Data comparison between rats and embryonic chicks. (a, b) Mean resistivity ( $\pm$ SD) vs. percentage depth profiles. (c, d) PRF vs. resistivity plots.





## FEM-BASED INTEGRATED SIMULATION FRAMEWORK

---

### 4.1 INTRODUCTION

Before venturing into the simulation of implantable retinal prostheses, a validated simulation framework was established. As mentioned earlier in Chapter 1, construction of such a sophisticated computational framework involves consideration of the physical, electrical and the biological aspects of a typical retinal stimulation scenario. The essential components of a simulation framework consists of a model for the retina, volume conductor and the associated parts of a retinal prosthesis. A realistic geometry of these elements adapted for the system under investigation are inputs to this simulation framework. The nature of the framework suggests a non-analytical approach in solving the complex bio-electric fields, currents and voltages in the retina and the volume conductor. Finite element method has been used in this dissertation to compute the quantities necessary for analysing retinal stimulation.

A description on the integration of the various elements along with a retina model into a simulation framework for studying performance of current implantable retinal prostheses is presented in this chapter. A discussion of the geometrical factors affecting retinal stimulation followed by elements of the simulation framework is provided in the following sections.

### 4.2 GEOMETRICAL FACTORS

Two significant geometrical factors that affect stimulation thresholds for a retinal prosthesis are: the distance between electrode and retina; and the electrode size. These factors contribute in either affecting the path of electric currents and/or affecting the electric field distribution around the electrode. The representation of these factors in the simulation framework is explained below.

#### 4.2.1 *Electrode-retina gap model*

Let us consider the stimulation electrode separated from the retina by a small gap filled with physiological fluid (PF) of high conductivity. Under these circumstances,

a major change in the field lines penetrating the retinal tissue is expected as shown schematically in Figure 4.1.

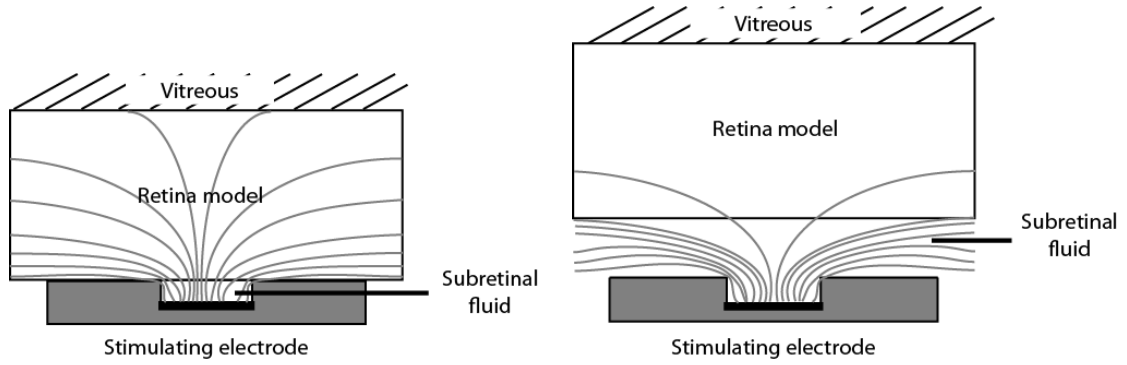


Figure 4.1: Schematic diagram of the electric field lines in the retina when the tissue is in contact with the electrode (left) and when a layer of PF is present between the retina and the electrode (right). The gap is assumed to be filled with PF whose electrical conductivity is assigned a value of  $2 \Omega \cdot m$ .

The distance between the retina and the electrode is actually a volume. This volume is occupied by physiological fluid<sup>1</sup> depending on the implant placement scheme. Considering a two-dimensional electrode-retina gap, distances of up to  $1500 \mu m$  for epiretinal and up to  $50 \mu m$  for subretinal stimulation schemes were used for simulations.

#### 4.2.2 Electrode size

In Chapter 1, it was mentioned that disc electrodes are the most commonly used geometries in current implantable retinal prostheses. In general, the simulation framework presented in this chapter is capable of simulating electrodes of any shape and sizes that can be used in retinal prostheses. The planar disc electrode sizes employed to study epiretinal and subretinal prostheses (Chapters 5 and 6) is documented in Table 4.1. These electrode sizes were specifically chosen in order to validate the simulation framework.

Results from the simulation framework will be compared with different sources in the literature (primarily Argus I) and from the in vitro experiments conducted by our collaborators at HUG using the polyimide-based retinal implant fabricated during this doctoral work.

<sup>1</sup> For an epiretinal scheme, the fluid is obviously vitreous humour; and for subretinal scheme it is known as subretinal fluid, an exact composition of such a fluid has not been studied yet.

STIMULATION SCHEME	EXPERIMENT (s)	DISC ELECTRODE DIAMETER ( $\mu\text{m}$ )
Epiretinal	Argus I (clinical trials)	260, 520
	and <i>in vitro</i> data from literature	and ~25-500
Epiretinal	EPFL-HUG ( <i>in vitro</i> )	50
Subretinal	<i>In vitro</i> data from literature	5-200
	EPFL-HUG ( <i>in vitro</i> )	50

Table 4.1: Disc electrode sizes used for comparison with simulated scenarios.

*EPFL implant (epiretinal and subretinal)*

With an intent to study retinal implants, EPFL has been involved with a collaborative retinal implant project with several partners, since 1999. Under this framework, based on psychophysical studies conducted by one of EPFL's partners - HUG<sup>2</sup>, a reliable technology for the fabrication of implantable microelectrode arrays was developed [Metz *et al.* 2004]. This was the same technology utilised for fabricating the flexible microprobe employed for resistivity profiling in the retina (Chapter 3).

The passive electrodes (i. e., without CMOS electronics) were fabricated for *in vitro* electrophysiology experiments [Lecchi *et al.* 2006] and for *in vivo* experiments with rats [Salzmann *et al.* 2006]. These electrodes were polyimide-based implants with four platinum electrodes of 50  $\mu\text{m}$  diameter each. These electrodes were surrounded by a large arc shaped return electrode having a width of 100  $\mu\text{m}$ . The implant is shown in Figure 4.2. The electrodes are recessed and placed on the polyimide insulation layer. The recess configuration is practically beneficial [Rubinstein *et al.* 1987, West 1991] for neurostimulation electrodes in limiting the high electric fields appearing at the electrode edge [Wiley and Webster 1982, Shepherd *et al.* 1985].

These passive implants catered to two applications with respect to this dissertation. Firstly, they were used in both epiretinal and subretinal experiments conducted by our collaborators in HUG and CMU<sup>3</sup>. Secondly, a total of more than 100 rats were

<sup>2</sup> HUG - Ophthalmology Department at University Hospital of Geneva jointly headed by Prof. A. B. Safran and led by Prof. M. Pelizzone

<sup>3</sup> CMU - Department of Physiology of the University of Geneva headed by Prof. D. Bertrand.

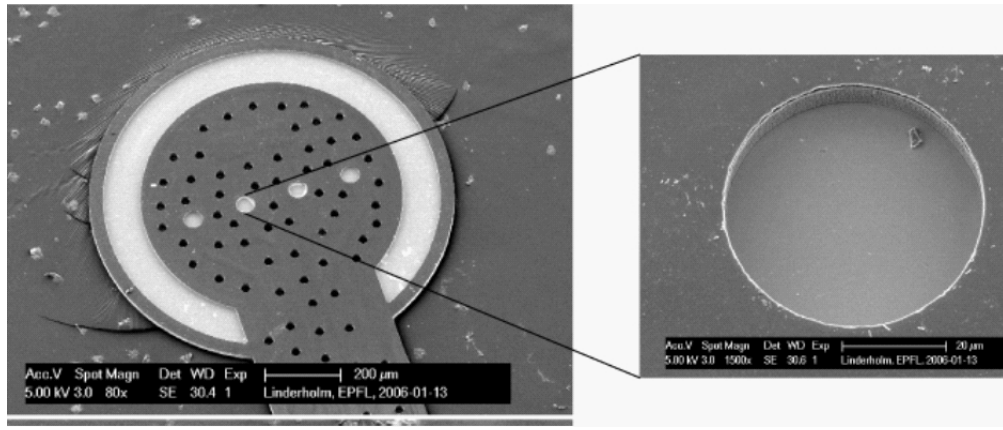


Figure 4.2: A SEM image of the electrode array of the EPFL passive implant. The electrode array consisted of  $50\mu\text{m}$  diameter disc electrodes arranged in a straight line, with centre-to-centre separation of  $150\mu\text{m}$ . The entire array covered  $2\times 2\text{ mm}$  of retinal space. There are  $20\mu\text{m}$  perforations in the implant to permit nutrient exchange between the retina and the RPE.

implanted with these implants in collaboration with INSERM Paris<sup>4</sup>. A reliable surgical procedure was set-up and good implantation results obtained [Salzmann *et al.* 2006]. A quantitative assessment of the electrode-tissue interaction was made by monitoring the electrical impedance for more than two months (refer Chapter 6).

#### *Other epiretinal implants*

The most experimented epiretinal prosthesis until now has been the 16-electrode Argus I epiretinal implant developed by Second Sight Medical Products. They epiretinally implanted human patients' eyes with a four by four array of disc electrodes in the macular region. Electrodes were either  $260\mu\text{m}$  or  $520\mu\text{m}$  in diameter, arranged in an alternating checkerboard pattern with  $800\mu\text{m}$  of centre-to-centre separation between each electrode as shown in Figure 4.3.

The other studies that have been used for comparison are based on *in vitro* results from Jensen *et al.* [Jensen *et al.* 2005b] and Sekirnjak *et al.* [Sekirnjak *et al.* 2006].

#### *Other subretinal implants*

Studies from Tsai *et al.* and Stett *et al.* have been used to compare with some results obtained from simulations on subretinal prosthesis in this dissertation (Chapter 6). Unfortunately, there has been no access to stimulation related data in human subjects implanted with subretinal prostheses except for an abstract [Wilke *et al.* 2010a]. Hence, we are not in a position to make comparisons to clinical studies with subretinal implants.

<sup>4</sup> INSERM - Centre de Recherche INSTITUT DE LA VISION, UMR\_S968 INSERM / UPMC/ CNRS 7210 / CHNO des Quinze-Vingts headed by Prof. J. Sahel and led by Dr. Serge Picaud

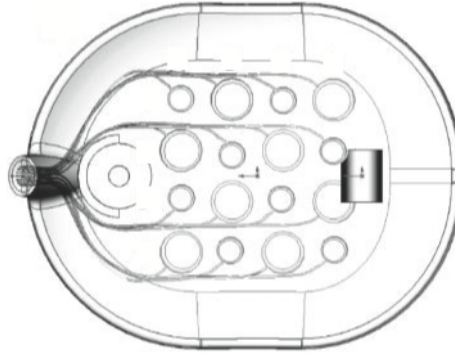


Figure 4.3: Electrode array. The electrode array consisted of  $260\text{ }\mu\text{m}$  or  $520\text{ }\mu\text{m}$  electrodes arranged in a checkerboard pattern, with centre-to-centre separation of  $800\text{ }\mu\text{m}$ . The entire array covered  $2.9 \times 2.9\text{ mm}$  of retinal space (from [Horsager *et al.* 2009]).

### 4.3 SIMULATION FRAMEWORK

The elements of a simulation framework essentially consist of organised subdomains (constituents), well defined boundary conditions and specifications (hypotheses) necessary for extracting the required quantities (extracted parameters). These elements will be described in the following sections.

In the context of a retinal prosthesis, the constituents of the framework can be subdivided into physiological fluid, stimulation and return (ground) electrodes, retina and the pigment epithelium (RPE)-sclera combination.

#### 4.3.1 Constituents of the framework

##### *Physiological medium*

Physiological medium encompasses the implant when it is not in contact with the retina and was defined to have a resistivity of  $\sim 1.5\text{-}2\text{ }\Omega\cdot\text{m}^5$ .

##### *Stimulation electrode*

The stimulation electrode is positioned on RGC layer side or subretinal side of the retina based on the investigated stimulation scheme (epiretinal or subretinal). The stimulation electrode is represented in the form of a planar disc embedded in an insulated substrate and located at the geometrical centre of the entire model geometry. The  $12\text{-}15\text{ }\mu\text{m}$  thick insulation (flexible sheet of the implant) was defined with a resistivity of  $1 \times 10^{17}\text{ }\Omega\cdot\text{m}$  [Smith *et al.* 1987] corresponding to Polyimide and an electrode resistivity of  $106\text{ n}\Omega\cdot\text{m}$ , a standard value for bulk platinum.

<sup>5</sup> a value based on measurements using bipolar microprobe in Chapter 3 on rat and embryonic chick isolated retinal slices.

### Ground electrode

The placement of the ground electrode was based on the stimulation scheme. As monopolar stimulation was used in the investigations and comparisons from literature, the ground electrode was always placed far away from the stimulation electrode. For all experimental combinations, the ground electrode was analysed for two configurations. Firstly, when it is placed in the physiological medium on the photoreceptor (subretinal) side and axially shifted by 15 mm away from the stimulation disc electrode. The ground was defined as a 100 mm diameter platinum disc electrode. Secondly, for studying Argus I implants, the ground electrode was placed on the sclera. A summary of the various placements studied in this dissertation is provided in Table 4.2.

STIMULATION SCHEME	EXPERIMENT (S)	GROUND PLACEMENT
Epiretinal	Argus I (clinical trials)	on sclera
	and <i>in vitro</i> data from literature	and in the medium (far)
Epiretinal	EPFL-HUG ( <i>in vitro</i> )	in the medium, axially shifted (far)
Subretinal	<i>In vitro</i> data from literature	in the medium (far)
Subretinal	EPFL-HUG ( <i>in vitro</i> )	in the medium, axially shifted (far)

Table 4.2: Placement of the ground electrode for different simulated scenarios.

### RPE and sclera

The RPE and sclera together are represented by a highly resistive block, which is set to a resistivity of  $500 \Omega \cdot \text{m}$ . Their position is fixed with respect to the retina's orientation which in turn is dependent on the stimulation scheme under investigation.

### Electric model of the retina

The electric model of the retina is based on the varying cell densities along its thickness. We define a piecewise linear model to represent the electrical resistivity of the retina

as shown in Figure 4.4. The data is extrapolated to obtain the resistivity model for the human eye by scaling the dimensions of the macaque retina to the human retina. Even though mammalian eyes exhibit differences in sizes, thickness of retinal layers (including the nerve fibre layer), etc. which are all critical factors under consideration, the reason for the extrapolation is that the anatomical organisation of the primate retina closely resembles that of humans [Sernagor *et al.* 2006].

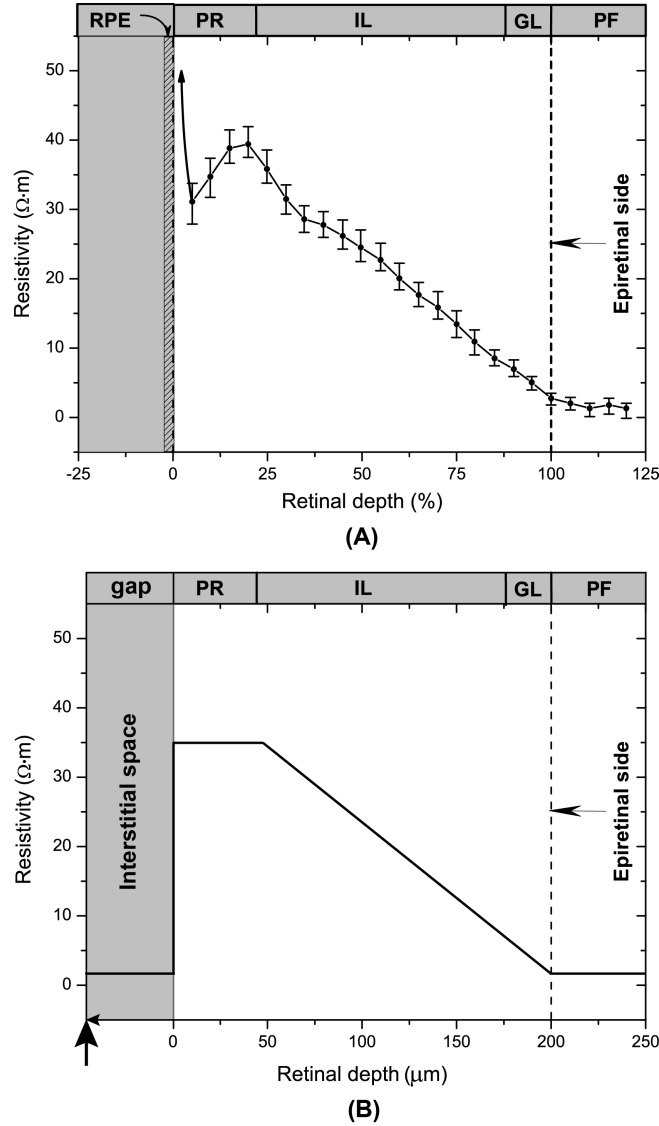


Figure 4.4: (A) Replica of the plot showing the local resistivity (vs. percentage retina thickness) of the various layers of the retina measured on a macaque retina by Heynen and Van Norren [Heynen and van Norren 1985]. (B) Electric model of the retina represented as variations in electrical resistivities, based on the resistivity changes in the macaque retinal tissue as seen in (A) and extrapolated to a human retina bearing a thickness of 200  $\mu m$ . The depth of the retina is calculated between the photoreceptors (subretinal side) and the ganglion cell layer (epiretinal side). Legend – RPE: Retinal pigment epithelium; PR: Photoreceptor layer; IL: Intermediate layers; GL: Ganglion cell layer; PF: Physiological fluid. Arrow indicates the position of the implant for modelling purposes.

In Heynen's experiment, the resistivity measurements extend into the retinal pigment epithelium (RPE). We compositely modelled the Photoreceptor (PR) and the Intermediate cell (IL) – Ganglion cell (GL) regions (Figure 4.4) based on the linear approximation of the experimental data. The resistivity varies from  $35 \Omega \cdot \text{m}$  at the PR to  $2 \Omega \cdot \text{m}$  which is set as the resistivity of physiological fluid filling the interstitial space. As in most cases, when the electrode is not in intimate contact with the retina, an electrode-retinal gap filled with ophthalmic physiological fluid (PF) is considered.

The selection for thickness of the retina depends mainly on the location of the retinal implant. Typically, in retinal implantation trials [Chow *et al.* 2001], the implant is placed closer to the fovea, but not over it [Perez Fornos 2006] due to the absence of ganglion and bipolar cells in the fovea. The retinal thickness in the region surrounding the fovea is known to vary between  $\sim 100 \mu\text{m}$  at the foveal floor to  $\sim 320 \mu\text{m}$  at the foveal rim [Bonanomi *et al.* 2006]. Considering that the location of the implant near the fovea is not precise, the chosen value for the retinal thickness was  $200 \mu\text{m}$ .

The retinal thickness value of  $200 \mu\text{m}$  was used for analysis on the Argus I and other *in vitro* experiments from the literature. For the EPFL-HUG experiments, a value of  $175 \mu\text{m}$  [Huang *et al.* 1998] with a re-adjusted retina model was used.

#### *Inclusion of geometric factors*

The two geometrical factors affecting the stimulation thresholds (discussed in Section 4.2) were included in the simulation model as variable parameters: electrode-retina distance ( $g$ ) and electrode disc diameter ( $d$ ). The retinal resistivity model is positioned according to the electrode-retina distance, between 0 and  $1500 \mu\text{m}$  (refer 4.2.1). Other variables defined in the model are:  $h_{GL}$  – depth at which ganglion cells are assumed to be located, and  $h_{Ret}$  – depth where the retina ends and the RPE starts.  $h_{GL}$  was defined to be  $20 \mu\text{m}$  outwards from the epiretinal side, *i. e.*,  $(g+20) \mu\text{m}$  from the surface of the implant. Figure 4.5 presents a schematic representation of the above mentioned elements (excluding the ground electrode) and the variable parameters together with a graph representing the resistivity change as a function of the retina depth. These values were employed for simulation of an epiretinal prosthesis.

For a subretinal scheme, apart from the orientation change of the retina, the depth of RGCs ( $h_{GL}$ ) is assumed to be at  $175 \mu\text{m}$  from the subretinal surface of the retina.

For modelling based on *in vitro* experiments conducted by our HUG collaborators, apart from a geometric change in the implant size, the electric model is constructed



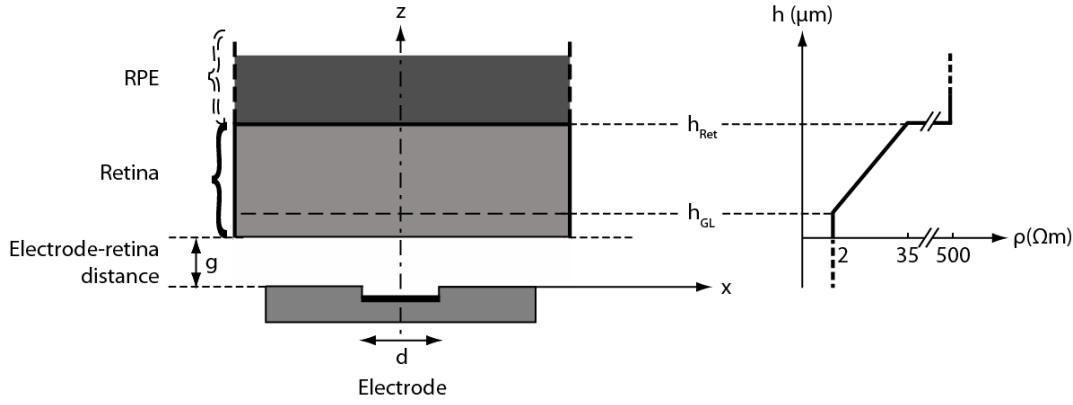


Figure 4.5: Schematic representation of the various elements of the simulation framework (for an epiretinal scheme). A schematic representation of the constituents the simulation framework (excluding the ground electrode) and a graphic representation of the resistivity change as a function of the retina depth. RPE is the retinal pigment epithelium,  $h_{GL}$  is the depth at which ganglion cells are assumed to be located,  $h_{Ret}$  is the depth where the retina ends and the RPE (not shown) starts,  $g$  is the electrode-retina distance and  $d$  is the electrode disc diameter.

based on extracted data from resistivity profiling experiments on isolated retina slices from embryonic chicks. The resistivity varies from  $\sim 9 \Omega \cdot m$  at the PR to  $2 \Omega \cdot m$  which is set as the resistivity of physiological fluid filling the interstitial space. An appropriate model is used for epiretinal and subretinal configurations. All computations for these modelling studies were made with the assumption that retina is in contact with the implant and that no electrode-retina gap exists.

#### 4.3.2 Hypotheses for RGC activation

##### Threshold criterion

The threshold current necessary for activation of an RGC by means of extracellular stimulation has been both experimentally and theoretically demonstrated to depend upon various parameters such as activation of soma versus axon (axon initial segment) [Schiefer and Grill 2006, Behrend *et al.* 2009, Fried *et al.* 2009], stimulus pulse type (cathodic or anodic), polarity (monophasic or biphasic) and shape (pulse duration) [Fried *et al.* 2006, Boinagrov *et al.* 2010]. For the purpose of our study, we consider a spherical RGC soma (without axon and dendrites) activated using a single, balanced, cathodic pulse duration of 0.975 ms/phase (epiretinal) and 0.1 ms (subretinal) at threshold excitation. The rationale behind choosing a spherical model of an RGC soma instead of planar (disc-like) or cylindrical (unmyelinated axon-like) was based on a recent modelling study by Boinagrov *et al.* [Boinagrov *et al.* 2010] employing the six-channel salamander RGC model [Fohlmeister *et al.* 1990].

For epiretinal scheme in our simulation studies, a threshold criteria was chosen following strength-duration curves based on the spherical soma model (Figure 12, Pg. 2245 of [Boinagrov *et al.* 2010]) and demonstrated good matching with experimental data [Jensen *et al.* 2005b] that was generated using large electrode (125  $\mu\text{m}$  and 500  $\mu\text{m}$  in diameter) stimulation. Similar range of sizes were used for electrodes used in Argus I trials. The stimulus pulse parameters were taken from Argus I clinical trials in order to be relevant for comparison with results from our study. An RGC activation threshold criterion can be extracted from one of the multiple strength-duration curves computed by Boinagrov *et al.* [Boinagrov *et al.* 2010] using a planar Hodgkin-Huxley (HH) cell model studied using a single, charge-balanced, cathodic-first, biphasic stimulus (type used in Argus I trials). The threshold current injected to create a voltage gradient to activate an RGC located at a distance from the electrode (cell activation depth) leads to a local electric field near the cell. In the current study, an electric field criterion of 1000 V/m is chosen, assuming uniform electric field around the cell. This value corresponds to a local voltage drop (transcellular) of 10 mV for a biphasic 1 ms stimulus pulse duration and a planar Hodgkin-Huxley cell with a cell polarisation time RC of  $10^{-4}$  ms (refer Figure 5A in [Boinagrov *et al.* 2010]). The model also demonstrates that biphasic stimulation thresholds for planar cells are lower than those of a spherical cell by a factor of 1.7-1.8 throughout all pulse durations. In spite of this factor, we considered a transcellular potential of 10 mV created across an RGC soma of around 10  $\mu\text{m}$  in diameter, a typical RGC size in primates used in modelling studies previously [Greenberg *et al.* 1999]. By neglecting the factor and considering soma to be spherical, a compromise between experimental (or clinical) and modelling inaccuracies was made. The influence of pulse type and duration on RGC activation was neglected from epiretinal simulations as this was considered directly in the assumption for activation criterion (explained above).

By selecting another threshold electric field criterion (here, based on the strength-duration curve) would merely cause a scaling on the computed threshold voltages which affects related parameters (e.g. threshold currents, electric field distribution, etc.). An illustration of a change in criterion is explained below and demonstrated in subretinal simulations (Chapter 6).

For comparisons with subretinal *in vitro* data from literature and *in vitro* data for both epiretinal and subretinal obtained by our HUG collaborators, in our simulation studies, the threshold currents were computed based on a threshold criterion of 3000 V/m, an

approximation derived from literature [Palanker *et al.* 2005] under uniform electric field conditions. This corresponds to a voltage of 30 mV created across a cell of  $10\text{ }\mu\text{m}$  in diameter [Palanker *et al.* 2005]. However, the depolarisation of a cell membrane by 10-25 mV (transmembrane) is usually sufficient to activate a retinal neuron. This provides a range of transcellular voltage values between 2000-5000 V/m (twice the transmembrane voltage) to choose from as a threshold criterion.

#### *Depth of RGC activation*

RGCs are considered to produce robust responses when directly activated regardless of the scheme of stimulation [Tsai *et al.* 2009a, Boinagrov *et al.* 2010]. Therefore, it was assumed generally in our studies that the retina can be directly stimulated at the depth  $h_{GL}$ , in other words at the RGC layer.

### 4.4 INTEGRATED FEM MODEL

The components of the simulation framework are assembled together into a FEM model bound by well defined conditions. In the FEM simulations presented in this work, we have used a monopolar stimulation scheme for which the ground electrode is located far away from the stimulation electrode. The stimulation and ground electrodes are placed as defined in the section 4.3.1. An external bounding box of  $44 \times 25\text{ mm}$  (epiretinal) and  $18 \times 12\text{ mm}$  (subretinal) drawn from the axis of the stimulation electrode and confining the implant is used to limit the computation space. The retinal resistivity model presented before is placed in close contact with the electrodes except during the case studies on electrode-tissue gap.

The time-varying bio-electric fields, currents and voltages in a biological medium can be examined in the conventional quasistatic limit [Plonsey and Heppner 1967]. Under these circumstances, the electric scalar potential,  $V$  in the biological medium is defined by solving the Laplace's equation:

$$\nabla \cdot [(\sigma + i\omega\epsilon_0\epsilon_r)\nabla V] = 0 \quad (4.1)$$

where,  $\sigma$  and  $\epsilon_r$  are the conductivity and relative permittivity of the medium respectively. The angular frequency of the driving stimulus is  $\omega = 2\pi f$ ,  $\epsilon_0$  is the permittivity of vacuum, and  $i$  is the imaginary unit. The current density on the electrode,  $\mathbf{J}$  is related to  $V$  given by Ohm's law:

$$\mathbf{J} = -(\sigma + i\omega\epsilon_0\epsilon_r)\nabla V \quad (4.2)$$

We computed the threshold current and the impedance using both harmonic and DC modes of representing the biological medium.

In the harmonic mode, frequencies of  $1\text{ kHz}$  ( $1\text{ ms}$ ) and  $10\text{ kHz}$  ( $0.1\text{ ms}$ ) were used based on the time scale of commonly applied pulses for stimulation. The biological medium was represented by conductivity and permittivity values considering the dispersive (frequency dependent) properties of the tissue. The electrode-electrolyte interface impedance was also implemented into this mode in the form of a thin-layer approximation as described by Cantrell *et al.* [Cantrell *et al.* 2008]. Simulations indicated that above certain values of the electrode potential, the potential drop seen across the electrode, also known as overpotential, is negligible compared to the potential drop across the tissue impedance (refer Appendix C). Furthermore, an estimate of the capacitive component of the tissue impedance at the given frequency is more than an order of magnitude higher than the resistive component for both the frequencies. Finally, the RPE and sclera do not contribute to the dynamic changes in voltages across them due to the low value of scleral resistance compared to its capacitance. This renders them to be represented as resistive contribution to the flow of current through them. These observations suggest that the simulation problem could be reduced to a simple and computationally less expensive DC model. Consequently, a frequency independent DC model considering the biological medium as purely resistive along with the neglected electrode interface impedance was modelled.

Simulations were performed with the Comsol Multiphysics® (versions 3.5 and 4.1) finite element modelling software. An axisymmetric finite element model of the stimulation and the ground electrodes were created with a mesh resolution of up to 2 Million (epiretinal) and approximately 0.5 Million nodes (subretinal). By default, the Delaunay (normal or advancing front) triangulation meshing algorithm of Lagrange-quadratic element type was utilised in Comsol for meshing the simulation volume. Element refinement (high density meshing) was performed on the stimulation ( $40\text{ nm}$  mesh element size) and the ground electrodes to ensure current conservation. Appropriate Dirichlet, von Neumann and continuity boundary conditions (only for harmonic simulations) were used to define the electrode-retina interfaces, the insulating material-retina interfaces and the boundaries of the simulation bounding box. Table 4.3 displays the boundary conditions and equations employed in the simulation framework operated in DC. Material properties, in this case, electrical resistivities of platinum (Pt) electrode, insulator (assumed as Polyimide) and PF were adjusted parameters. Table 4.4

displays the constants employed for the quasistatic and/or conductive DC simulations performed using FEM model.

DOMAIN/BOUNDARY NAME	TYPE OF CONDITION	EQUATION (s)
Physiological fluid	Current conservation	$\nabla \cdot \mathbf{J} = 0$
Retina model		$\mathbf{J} = \sigma \mathbf{E}$
Substrate insulation		$\mathbf{E} = -\nabla V$
Bounding box	Electric insulation	$-\mathbf{n} \cdot \mathbf{J} = 0$
Stimulation electrode	Electric potential	$V = V_{stimulation}$
Ground electrode	Ground	$V = 0$
Equation to compute electric scalar potential, $V$ in the medium due to an electrode stimulation		$\nabla \cdot [\sigma \nabla V] = 0$
Notations: $\mathbf{J}$ : current density on the electrode; $\mathbf{E}$ : electric field vector; $V_{stimulation}$ : amplitude of the voltage stimulus; $\sigma$ : conductivity of the physiological medium; $\mathbf{n}$ : normal vector.		

Table 4.3: Boundary conditions and equations employed in the simulation framework operated in DC.

The FEM model was solved using a direct linear solver known as PARDISO. A brief record of solver parameters is shown in Table 4.5. Simulations were performed under electrostatic conditions with an applied DC voltage between the stimulation and ground electrodes. A glimpse of surface voltage profile and current density streamlines for typical electrode stimulation is presented in Figure 4.6.

#### 4.5 EXTRACTED PARAMETERS

An element refinement of ten times normal meshing was made for the data extracted from the simulations which were subsequently post-processed in MATLAB® to generate the required plots.

SUBDOMAIN	CONDUCTIVITY ( $S/m$ )	RELATIVE PERMITTIVITY
Platinum	$94.35 \times 10^5$	1
Polyimide	$1 \times 10^{-17}$	4
Subretinal fluid	0.5 – 0.67	99 <sup>a</sup>
Retina	In accordance with the retina model	30,000 <sup>b</sup>

<sup>a</sup> <http://niremf.ifac.cnr.it/tissprop> – a value at 1 kHz for vitreous assuming that subretinal fluid has similar properties.

<sup>b</sup> <http://niremf.ifac.cnr.it/tissprop> – an approximate mean value for retinal tissue taken in the range between 1 and 10 kHz.

Table 4.4: Constants employed for the quasistatic and/or DC simulations performed using FEM model.

#### 4.5.1 Current

The current delivered by the electrode was computed by a boundary integration of the normal component of current density over the ground electrode.

#### 4.5.2 Impedance

Impedance is computed as the ratio between the applied voltage stimulus and the resulting current seen at the electrode taking into consideration the retina with or without an electrode-retina gap.

#### 4.5.3 Lateral extent

During actual experiments, to ensure stimulation, there is a tendency to use stimulation currents 10-20% above the pre-determined minimum threshold current. In our study, we define lateral extent as the horizontal distance (measured from the electrode axis) covered at  $h_{GL}$  corresponding to a threshold electric field of 1 kV/m caused by a 20% excess on the threshold current. An illustration of the assumption and the lateral extent definition is presented in Figure 4.7. Implant resolution can be calculated based on the lateral extent of stimulation for the electrodes.

### 4.6 CONCLUSION AND OUTLOOK

The simulation framework developed in this chapter is a preliminary step in formulation of a full scale integrated simulation framework including complex models and criterion.

Direct (PARDISO) - Linear system solver	
PARAMETER	VALUE
Preordering algorithm	Nested dissection
Row preordering	On
Bunch-Kaufmann	On
Pivoting perturbation	$10^{-8}$
Relative tolerance	$10^{-6}$
Factor in error estimate	400
Stationary	
PARAMETER	VALUE
Linearity	Nonlinear
Relative tolerance	$10^{-6}$
Maximum number of iterations	5000
Initial damping factor	1
Minimum damping factor	$10^{-4}$

Table 4.5: A brief overview of solver parameters used for simulations.

This framework will be our basis to study epiretinal and subretinal prostheses presented in Chapters 5 and 6.

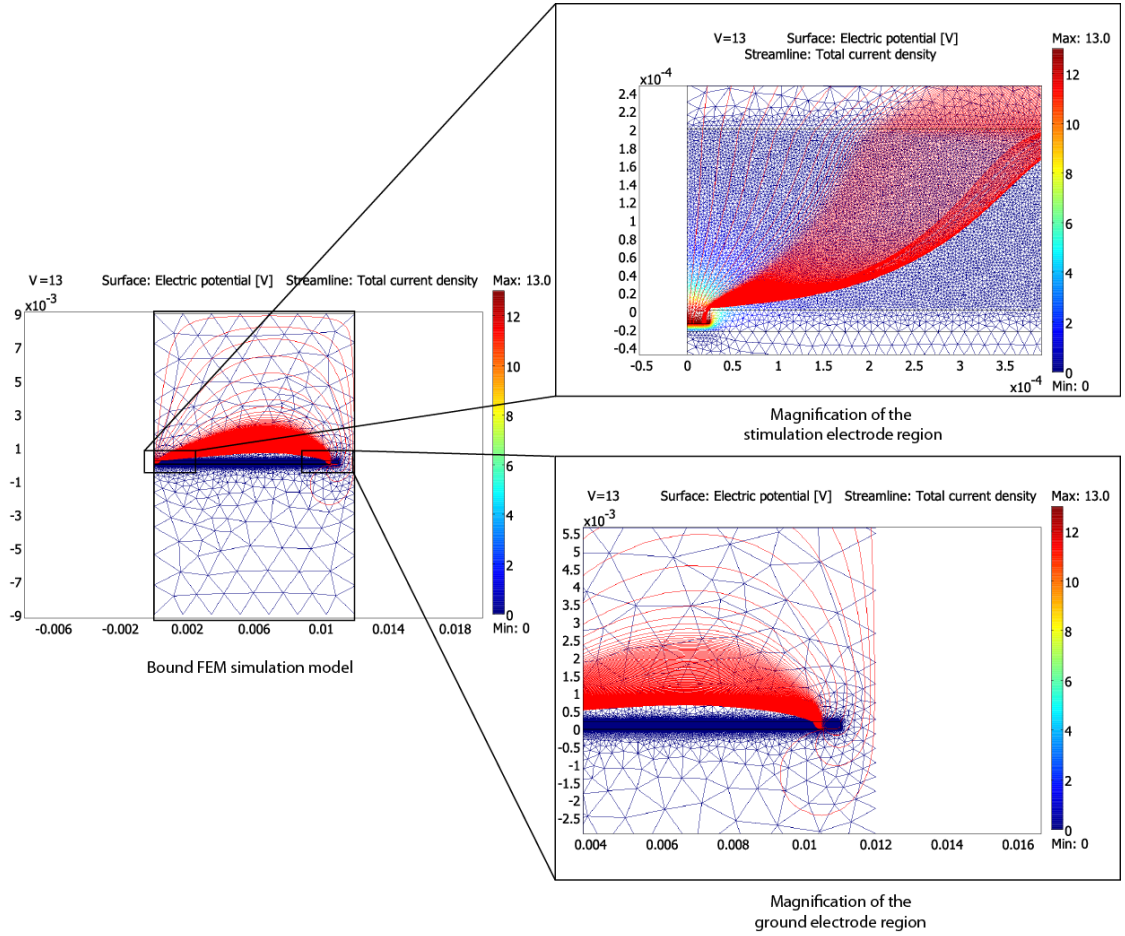


Figure 4.6: A graphical mapping of an electrostatic simulation of electrode stimulation with an applied DC voltage (13 V) where the retina is in contact with the implant surface. A wireframe-based surface voltage profile along with streamlines of current density is displayed. The wireframe representation indicates the element sizes employed during computation. Relevant magnifications in the regions of stimulation and ground electrodes are also illustrated for clarity. All designated dimensions are in metres. Note: please see PDF version for colour version of the figure.

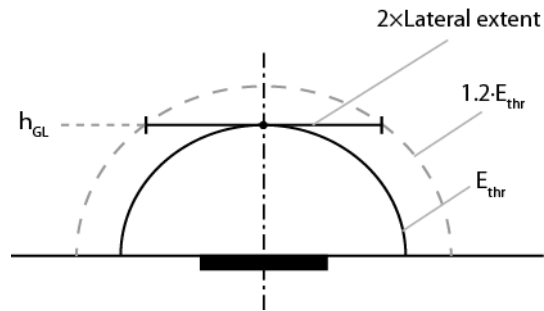


Figure 4.7: A graphical representation of lateral extent of retinal stimulation. An illustration of the definition for lateral extent of retinal stimulation. It is denoted by a horizontal distance measured at  $h_{GL}$ , where the threshold electric field criterion is reached for a 20% increase in stimulation amplitude. The dark block represents the stimulating electrode.



## SIMULATION OF EPIRETINAL PROSTHESES

---

### 5.1 BACKGROUND

Two major electrical parameters responsible for affecting the efficiency of retinal prostheses [de Balthasar *et al.* 2008] are: (i) the fluctuation of current amplitude for activation (threshold current) that can occur due to unstable positioning of the electrode array on the inner retinal surface, electrochemical alterations in the electrodes, or neurophysiological remodelling of the retina. (ii) The charge density necessary to elicit visual percepts to permit long-term stimulation without damaging the retina or the electrodes. The determination of threshold current and charge density is important for achieving safe stimulation. Appropriately, electrode-retina distances along with the electrode geometry are factors influencing the retinal stimulation. The development of an integrated simulation framework can predict the stimulation parameters by including these factors in the model.

An electrode-retina distance contributes to the varying current spread from the electrodes causing changes in the stimulation area in the retina and therefore affects the resolution of the prosthesis. *In vitro* electrophysiological data and analytical calculations suggest that the threshold currents rise rapidly with increasing distance of the electrodes from the retinal surface [Jensen *et al.* 2003, Palanker *et al.* 2005]. Electrode geometry has an effect on the current required for RGC activation. *In vitro* experiments [Sekirnjak *et al.* 2006] have established that the threshold current necessary to elicit spikes in RGCs has a power law relationship with electrode area. Incorporating these geometrical factors affecting perceptual thresholds in a simulation framework can be of interest to: design engineers of retinal implants—aiding them to determine optimal electrode schemes for retinal stimulation by predicting values for spatial extents (resolution) and probable electrochemical effects on the electrode surface; surgeons – assisting them after surgery to verify the distance between implant and the retina in addition to a visual confirmation [Humayun *et al.* 2003]; and electrophysiologists – to estimate the threshold current, voltage or charge needed during an actual stimulation trial [de Balthasar *et al.* 2008].

Presently, proximity of the retina to the electrodes is verified by two different techniques after implantation of retinal prostheses. Optical coherence tomography (OCT) is one of the methods which reveals only proximity of the edges of the device to the retina for a non-transparent retinal implant. The other technique, known as impedance analysis [Johnson *et al.* 2007] uses the changes in impedance to estimate the electrode-retina distance. The changes in impedance occur when the implant moves closer or away from the retina. The utilisation of an integrated framework can predict the impedance associated with an electrode-retina distance considering different electrode geometries.

For our studies, a simulation framework was built integrating the prosthesis-retina interface elements involved in an epiretinal prosthesis closely resembling the one used in the framework of the only and most comprehensive published human trials until now using Argus I epiretinal implants by de Balthasar *et al.* [de Balthasar *et al.* 2008]. Following are the features of our framework (detailed description in Chapter 4) that has not been dealt by previous modelling studies on epiretinal stimulation: (i) the location and dimensions of stimulation and ground electrodes were adapted to a real implantation scenario; (ii) a realistic representation of the electrical properties of the retina; (iii) choice of a simplified, yet realistic activation threshold criterion based on a recent analytical study [Boinagrov *et al.* 2010] that incorporates the critical stimulation parameters such as stimulus type (monophasic/biphasic), shape (cathodic/anodic) and duration under a single unified model (iv) Predictions on threshold currents and impedance with varying electrode-retina distances for different electrode dimensions. Using this framework, variation of threshold currents and impedances were computed using different electrode-retina distances and disc electrode sizes. In order to demonstrate the relevance of our simulation framework to implanted human epiretinal prosthesis, the frame of reference for the computed results is the most recent experimental data on geometrical factors affecting perceptual thresholds presented in Argus I trials. We estimated lateral extents of stimulation for the electrodes which provides an indication to the resolution of the epiretinal prosthesis used in those trials. Subsequently, this simulation model can be easily modified to predict the efficiency of novel electrode geometries for epiretinal prostheses.

## 5.2 METHODS

The adjustments in the simulation model, threshold current criterion, depth of RGC activation, electrode-retina gap and the construction of FEM-based simulation framework was based on explanation in Chapter 4 for an epiretinal scheme of stimulation. The necessary modifications to the framework in order to be able to study the two configurations proposed *i. e.*, Argus I and our implant is also mentioned in Chapter 4.

## 5.3 RESULTS AND DISCUSSION

The effectiveness of this computational study can be evaluated by directly comparing clinical and electrophysiological results with outcomes based on our simulation framework. One of the principal results for comparing our study are the only exhaustive measurements made during the clinical study conducted by de Balthasar et al. [de Balthasar *et al.* 2008] on human beings implanted by Argus I epiretinal implants. The scattered impedance and threshold data observed in their experimental study was associated with small movements of the electrode array. In order to determine a theoretical water window for electrodes used in Argus I experimental protocol, charge and charge density were calculated with a stimulus duration of 0.975 ms.

### 5.3.1 Stimulation thresholds as a function of electrode-retina distance

A computed threshold current is plotted as a function of electrode-retina distances for the two electrode sizes, 260  $\mu\text{m}$  and 520  $\mu\text{m}$  are presented in Figure 5.1. A factor two difference between the thresholds for both electrodes was noticed when the electrodes were in contact with the retina. We observed an approximate order of magnitude increase in thresholds when the electrode-retina distance reached half of the electrode diameter. Subsequently, for electrode-retina distances exceeding the electrode diameter, the threshold current becomes proportional to the square of the electrode-retina distance. For smaller distances ( $< 20 \mu\text{m}$ ), the threshold changes were less pronounced as also observed in *in vitro* experiments conducted by Jensen *et al.* [Jensen *et al.* 2003]. At large electrode-retina distances, above 300  $\mu\text{m}$ , the two electrodes are not differentiated as they showed nearly the same threshold current values. Threshold current variation as a function of electrode-retina distance obtained in this study (Figure 5.1), are within the range of values obtained in the experimental results of the Argus I clinical trials [de Balthasar *et al.* 2008].

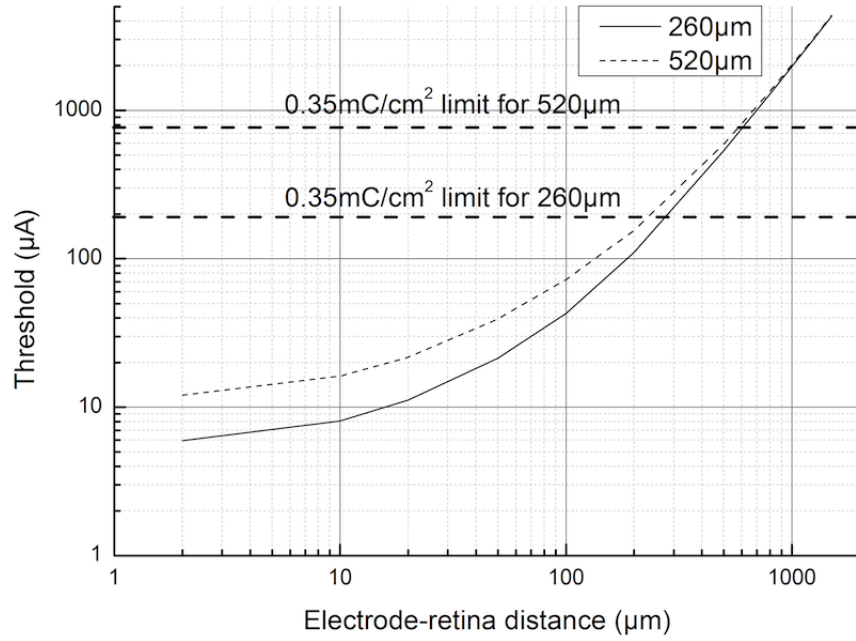


Figure 5.1: Threshold current versus electrode-retina distance. Evolution of computed threshold current with variation in electrode-retina distance for two electrode sizes (260  $\mu\text{m}$  and 520  $\mu\text{m}$ ). We observe that there is a factor two difference of threshold between the two sizes when the electrode is in contact with the retina. Approximately, an order of magnitude increase in threshold current is observed when the electrode-retina distance reaches half of the electrode diameter. When electrode-retina distance exceeds the electrode diameter, the threshold current becomes proportional to the square of the distance. The corresponding charge injection limit (for 0.975 ms pulses) is displayed for both electrode sizes.

Safe stimulation is critical for a chronic usage of a retinal prosthesis. Platinum electrodes have a charge density limit ranging between 0.05 [Rose and Robblee 1990] and  $0.49 \text{ mC}/\text{cm}^2$  [Brummer and Turner 1977] per stimulation pulse above which electrochemical reactions dominates at the electrode surface [Brummer and Turner 1977]. The range of charge densities (also known as reversible charge storage capacity) is related to considerations on real surface area, geometry of the electrode and on the stimulus pulse width [Merrill *et al.* 2005]. A theoretical charge density limit of  $0.35 \text{ mC}/\text{cm}^2$  was chosen for our study considering a real geometry of the electrode and a pulse width of 0.975 ms. Currents corresponding to this charge limit are  $190.6 \mu\text{A}$  for 260  $\mu\text{m}$  and  $762.4 \mu\text{A}$  for 520  $\mu\text{m}$  electrodes. It can be observed that the current injection limit can be reached at an electrode-retina distance of about 270  $\mu\text{m}$  for 260  $\mu\text{m}$  diameter electrodes and nearly 600  $\mu\text{m}$  for 520  $\mu\text{m}$  diameter electrodes. Close proximity of RGCs to the electrodes is thus a critical issue for safe and chronic retinal stimulation.

### 5.3.2 Stimulation thresholds as a function of electrode sizes

A range of disc electrodes with diameters ranging between  $10\text{ }\mu\text{m}$  and  $1500\text{ }\mu\text{m}$  were used to simulate the relationship between the stimulation threshold and electrode-retina distances –  $0\text{ }\mu\text{m}$  (in contact with retina),  $10\text{ }\mu\text{m}$  and  $100\text{ }\mu\text{m}$ . In retina contact condition presented in Figure 5.2 (axes plotted in logarithmic scale), it is observed that the threshold current is a power function of the square root of the electrode area (follows a power law with the electrode circumference) as inferred from the linearity between the quantities. The charge density increases to a high value with smaller electrodes, as the decrease in surface area outweighs the threshold current decrease, explaining the change in slope of the linear trend below electrode sizes of  $25\text{ }\mu\text{m}$ . Our simulation results for large electrodes ( $> 100\text{ }\mu\text{m}$ ) are in agreement with the trends observed in *in vitro* experiments conducted by Jensen [Jensen *et al.* 2005b] and the literature review by Sekirnjak [Sekirnjak *et al.* 2006] groups indicating that the threshold current necessary to elicit spikes within RGCs varies as a power law with electrode area. The thresholds obtained for smaller electrodes ( $< 25\text{ }\mu\text{m}$ ) cannot be compared with a previous report by Sekirnjak *et al.* [Sekirnjak *et al.* 2006] as the stimulus pulse widths used in their study was different. When the electrode is not in contact with the retina, the threshold is almost independent of the electrode size for all electrode-retina distances below a distance approximately equal to the electrode diameter and for distances above this, follows the power law again. This behaviour is explained by the electrode edge effect dominating at small electrode-retina distances. Another interesting result in relation to safe stimulation is an electrode with a radius smaller than the electrode-retina distance will typically require a stimulation current above its current injection capacity (refer Figure 5.2).

Computed threshold currents for  $260\text{ }\mu\text{m}$  and  $520\text{ }\mu\text{m}$  electrodes differ only slightly at electrode-retina distances from  $\sim 200\text{ }\mu\text{m}$  onwards. This similarity between threshold currents for the two electrodes was also observed in Argus I clinical trials [de Balthasar *et al.* 2008]. It is interesting to notice from their measurements (threshold versus electrode-retina distance, refer Figure 7b in [de Balthasar *et al.* 2008]) that the similarity in thresholds for the two electrodes, results from the electrode-retina distances being in the range of  $150\text{--}300\text{ }\mu\text{m}$ . The consistency offered by our predictions in comparison to the existing clinical measurements on thresholds correlating to electrode-retina distance reiterates the importance of a realistic framework.

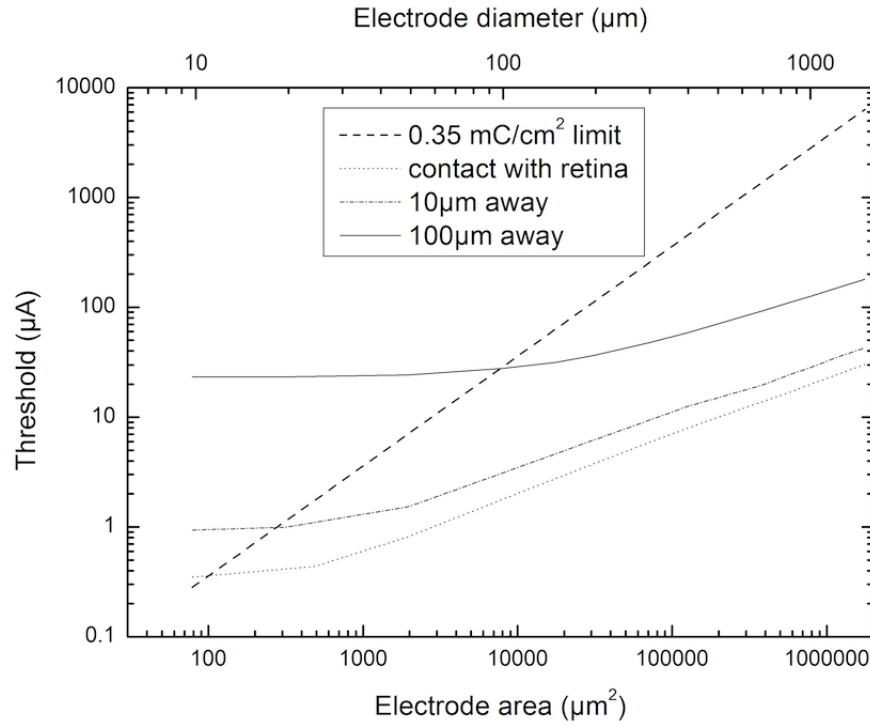


Figure 5.2: Threshold current versus electrode diameter/area. Computed trend for variation of threshold currents with changing electrode area (corresponding electrode diameter is shown on the top axis). Dotted line represents the charge density limit calculated for platinum electrodes using a stimulation pulse width of 0.975 ms. When electrodes are in contact with the retina, the threshold current varies with the square root of the electrode area (or proportional to the electrode circumference). When electrodes are not in contact with the retina, the threshold is almost independent of the electrode size until the electrode diameter is roughly equal to the electrode-retina distance, and then follows the square root law. This behaviour is explained by dominance of edge effects at small electrode-retina distances. The current injection limit trend line is also plotted on the graph. It is observed that for an electrode with a radius smaller than the electrode-retina distance will typically require a stimulation current larger than the injection limit.

Electrode-retina distance influences the threshold current values for various electrode sizes having a pronounced effect on safe stimulation of the retina. A trend line between threshold current limits for different disc electrodes based on the electrochemical limit for platinum ( $0.35 \text{ mC/cm}^2$ ) is plotted in Figure 5.2. The approximate electrode sizes below which the electrochemical limit (for platinum electrodes) is exceeded for the three electrode-distance conditions is as follows: (i)  $11 \mu\text{m}$  diameter when the electrode is in contact with retina, (ii) about  $20 \mu\text{m}$  diameter when the electrode is within  $10 \mu\text{m}$  distance from the retina and (iii) about  $100 \mu\text{m}$  when the electrode is within  $100 \mu\text{m}$  distance from the retina. Since both charge and charge density are to be considered for discussion on safe stimulation [Merrill *et al.* 2005], the stimulus pulse duration is critical. Our simulation framework is capable of computing threshold currents for different electrode geometries based on a stimulus pulse dependent threshold criterion, rendering it a powerful prediction tool.

### 5.3.3 Impedance variation based on electrode-retina distance

Impedance changes in neuroprostheses (e.g., cochlear implants) have been correlated with changes in the tissue resistivity surrounding the electrode [Duan *et al.* 2004] and electrochemical changes at the electrode surface with time [Hughes *et al.* 2001]. There has been no strong evidence for these phenomena in chronic epiretinal implantation studies [de Balthasar *et al.* 2008]. Moreover, the probability of an immune response (e.g. tissue encapsulation) in such implantations is low because the electrodes were observed to be in the vitreous significantly away from the retina during trials [Mahadevappa *et al.* 2005, McMahon *et al.* 2006]. Consequently, by neglecting effects influencing impedance changes, impedance measurements can be compared to the simulated values for obtaining information on distance of the retina with respect to the electrode array of the implant. As threshold currents reduce with closer proximity between the retina and electrodes, impedance can be used to predict threshold currents for retinal stimulation. Studies [McMahon *et al.* 2006, de Balthasar *et al.* 2008] based on frequent monitoring of impedance during the post implantation period suggest that there is a continuous change in distance between the electrode array and the retina influencing the variation in measured impedance.

Our framework computed the trend between impedance and electrode-retina distance and is shown in Figure 5.3. By using this trend, the threshold currents can then be directly predicted from computed impedance values knowing the relationship between threshold currents and electrode-retina distance (Figure 5.1). Higher impedances (electrodes closer to the retinal surface) means low thresholds for the activation of RGCs. Electrode-retina distances which affect the computed values of impedance indicate that there is no benefit of using a smaller electrode other than the capacity to place more electrodes within the same area; as at large electrode-retina distances (especially in the range 100-300  $\mu\text{m}$ ), there is small difference in thresholds for different electrode sizes. But, when multiple such electrodes are stimulated simultaneously, a higher resolution might be produced as shifting stimulation of an array of four small electrodes (for e.g., half the size of larger electrode) by one row could shift the stimulation by a smaller distance than shifting stimulation of larger electrodes by one row. Even though there is a large variability within the impedance measurements presented in Argus I clinical trials [de Balthasar *et al.* 2008] (reproduced in Figure 5.3 for convenience), they are grossly within our simulated range of values for impedance versus electrode-retina distance. Considering the data spread of impedance-distance measurements in the



Argus I clinical data; a fitting of the data is not totally relevant, but a fit would not be in contradiction with our simulations.

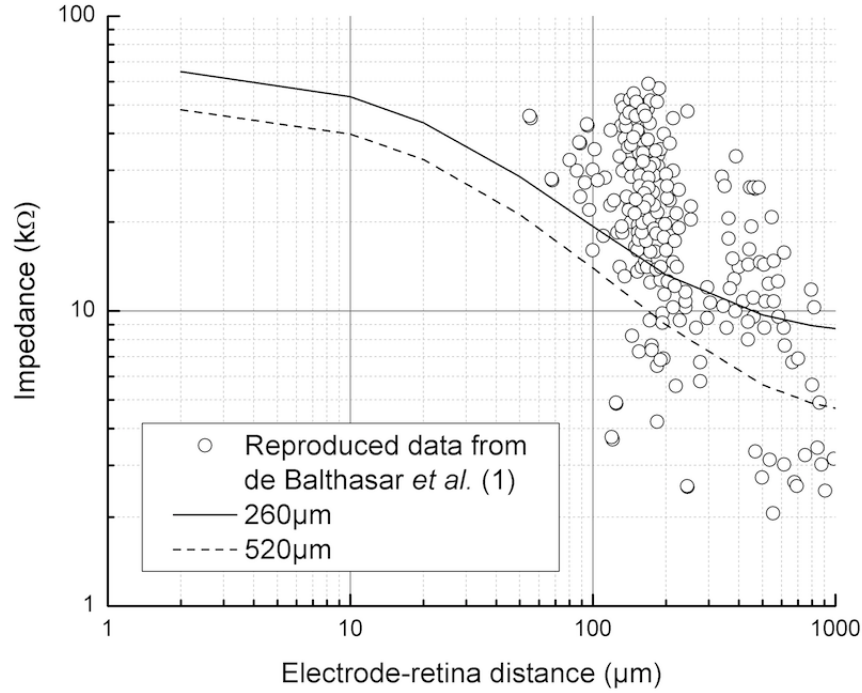


Figure 5.3: Impedance versus electrode-retina distance. Computed impedance change with variation in electrode distance from the retinal surface. The impedance during electrode-retina contact is not indicated. Impedance values for the contact condition for 260  $\mu\text{m}$  electrode: 70.5  $\text{k}\Omega$ ; 520  $\mu\text{m}$  electrode: 52  $\text{k}\Omega$ . Open circles are experimental data points from the Argus I clinical trials [de Balthasar *et al.* 2008]. The clinical data demonstrate large scattering of impedance but are grossly within the range of simulated values from our framework. A fitting of the experimental data is not completely relevant, but it would lead to an impedance-distance relationship that is not in contradiction with our simulations.

#### 5.3.4 Estimation of resolution based on spatial extent of stimulation

In our study, we have computed threshold currents for activation of a single RGC located at the cell activation depth ( $h_{GL}$ ) from the stimulation electrode. During actual experiments, to ensure stimulation, there is a tendency to use stimulation currents 10-20% above the pre-determined minimum threshold current. In our study, we define lateral extent as the horizontal distance (measured from the electrode axis) covered at  $h_{GL}$  corresponding to a threshold electric field of 1  $\text{kV/m}$  caused by a 20% excess on the threshold current (refer to Chapter 4 for illustration). Implant resolution can be calculated based on the lateral extent of stimulation for the electrodes. A relationship between the lateral extents of stimulation zone with varying electrode-retina distances for both the electrodes has been plotted in Figure 5.4. The lateral extent is proportional to the sum of the electrode-retina distance and radius of the electrode. The lateral



extent for a point source electrode (or very small electrodes) would be zero ideally. The linear-like relationship between the lateral extents of stimulation and the electrode-retina distance implies that the resolution of the implant drops with increasing electrode-retina distances for the electrode geometries studied.

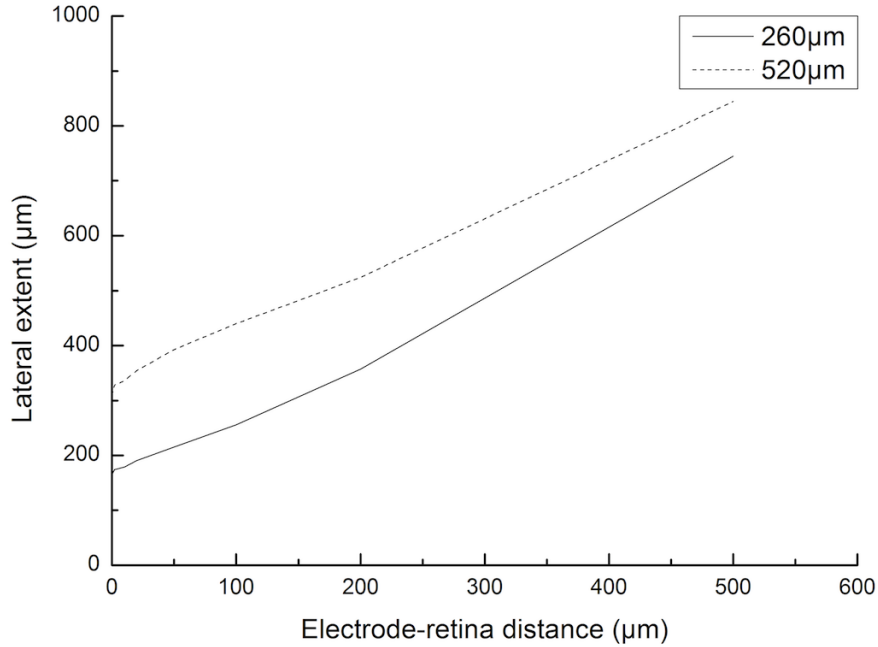


Figure 5.4: Lateral extent of stimulation versus electrode-retina distance. Relationship between the computed lateral extent of stimulation and the electrode-retina distance demonstrates that an increase in electrode-retina distances decreases the resolution of the retinal implant. The lateral extent is proportional to the sum of the electrode-retina distance and radius of the electrode. For a point source (or very small electrodes), the graph would cross the origin of the graph.

#### 5.3.5 Simulation vs. *in vitro* epiretinal stimulation - Our implant

In an attempt to simulate the *in vitro* experiments by our HUG collaborators, we computed the necessary thresholds and lateral extents under an epiretinal scheme for a model representing our implant.

Intracellular recordings were performed from individual ganglion cells in epiretinal configurations while electrical pulses were delivered through the electrodes in the array, one after the other, in order to determine individual cell activation thresholds as a function of distance from the stimulating electrode *i.e.* a lateral extent in a different form. The computed and experimental thresholds as a function of squared distance is presented in Figure 5.5.

A good agreement was found between the computed and experimental values of threshold measured as a function of the squared distance.

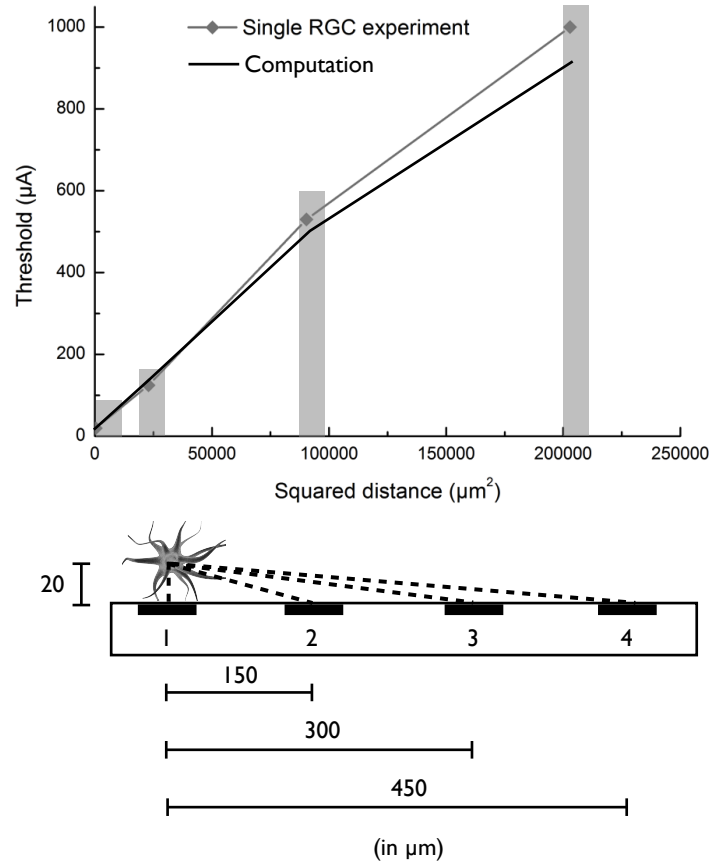


Figure 5.5: (Top) Thresholds as function of squared distance. Single RGC data is presented due to the difficulty with the experimental procedure. The computed profile is in good agreement with the experimental trend. (Bottom) An illustration of the squared distance (another definition for lateral extent) from the electrode position with respect to the neuron. The grey bars indicate threshold values for corresponding squared distance for each electrode. Courtesy: Unpublished data with kind permission from Dr. Alexandre Babalian (HUG)

#### 5.4 CONCLUSIONS

The simulations on the effect of geometrical factors, viz. electrode size and electrode distance to the retinal surface affecting impedance and threshold values is an indication of the importance of proximity between the electrode array and the retina for a successful retinal implant. The resolution of the implant can be estimated for different electrode-retina distances considering the computed lateral extents of stimulation.

Alternatively, the good accordance of simulations with *in vitro* experiments conducted by our HUG collaborators indicates the relevance of the measured resistivity profile of the chick retinas using our microprobe technique.

Electrode breakdown and tissue encapsulation effects, in spite of being extremely important in the viability of neural prostheses, have not been observed to be dominant in implanted human retinal prostheses studied until now. This could be due to the

fact that they have not been studied long enough to evaluate their performance under long term exposure to retinal milieus. Based on the threshold and impedance data collected during clinical epiretinal trials conducted in human subjects until now [de Balthasar *et al.* 2008, Mahadevappa *et al.* 2005], the variation in threshold current and impedance can be linked to changes in electrode-retina distance (Pg. 281, Chapter 14 of [Dagnelie 2011]). Hence, the pre-experimental computation of characteristic dependency between threshold and impedance is generally a significant guideline and supplemental information for surgeons and electrophysiologists. Furthermore, the presented simulation framework is a powerful and useful tool for implant designers - as it can be used to predict threshold of each electrode, irrespective of its geometry, in arrays of high electrode count targeted at high-resolution retinal stimulation in future.

An integrated simulation framework computing electric fields in the electrode-retina interface could help in understanding the effective operation of a retinal implant. Knowledge of current densities in the retinal tissue can resolve significant questions which include: design of implantable electrode arrays, a proper location for the implant to be placed, optimal electrode geometry and ground placement, efficiency of different shapes and sizes of electrodes, optimal inter-electrode spacing, maximum amount of current injected safely for a given configuration, efficiency of current injection and current circulation in a tissue for a particular scenario.



## SIMULATION OF SUBRETINAL PROSTHESES

---

### 6.1 INTRODUCTION

Most prostheses designed to interface with the retina rely on the hypothesis that a direct stimulation applied either to the outer layers of the retina or to the ganglion cell layer could restore sight to the patients.

Ganglion cells form the innermost retinal cell layer, relaying the transformed visual input to the brain, implying that they are the targets in either subretinal or epiretinal stimulation schemes. They can be excited either by direct or indirect electric stimulation applied through the intermediate retinal network. Indirect stimulation of ganglion cells is experimentally observed through activation of bipolar and amacrine cells [Fried *et al.* 2004] and also predicted theoretically by modelling bipolar cell stimulation [Gerhardt *et al.* 2010]. Based on the result that “short stimulation pulses are preferable for safety and efficacy considerations in subretinal prostheses and that direct activation of ganglion cells will be necessary for reliable activation during high-frequency stimulation” [Tsai *et al.* 2009a]; in this study, we are modelling direct activation of ganglion cells by extracellular stimulation. A simple passive model of extracellular stimulation [Coburn 1989] of the soma of a ganglion cell has been considered before for analytical studies [Palanker *et al.* 2005]. We consider a ganglion cell as a spherical neuronal soma and hypothesise its activation by assigning a cross-membrane depolarisation condition.

Patch clamp and extracellular multi-electrode recordings have been used to measure the threshold currents required to activate ganglion cells in both subretinal [Stett *et al.* 2000, Jensen and Rizzo 2007] and epiretinal [Jensen *et al.* 2005a, Sekirnjak *et al.* 2006] approaches. The threshold stimulation current applied on electrodes is one of the key elements in determining the performance of a retinal prosthesis. Palanker and co-workers [Palanker *et al.* 2005] approximated a threshold electric field of 3000 V/m to perform analytical calculations and draw predictions on various parameters affected during stimulation. In the present study, we define a typical threshold as the minimum stimulation current required to obtain an electric field of 3000 V/m at a certain distance between the stimulating electrode and the retinal ganglion cell.

A recent psychophysical study in blind human volunteers demonstrated a strong decrease in threshold charge delivered by the electrodes as a function of time after implantation [Wilke *et al.* 2010a]. We hypothesise that this decrease is linked to the discharge pattern of the current above the electrode as a result of changing measured impedance. Impedance variations may occur due to changes in electrode impedances due to various factors like physical and chemical changes in electrodes, mechanical alterations, retinal tissue remodelling in the process of degeneration, etc. Under ideal implantation conditions and assuming that electrode corrosion does not occur [de Balthasar *et al.* 2008], the impedance variation can be explained by two main theories:

1. Gliosis theory – a proliferation of glial cells at the site of a tissue injury or neuronal loss caused by surgical intervention and insertion of the implant.
2. Gap theory – soon after implantation, the retina may not be in intimate contact with the electrodes giving rise to a gap. This gap is predicted to be very small in the order of a few microns. It is likely that a close contact between the retina and electrodes is recovered within a few days. Similar post-implantation effect of an electrode-tissue gap is also observed between the target tissue and the stimulation electrodes immediately after a deep brain implantation [van Kuyck *et al.* 2007].

In the case of a glial reaction, new cells surround the electrode surface resulting in retinal ganglion cells moving farther away from the electrode. The highly resistive glial cells increase the impedance and consequently raise the threshold stimulation currents. On the contrary, when the retinal cells move closer to the electrode and fill the electrode-retina gap, it has the same effect of increasing the impedance due to the higher resistivity of the retinal cells [Heynen and van Norren 1985] and eventually reducing the threshold of stimulation currents.

A number of studies related to the experimental determination of threshold stimulation currents in subretinal stimulation on various species *in vitro* have been reported [Stett *et al.* 2000, Jensen and Rizzo 2008, Tsai *et al.* 2009a]. Despite the extent of literature on the stimulation parameters and methods, there is still a lack of understanding on the relationship between the electrical properties of the retinal tissue and the microelectrode specifications.

The aim of this chapter is to predict the threshold currents for subretinal stimulation of the retina by using a layered resistivity model of the retinal tissue. The stimulation of the retina is based on the direct activation of ganglion cells neglecting the contribution

of the inner layers within the retina. We assume a spherical neuronal soma model of a retinal ganglion cell with an electric field stimulation criterion of 3000 V/m. A lateral extent of the stimulation zone is estimated at the ganglion cell layer depth in the retina for a given value of stimulation current. Finally, the effect of an electrode-tissue gap on the threshold currents and impedance is analysed. We demonstrate a simple finite element simulation framework aimed at predicting the activation threshold currents for ganglion cells in the retina. We also demonstrate that the threshold stimulation currents can be correlated to the changes in impedance due to variations in the gap between the tissue and electrode.

## 6.2 METHODS

The reader is kindly advised to refer to Chapter 4 for more details on this section in relation with subretinal stimulation scheme as directed below at various places.

### 6.2.1 *Hypotheses for retinal stimulation*

The threshold current criterion and depth of RGC activation, was based on explanation in Chapter 4 for a subretinal scheme of stimulation.

### 6.2.2 *FEM modelling*

The adjustments in the FEM-based simulation framework was based on explanation in Chapter 4 for a subretinal scheme of stimulation. The necessary modifications to the framework in order to be able to study *in vitro* results from literature and from our HUG collaborators using our implant is also mentioned in Chapter 4.

### 6.2.3 *Animal model and impedance spectroscopy*

Impedance recordings were performed on P23H line 1 rats at least 3 months old which were implanted with custom made polyimide-based implants under a well defined surgical intervention protocol [Salzmann *et al.* 2006]. As described previously [Salzmann *et al.* 2006], the implants consisted of a 1 mm circular head and a 40 mm long shaft. The thickness was 22  $\mu\text{m}$ . There were four stimulating 50  $\mu\text{m}$  disc electrodes on each implant, surrounded by a large return electrode. The electrode geometry used in this modelling study is based on the electrode design used in these implants.

The impedance spectra were acquired using an Agilent 4284A impedance analyser, controlled by proprietary Java software. Electrodes were connected to the impedance

analyser via a 150 mm long, 5 pole-cable and a DIP-switch (Grayhill 90HBW05) mounted on a printed circuit board, to which the impedance analyser was connected. Measurements were carried out using a voltage of 50 – 1000 mV RMS with each frequency spectrum taken between 100 – 1 MHz, with the sweep starting at the highest frequency. The measurements were made between one of the four 50  $\mu\text{m}$  electrodes and the surrounding return electrode. The commercial software ZView<sup>TM</sup> was used to analyse the impedance data. The individual electric elements modelling the electrode-tissue measurement setup were extracted using a complex non-linear least squares fitting algorithm (CNLS) built into ZView<sup>TM</sup>.

A stimulation amplitude of 50 mV was selected for the subsequent impedance measurements to minimise the risk of tissue and electrode damage by excessive current densities. Smaller amplitudes however contributed to noisy measurements. The tissue impedance extracted from the electrical equivalent model was calculated at 10 kHz due to two main reasons:

1. Relevant as the applied stimulation pulse width is around 0.1 ms in high frequency stimulation.
2. This frequency appeared as a compromise for the different sample frequency spectra studied, *i.e.* the largest change in impedance occurred around 100 kHz right after implantation, whereas it occurred closer to 1 kHz after a few weeks.

### 6.3 RESULTS

#### 6.3.1 *Spatial extent of the threshold current*

For a given depth in the retina, the threshold current is increased for the cells located away from the axis of the electrode. In subretinal implants, the spatial extent of the stimulation represented in a cross section of the retina just above an electrode is shown in Figure 6.1. The different curves show the area that is stimulated by the electrode with the 3000 V/m criteria at different stimulation currents. For instance, the plot corresponding to the stimulation current of 3.5  $\mu\text{A}$  applied on the electrode is the locus of the electric field strength criterion. The threshold current value on the electrode axis is 39  $\mu\text{A}$  for GL. In this case, theoretically, just one cell is stimulated right above the electrode at the height measured subretinally. Higher values of stimulating current correspondingly stimulate cells over a wider space above the electrode. This can be seen from the curve corresponding to the locus of 59  $\mu\text{A}$  stimulation current, where the



lateral stimulation zone extends to about  $190\text{ }\mu\text{m}$  off-axis from the electrode for GL layer. The simulations show that the excitable cells in the GL region can be stimulated with threshold currents above  $39\text{ }\mu\text{A}$  using our subretinal electrodes. It is also seen that the ganglion cells can no longer be stimulated at a lower value than this threshold current.

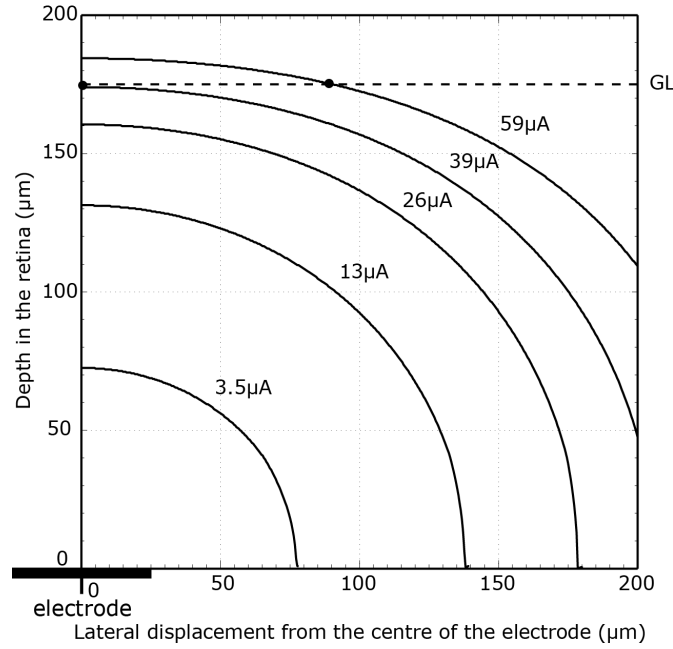


Figure 6.1: Spatial extent of threshold stimulation criterion met for different electrode currents in a subretinal scheme. The points along the horizontal line at GL ( $175\text{ }\mu\text{m}$ ) represent the lateral extent of stimulated cells with two different currents. The thick black horizontal bar represents the location of the electrode.

Figure 6.2 shows the evolution of the threshold currents with the lateral distance from the axis of the stimulation electrode. The off-axis threshold currents increase almost in a quadratic manner with lateral distance from the electrode axis implying that larger currents are required to stimulate wider area of cells away from the axis of the electrode.

A maximal admissible current during stimulation is based on the hypothesis of an electrochemical limit. For an electrode current  $\sim 69\text{ }\mu\text{A}$  applied for  $0.1\text{ ms}$  on a  $50\text{ }\mu\text{m}$  diameter disc electrode, the electrochemical limit of  $\sim 0.35\text{ mC/cm}^2$  [Brummer and Turner 1977] for platinum is reached. It is seen that the computed minimum threshold stimulation current of  $\sim 39\text{ }\mu\text{A}$  required for stimulating the GL is approximately a factor two below the electrode current at the electrochemical limit.

### 6.3.2 Effect of a gap between the electrode and the retinal tissue

The electrode-tissue gap plays an important role in the electric potential distribution above the stimulation electrode and consequently the strength of the threshold currents originating from the electrode. There is also a significant impact on the impedance due

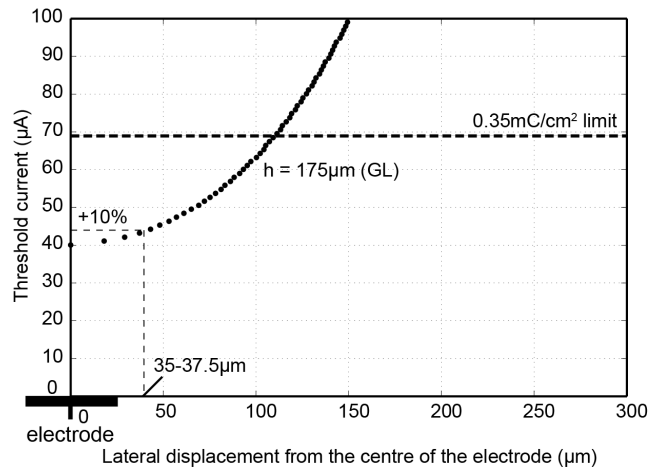


Figure 6.2: Evolution of the threshold currents (3000 V/m criterion) in the GL vs. the lateral distance from the electrode axis. The thick black horizontal bar represents the location of the electrode. A 10% increase in stimulation current from minimum stimulation current results in a lateral extent of 70-75  $\mu\text{m}$  in the GL.

to the space between the electrode and the retinal tissue being gradually replaced by a fluid more conductive than the retina itself. We will now study both these effects of a gap between the electrode and the tissue by varying the gap between the retina and implant surface in the FEM model.

#### *Effect on threshold currents*

Figure 6.3 shows the dependence of the on-axis stimulation current required to reach the 3000 V/m criterion in the GL as a function of the gap between the stimulation electrode and the bottom surface of the retina. It is seen that the threshold current increases rapidly in the GL as the gap between the electrode and the tissue increases. As a result, the electrode electrochemical limit is reached when the gap exceeds 5  $\mu\text{m}$  for GL stimulation.

#### *Effect on impedance*

Knowledge of impedance can be used as an indirect measurement of the electrode-tissue gap. Previously, impedance analysis [McMahon *et al.* 2006, Johnson *et al.* 2007] has been employed to estimate the electrode-retina distance by measuring the changes in impedance that occur when the implant moves closer or away from the retina. It is also well known that Advanced Optical Coherence Tomography (OCT) imaging technique can be used to determine the distance between an electrode and tissue in *in vivo* post-implantation [de Balthasar *et al.* 2008]. On the contrary, for a non-transparent

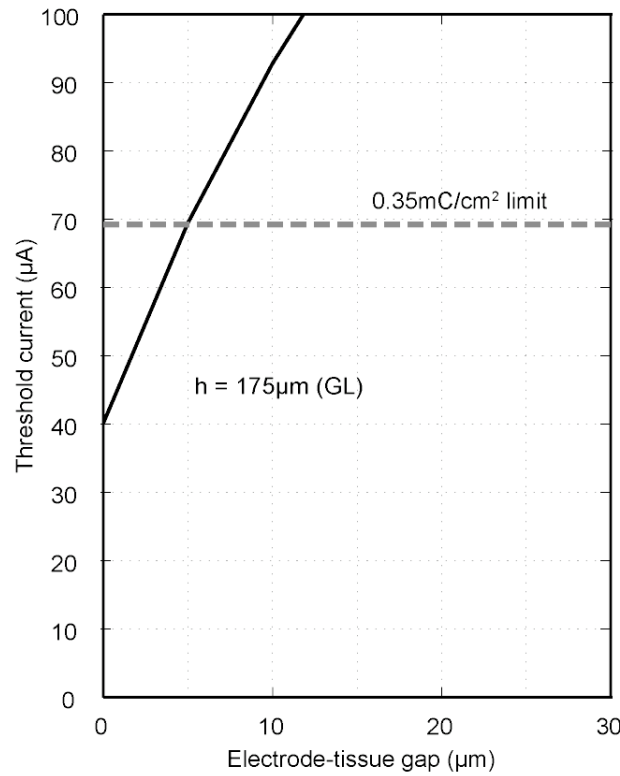


Figure 6.3: Dependence of the on-axis threshold current with the electrode-tissue gap at GL in the retina.

implant, OCT methods have the drawback of revealing only the proximity of edges of the implant with respect to the retina.

Our simulation framework can predict the gap between an electrode and tissue by relating computed values with actual measurements of impedance. Figure 6.4 shows the computed impedance as a function of the gap between the retina and the stimulation electrode. The impedance decreases with increasing gap values. A gap of  $50\mu\text{m}$  is sufficient to decrease the impedance by a factor of 10 and almost attain a resistivity equivalent to that of the PF. The line at  $36\text{ k}\Omega$  corresponds to the computed impedance of the PF as seen by the stimulating electrode with respect to the ground.

*In vivo* impedance measurements, presented in Figure 6.5, demonstrate that the impedance measured just after subretinal implantation in rats [Salzmann *et al.* 2006] is appreciably lower than the expected value obtained when there is a close contact between the electrode and retina. This corresponds to the hypothesis of an electrode-tissue gap. Typically, after 20 days, the electrode impedance increases to a high value. It is observed from additional measurements after two months that the attained high value remains stable. This situation corresponds to a small electrode-tissue gap in our model.

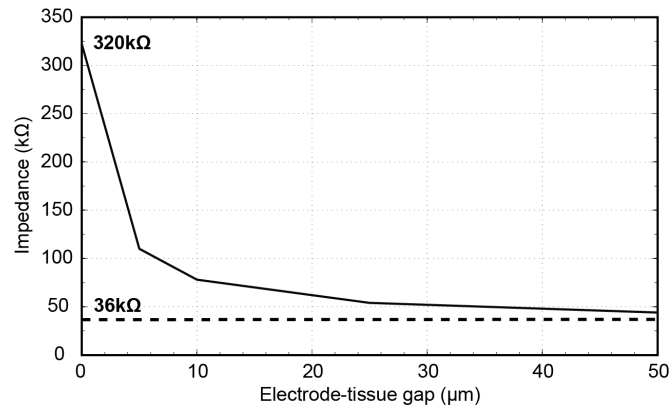


Figure 6.4: Variation of impedance with changes in electrode-tissue gap.

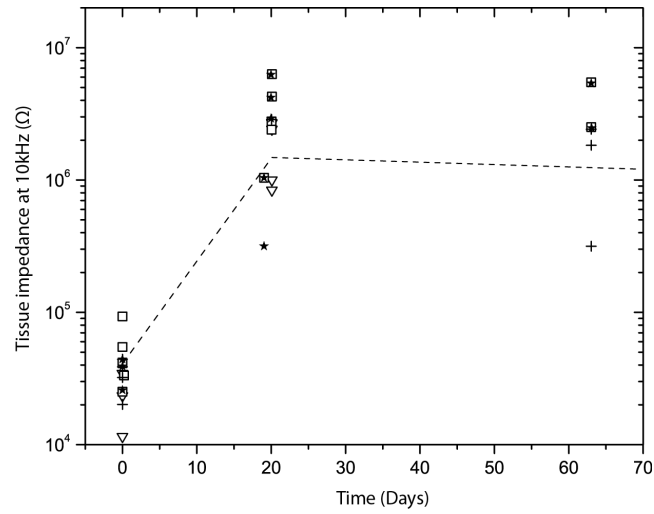


Figure 6.5: Evolution of the *in vivo* electrical impedance of retinal tissue measured at 10 kHz in rats during a two-month period. The impedance measurements were performed with implanted rats that exhibited low fibrous reaction.

## 6.4 DISCUSSION

Using FEM simulations, this report investigated the estimation of spatial extent of the threshold currents and the evolution of threshold currents with lateral distance in the GL for subretinal stimulation. The effect of electrode-tissue gap on the threshold current and impedance was also studied.

### 6.4.1 Threshold current

Stimulation experiments conducted by independent research groups indicate that the thresholds for activating the ganglion cells vary depending on the manner of activation – direct or indirect, pulse type, time-course, polarity and many other unknown parameters. Based on our assumptions, the computed thresholds for direct activation were expressed as charge densities. The value is in the order of  $0.2 \text{ mC/cm}^2$  in the GL for a balanced,

cathodic-first, rectangular stimulus with a pulse duration of 0.1 ms. These compare with the threshold charge density values obtained from *in vitro* subretinal stimulation trials by Tsai *et al.* [Tsai *et al.* 2009a]. They experimentally determined that short balanced biphasic pulses of the order of 0.1 ms/phase directly activated retinal ganglion cells with a threshold charge density ranging between  $0.06 \text{ mC/cm}^2$  and  $0.12 \text{ mC/cm}^2$ .

Considering the limitations of our passive model, the computed thresholds were close to the values obtained by Tsai *et al.* Based on the comparison with their measurements, we predict a higher limit for the threshold currents.

#### 6.4.2 Spatial extent of stimulation

The spatial resolution of a local electrical stimulation triggered by a monopolar electrode is related to the spatial extent of the elicited retinal response. The retinal response is directly related to the activation of spatially distributed ganglion cells in the GL. We computed a near-quadratic variation of threshold current with increasing lateral distances from the electrode centre for the geometry presented. During actual experiments, to ensure stimulation, there is a tendency to use stimulation currents 10-20% above the pre-determined minimum threshold current. For a 10% excess on the minimum threshold current, it is observed from Figure 6.2 that a spatial region of  $70\text{-}75 \mu\text{m}$  is in the zone of stimulation at GL. Eckhorn *et al.* [Eckhorn *et al.* 2006] quote in their paper concerning *in vitro* experiments performed by Stett *et al.* in normal and degenerated rat retinas that the spatial resolution at retinal level, subretinally stimulated by multi-electrode arrays, is at least  $70 \mu\text{m}$ . This limiting value is a good starting point to associate with the spatial resolution computed at the GL in our FEM model. Our FEM framework predicts a realistic spatial resolution for the simulated geometry and retina model presented. Consequently, these values can be used as a guideline for determining density of stimulation electrodes needed to attain reasonable resolution using current and future retinal implants.

#### 6.4.3 Effect of electrode size

In this study, the effects of an inhomogeneous retina and the electrode-retina gap on subretinal stimulation using a  $50 \mu\text{m}$  diameter disc electrode were computed. Increasing electrode size has proven to increase thresholds in epiretinal stimulation [Sekirnjak *et al.* 2006]. It also has the effect of reducing the spatial resolution for epiretinal stimulation. In contrast to these results, we performed simulations in subretinal mode to predict the

direct ganglion cell stimulation thresholds and the lateral extents. The lateral extents for smaller electrodes (up to  $5\mu\text{m}$ ) were only slightly lesser than with the  $50\mu\text{m}$  discs. For larger sizes (up to  $200\mu\text{m}$ ), both the stimulation threshold and the lateral extents increase marginally. Table 4 displays the computed threshold values for each of the electrode sizes simulated.

ELECTRODE SIZE ( $\mu\text{m}$ )	STIMULATION THRESHOLD ( $\mu\text{A}$ )	LATERAL EXTENT ( $\mu\text{m}$ )
5	39.5	65-70
10	39.5	65-70
25	39.6	70
50	40.5	75
100	43	100
200	54.7	140

Table 6.1: Computed thresholds of stimulation and lateral extents for different electrode sizes.

We also deduced that in smaller electrodes up to  $50\mu\text{m}$ , similar values of threshold currents imply large current densities eventually giving rise to electrochemical problems during stimulation. Additionally, reducing electrode size implies a larger impedance which leads to higher voltages on the electrode surface. This has an impact on the voltage delivering capabilities of the power source used for firing up the electrodes.

#### 6.4.4 *Effect of electrode-tissue gap*

In chronic retinal implantations, there have been no observations of a fibrotic or gliotic capsule surrounding the implant area [Chow *et al.* 2001, de Balthasar *et al.* 2008]. A mention on the stimulation electrodes unaffected by corrosion [de Balthasar *et al.* 2008] also indicates that they are mostly electrochemically stable. To our best knowledge, explicit records of impedance measurements over a period of time after subretinal implantations are not available apart from the ones (refer Figure 6.5 above) shown in this study. But, recent results [Wilke *et al.* 2010a] on post subretinal implantation threshold voltage measurements with time along with computed threshold charge suggest a time variation of impedance in agreement with our hypothesis. This may

imply that the change in impedance is mainly due to the gap between the tissue and the electrode. Our FEM computations on the effect of an electrode-tissue gap on the impedance anticipate that it is the gap closing between the electrode and the retina which contributes mainly to the increase of impedance and not the resistivity of the encapsulating tissue surrounding the implanted electrode in retinal implantations.

From the simulation results it can be concluded that the impedance measured immediately after subretinal implantation may correspond to the electrode-tissue gap filled with PF. The value of the impedance reached post-implantation after a certain settling period corresponds to the impedance measured for a small electrode-tissue distance. This hypothesis is supported substantially by the impedance variation over time measured *in vivo* as demonstrated in Figure 6.5. Consequently, the low impedance measured immediately after implantation corresponds to a leakage of current resulting from the gap present between the electrodes and the tissue. The increase of impedance is a sign of the achievement of an intimacy between them.

Interestingly, we can deduce a relationship between variations in threshold current with changes in impedance. The association between them is presented in Figure 6.6 which is essentially a combination of results in Figure 6.3 and Figure 6.4. Similar behaviour has been observed in measurements with epiretinal implants on human subjects [de Balthasar *et al.* 2008]. We postulate that monitoring impedance is not only an effective and simple method to check the integrity of the implant; but with an appropriate electrical model of the retina it can predict a realistic stimulation current.

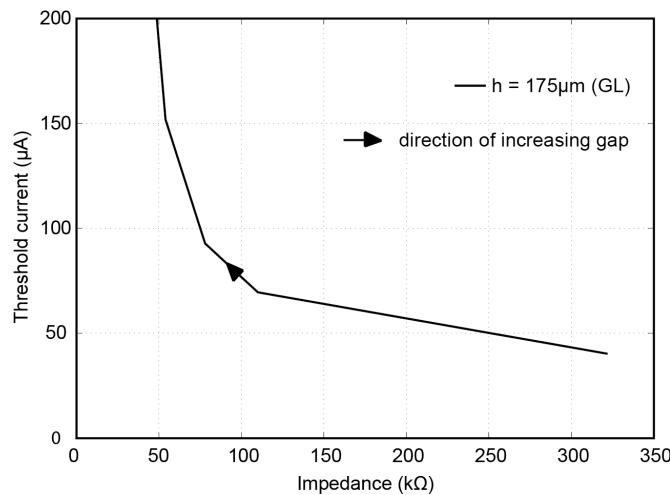


Figure 6.6: Relationship between the threshold current and the corresponding impedance for increasing electrode-tissue gap values. No gap ( $0\mu\text{m}$ ) corresponds to an impedance of  $320\text{ k}\Omega$  as shown in Figure 6.4. Higher values of gap result in lower impedance and higher thresholds.

#### 6.4.5 Simulation vs. *in vitro* subretinal stimulation - Our implant

In an attempt to simulate the *in vitro* experiments by our HUG collaborators, we computed the necessary thresholds and lateral extents under a subretinal scheme for a model representing our implant.

Intracellular recordings were performed from individual ganglion cells in subretinal configurations while electrical pulses were delivered through the electrodes in the array, one after the other, in order to determine individual cell activation thresholds as a function of distance from the stimulating electrode *i.e.* a lateral extent in a different form. The computed and experimental thresholds as a function of squared distance is presented in Figure 6.7.

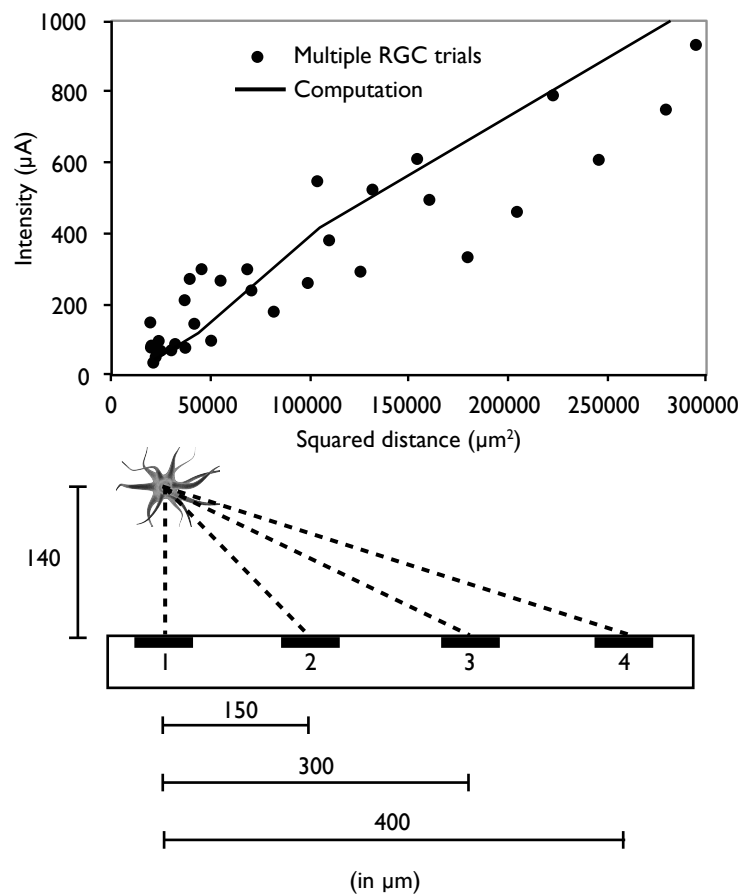


Figure 6.7: (Top) Thresholds as function of squared distance. Data from 15 RGCs is presented. The computed profile is in good agreement with the experimental trend. (Bottom) An illustration of the squared distance (another definition for lateral extent) from the electrode position with respect to the neuron. Courtesy: Unpublished data with kind permission from Dr. Alexandre Babalian (HUG)

A good agreement was found between the computed and experimental values of threshold measured as a function of the squared distance.



## 6.5 CONCLUSION

Understanding electrode-tissue interactions is a key to efficient and successful stimulation by a retinal prosthesis. Through the current study, we have shown that it is possible to study subretinal stimulation applying an electric resistivity model of the retina in a finite element simulation framework. The following conclusions can be drawn based on our simulation study:

1. Employing the 3000 V/m criterion on a spherical neuronal soma model of a retinal ganglion cell results in the prediction of the maximum limits of threshold current and lateral extent of stimulation to which *in vivo* experiments conducted by various researchers can be benchmarked.
2. The effect of an electrode-tissue gap is to increase threshold currents and decrease the impedance. The increasing impedance related to a closer proximity of the retina to the electrodes in our model is well supported by *in vivo* tissue impedance measurements. Therefore, the impedance can be a tool to monitor electrode-tissue gap and predict stimulation current simultaneously.

Alternatively, the second occurrence of good agreement between simulations and *in vitro* experiments conducted by our HUG collaborators confirms the relevance of the measured resistivity profile of the chick retinas using our microprobe technique.

We conclude that the importance of performing impedance measurements after implanting stimulation devices, ensuring the close contact of target neural tissue with the stimulation electrodes, is instrumental in successful neural stimulation. With further refinement and validation, it may be possible to use our method to design and simulate different electrode geometries that optimise stimulation efficiency of the retina, and the techniques used in this method can be expanded to electrodes used in other neural stimulation devices.



## CONCLUSION

---

### 7.1 SUMMARY OF MAIN RESULTS

The contribution of this dissertation can be summarised by two key points. First, a simulation platform that can assess the factors that affect RGC activation by retinal prostheses was formulated and constructed with preliminary validation. Secondly, using a specially microfabricated bipolar microprobe, measurements were conducted to determine a high resolution resistivity profile of the cross-sectional layers of a retina.

The requirement for modelling approaches is to understand the mechanisms that underlie retinal stimulation. Factors that can influence the electrode-retina interface include the stimulus pulse, electrode shape, electrode position, and retina cell density. Two of these factors, namely electrode size and electrode position with respect to the retina, and their effect on the activation of retinal ganglion cells was estimated in this dissertation using a simulation framework. Effect of both factors on stimulation thresholds was documented and compared to previously published results. For both epiretinal and subretinal configurations, they were found to be in agreement. Furthermore, evaluation on lateral extents of stimulation provided an insight into the resolution capabilities of the retinal implant under monopolar stimulation scheme. By impedance computations with varying electrode-tissue gap, it is even possible to predict the proximity of the retinal tissue to the electrodes of the implant as shown in the chapter of subretinal simulations (refer Chapter 6). In addition to the computation of current, charge density and the neural stimulation threshold, it is also possible to determine the neural injury and electrochemical limits. Owing to the wide range of study possibilities that this simulation framework offers, it should be considered to be the primary contribution offered by this dissertation.

As a *raw material* for the first contribution, an electric retinal model was a necessity in the building of a simulation framework. It is well known that the inherent electrical inhomogeneity of the retina alters the potential and electric field distribution within the retina created by extracellular stimulation. The activation of RGCs depend on the spatial formation of voltage gradients in their own vicinity. In this work, a localised,

direct method for experimentally determining the anisotropic electric properties of the retina is presented. The device was validated by profiling rat and embryonic chick retinas. The resistivity at each retinal depth was calculated based on tissue resistance extracted by peak resistance frequency methodology. Although, it was qualitatively established that the resistivity-depth profiles were in accordance with earlier studies, but were quantitatively different due to a configuration attributed by local and probably more accurate resistivity measurements. It was observed that resistivity at any arbitrary retinal depth is characterised by a unique peak resistance frequency. The computations, using the constructed electric model of chick retina, corresponded well to the *in vitro* stimulation experiments conducted by our collaborators at HUG using our implant; confirming the relevance of the obtained resistivity data in embryonic chicks and the used measurement method. This method is another major contribution of this work and to the area of modelling retinal stimulation since it provides a robust experimental method to extract resistivity profiles from the retina of any species including humans.

## 7.2 SIGNIFICANCE OF CONTRIBUTION TO KNOWLEDGE

The capability of modelling studies to evaluate factors affecting retinal stimulation can significantly improve the quality of future retinal prostheses, and will be an aid to surgeons and neurophysiologists. Previous methods attempting to model retinal prostheses, either do not consider a realistic geometry of the bioelectronic system; or study the sole influence of one of the factors like electrode geometry/size or electrode-retina distance only. By integrating the various elements of a retinal prosthesis into a single simulation framework, simply provides more accurate assessment of efficacy and safety of retinal stimulation. A platform has been set for future improvements on our framework to address other factors and move a step closer to a more complete modelling framework.

The most important element of a model for retinal stimulation is the retina itself. Until now, most researchers in this field have not considered an accurate model of the retina. In an ideal biophysical model of the retina, it would be essential to have detailed mapping of the resistivities across its various layers. Such demands for high resolution retina resistivity profiling has been accomplished by the measurement technique demonstrated in this work.

### 7.3 FUTURE OUTLOOK

It is possible to consider many other parameters and factors and incorporate in the simulation framework presented in this dissertation which is relatively in its infancy, in terms of options currently forming its repertoire. The limitations specified in Chapter 1 (refer section 1.6) will always be candidates for the upgraded version of the simulation framework. Relatively simple to implement but probably computationally intensive additions to the framework could be to consider electrode surface properties, ganglion cell density, etc. The most interesting future directions in the opinion of the author are:

#### 7.3.1 *Comsol-NEURON integration*

The most exciting of the approaches involves an integration of multiphysics properties of Comsol and the neurophysiological computing power of NEURON. The methodology is more useful for simulating indirect stimulation of retina as the full potential of NEURON in handling intercellular connections within retina is tapped. The working mechanism is rather simple. Voltages in three dimensional space within the volume conductor or retina caused by extracellular stimulation is captured by Comsol for a given excitation on the electrode(s). These voltages can subsequently be fed into different compartments of the target cell by voltage clamps in NEURON. Based on the time variation of voltage and the stimulus shape, there would be specific electrophysiologic processes activated within the cell. It would then be possible to verify if the cell has fired an action potential or in other words reached the state of activation. Hence, it is possible to benefit from the physical accuracy of FEM based Comsol and the neurophysiological activity simulator in Neuron making the simulation framework closer to being ideal. A more powerful approach consists of writing a stand-alone Matlab code that functions like NEURON and since Comsol is based on Matlab, a full integration could be achieved.

#### 7.3.2 *Electrode array*

Future generations of high resolution retinal prostheses comprise dipolar or multipolar electrode arrays [Wilke *et al.* 2010b]. This dissertation considers monopolar configuration alone. It is a computing challenge for Comsol to represent simultaneous stimulation by 1000 electrodes, as an example. Once a methodology to represent an electrode array is established, various analyses like crosstalk between electrodes, heat dissipation of the implant, etc. can be performed. Subsequently, an estimation of efficiency of such retinal implants can be easily determined.

### 7.3.3 *Pulse dependent stimulation*

In Chapter 2, it was mentioned that charge and charge density together contribute towards safe stimulation of the retina. Based on the pulse shape and duration, time dependent simulations using electrostatics combined with thermodynamics module, a heat profile can be generated. This can be used to compute the temperature increase in the volume conductor indicating retinal damage, if any. Cell membrane properties can be modelled permitting us to study electroporation [Palanker *et al.* 2007] related phenomena as well. By integrating this module with the ones explained above and existing properties of the framework described in this dissertation, it is possible to achieve a simulation framework closer to the actual implantation conditions.

## 7.4 VERDICT

Owing to nature, not every biological problem has a mathematical or physical explanation and therefore it is almost impossible to have a simulation framework that considers all phenomenon occurring during retinal stimulation. Even if there is, it would probably be practically impossible or time consuming to compute such a complex mathematical problem.

This dissertation attempts to utilise a piecewise linear electric model of the retina obtained from a robust experimental setup to extract resistivity profiles from the retina of any species including humans. In conjunction with the electric model of retina, the finite element model and simulation framework proposed for electric field estimation in retina provides scope to incorporate many of the discussed parameters and factors affecting neural stimulation and evaluating the efficiency of retinal prostheses. The developed simulation framework computes stimulation thresholds and impedance that can form a reference for quality control during surgery while inserting implants in the eye and functionality checks by electrophysiologists. Furthermore, this framework is useful in deciding the specifications of stimulation electrodes such as optimal size, shape, material, array density, and the position of the reference electrode to name a few. The work presented here offers to aid in optimising retinal prostheses and implantation procedures for patients and eventually contribute towards improvement of their life quality.

## Part II

### APPENDICES





## MICROFABRICATION PROTOCOL FOR THE MICROPROBE

Substrate: Silicon test wafer, <100>, 4", 525  $\mu\text{m}$







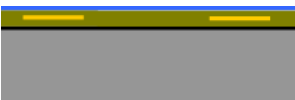
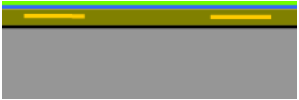


Illustration	Description
	1. Deposit TiW (500 nm) / Al (1000 nm) sacrificial layer
	2. Spin Polyimide PI2611 (several layers, 1400 rpm each) and hard bake
	3. Deposit Ti (50 nm) / Pt (200 nm) / Ti (50 nm) using SPIDER with Ti using RF target
	4. Photolithography, METAL mask. S1818 3.5 $\mu\text{m}$ might require double bake. 12 s exposure at 10 mW
	5. Pt etch using STS. Pt etch also does Ti layers. Resist removal.
	6. 2nd polyimide layer coating and hard bake. Slow ramp up to 300°C.
	7. Deposit SiO <sub>2</sub> using SPIDER

Illustration	Description
	8. HMDS/Oxygen plasma treatment for 20 minutes for making sure the adhesion resist in the next to SiO <sub>2</sub>
	9. Photolithography, PI mask. S1818 3.5 μm might require double bake. 12 s exposure at 10 mW. Manual development preferred
	10. Oxide, Polyimide and Oxide etch in STS. Polyimide etch time varies (~1 μm/min)
	11. outside of clean room: Aluminium dissolution and 5s of 1% HF dip to remove the protective Ti layer

## SUPPLEMENTARY INFORMATION ON RESISTIVITY PROFILING EXPERIMENT

All simulations were performed considering the electrode interface components at the experimental PRF of 375 kHz (frequency at which the solution resistance is extracted during actual measurements). The electrode interface behaviour was modelled based on a thin layer approximation similar to the one implemented by Cantrell *et al.* [Cantrell *et al.* 2008].

### B.1 ELECTRIC FIELD PENETRATION DEPTH

Refer to the section *materials and methods* (subheading 'Electrode design and fabrication')

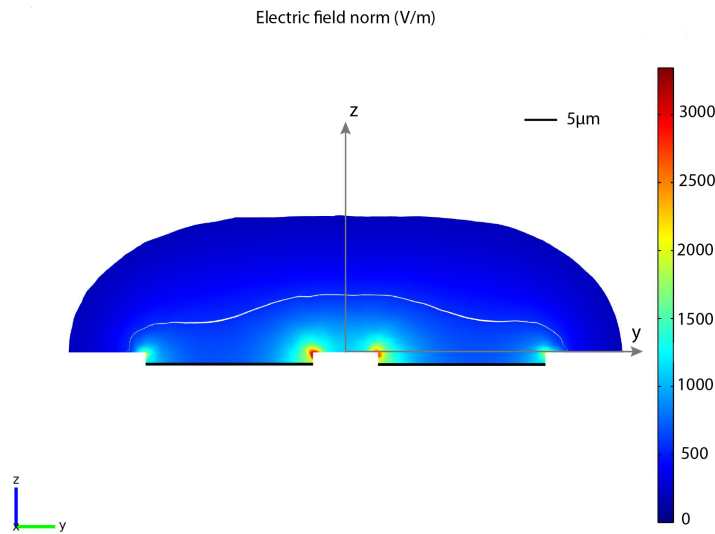


Figure B.1: Quasistatic simulation (Comsol 4.1) of the electric field norm for the bipolar electrodes in Ringer's solution ( $1.5 \Omega \cdot m$ ) for an excitation of 25 mV at 375 kHz (frequency at which the solution resistance is extracted during actual measurements). The penetration depth of electric field is achieved at  $8.3 \mu m$  (on the z-axis) where the electric field is half the value obtained on the axis ( $y=0$ ) of the microprobe surface ( $1100 V/m$ ). The white band in the plot represents the zone for penetration depth across the geometry. The two thick black lines represent the electrodes.

## B.2 COMPUTED CELL CONSTANT

Refer to the section *materials and methods* (subheading 'Measurement method and modelling') of Chapter 3.

The cell constant from simulation of the bipolar electrodes can be calculated as follows. Using Comsol, an integration of current density norm over the return electrode gives a current of  $\sim 0.72 \mu\text{A}$  for an applied excitation voltage on the electrode,  $V_a$  of 25 mV. The computed solution resistance,  $R_{sc}$  is calculated as:

$$R_{sc} = \frac{V_a}{I_c}$$

where,  $I_c$  – computed overall current in the system

Leading to an  $R_{sc} = 34830 \Omega$ .

We know that cell constant,  $k_{bipolar}$  in Ringer's solution of known resistivity,  $\rho_{Ringer} = 1.5 \Omega \cdot m$  can be calculated knowing the resistivity of the medium and the solution resistance as follows:

$$k_{bipolar} = \frac{R_{sc}}{\rho_{Ringer}}$$

Hence, we obtain a cell constant of  $232.2 \text{ cm}^{-1}$  from simulation.

## B.3 IMPEDANCE STABILISATION WITH TIME

Refer to the section *materials and methods* (subheading 'Measurement apparatus and protocol') in Chapter 3.

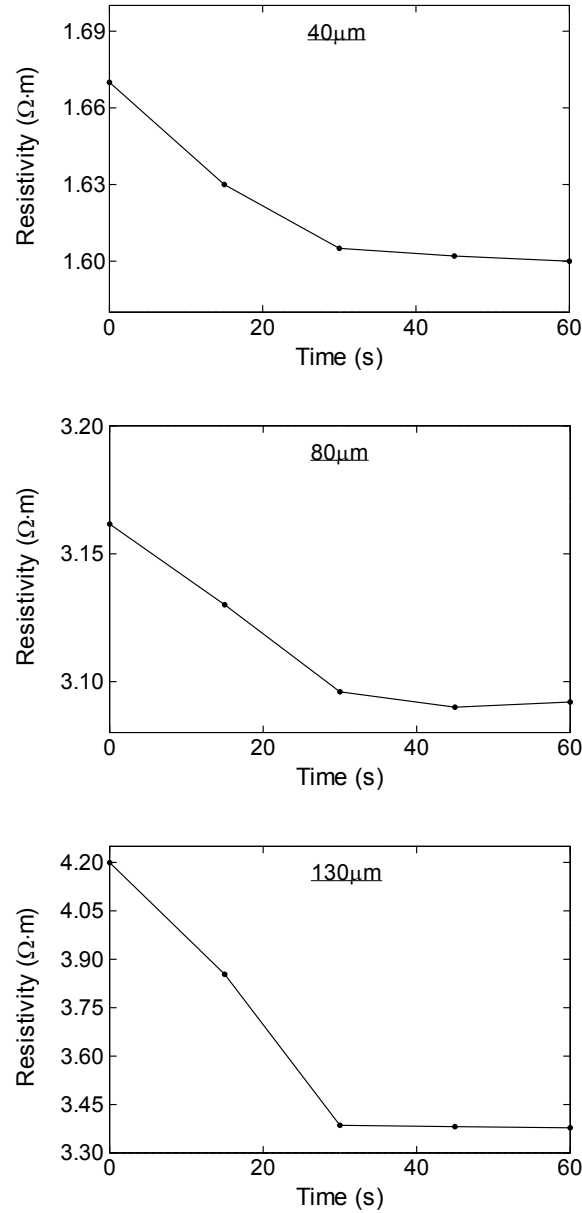


Figure B.2: Resistivity (directly calculated from impedance at peak resistance frequency) stabilisation with time for measurements at three arbitrary depths (40  $\mu m$ , 80  $\mu m$  and 130  $\mu m$ ) in a rat retinal slice is presented above. After the microprobe was displaced to a depth in the retina, a series of impedance spectra were recorded within intervals of 15 seconds each. Based on the above resistivity changes with time, it was established that the time to wait before valid measurements be recorded was 30 seconds.

#### B.4 SIMULATION ON REDUCTION OF FRINGING EFFECTS

Refer to the *discussion* section (First paragraph on reduction of fringing effects) of Chapter 3.

Using Comsol 4.1, a DC simulation between bipolar electrodes with sharp and rounded corners was simulated. The current density norm - surface and contour plots were generated at an excitation voltage of 25 mV.

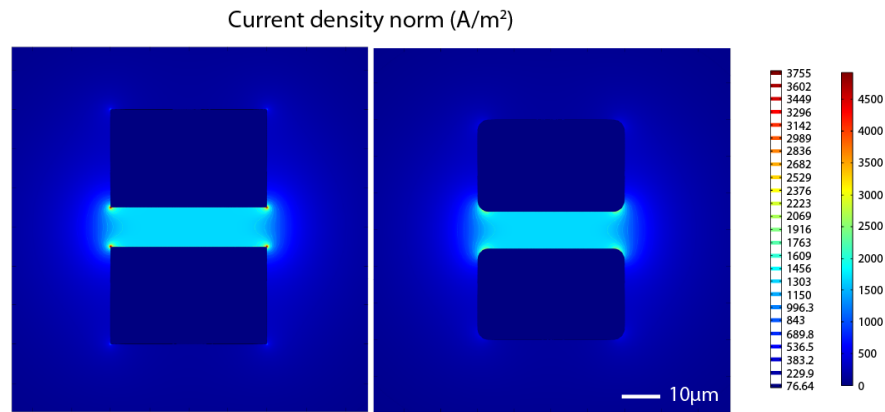


Figure B.3: Comparison through a DC simulation of bipolar electrodes with sharp corners (left) and rounded corners (right) used in this study. Sharp electrode edges produce high electric field zones that may lead to fringing effects and local tissue heating and damage during an actual trial.

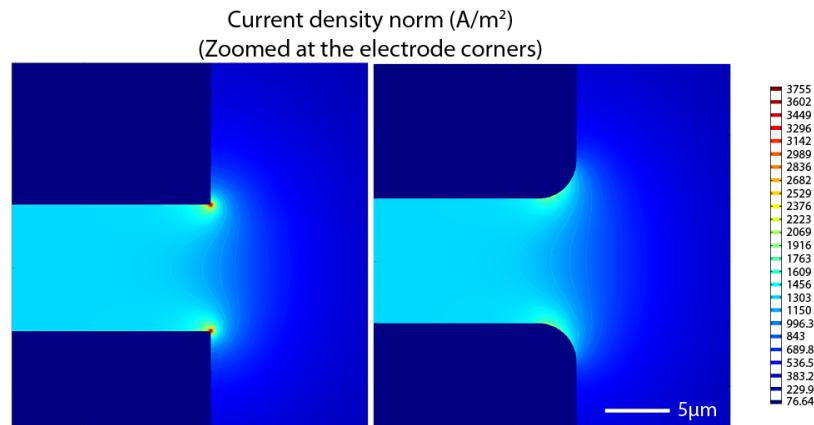


Figure B.4: A zoom in the region of electrode corners reveals an improvement against fringing effects of rounded corner electrodes in comparison with their sharper counterparts.

## MISCELLANEOUS SIMULATIONS AND CALCULATIONS

---

### C.1 VALIDATION FOR NEGLECTING ELECTRODE INTERFACE

The model of the electrode-electrolyte interface followed by calculations is contained in this section.

#### C.1.1 *Electrode-Electrolyte Interface*

The electrode-electrolyte interface is composed of Faradaic (charge transfer resistance,  $R_{CT}$ ) and non-Faradaic (constant phase element,  $Z_{CPA}$ ) components.

Equations used:

$$Z_{CPA} = K \cdot (i\omega)^{-\beta} \quad (C.1)$$

where  $K$  and  $\beta$  are considered to be constants in most early studies of the electrode-electrolyte interface, but Richardot and McAdams have examined these values and demonstrated that while they remain relatively constant at low driving voltages, they show a strong dependence on overpotential when those voltages are increased.

$$R_{CT}(\eta) = \frac{\eta}{I_0} \cdot \left( e^{\alpha_a \cdot \frac{nF}{RT} \cdot \eta} - e^{-\alpha_c \cdot \frac{nF}{RT} \cdot \eta} \right)^{-1} \quad (C.2)$$

where,

- $R$  universal gas constant,
- $T$  temperature in Kelvin,
- $F$  Faraday's constant,
- $n$  number of electrons per molecule participating in the reaction,
- $I_0$  exchange current,
- $\eta$  overpotential, and
- $\alpha_a$  and  $\alpha_c$  transfer coefficients.

Constants used (refer [[Cantrell \*et al.\* 2008](#)] and [[Richardot and McAdams 2002](#)]):

The values were normalised for electrode surface area appropriately:

$$K = 1.57 \Omega \cdot m^2 s^{-\beta}, \beta = 0.91, n = 2, I_0 = 6.41 \times 10^{-4} A \cdot m^2 \text{ and } T = 298 K$$

$$K = A \cdot e^{-\left(\frac{|\eta|}{\sigma}\right)^2}$$

$$\beta = a \cdot (|\eta|)^4 + b \cdot (|\eta|)^3 + c \cdot (|\eta|)^2 + d \cdot (|\eta|) + e$$

$$A = 1.5785 \Omega \cdot m^2 s^{-\beta}, \sigma = 0.1552, a = -3.736, b = 3.852, c = 0.3697$$

$$d = -1.2112 \text{ and } e = 0.9244$$

Additional constants for the Butler-Volmer equation for  $R_{CT}$ :

$$\alpha_a = 0.5, \alpha_c = 0.5, n = 2 \text{ and } T = 298 K$$

$$F = 96484.6 C \cdot mol^{-1}$$

$$R = 8.3144 J \cdot K^{-1} \cdot mol^{-1}$$

Insulator-electrolyte interface was incorporated also as described by Cantrell *et al.* [Cantrell *et al.* 2008] to avoid leakage of current into the insulator during simulations.

Equations C.1 and C.2 along with the values of constants were implemented in Comsol as shown in Figure C.1.

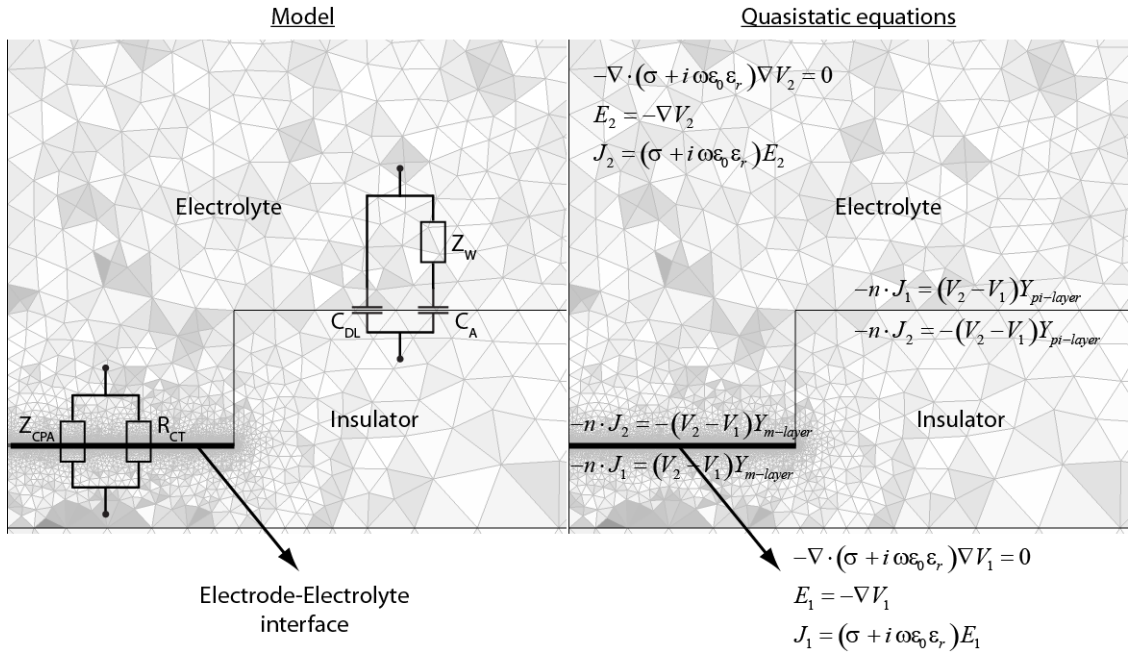


Figure C.1: (Left) Circuit equivalents and (right) quasi-static equations representing the boundary conditions



## C.1.2 Calculations

Incorporating equations C.1 and C.2 as described by Cantrell *et al.*, 2008 [Cantrell *et al.* 2008] in the simulation framework, following computations for a 50  $\mu\text{m}$  diameter disc electrode at 1 kHz (using a subretinal scheme with the 200  $\mu\text{m}$  thick electric model of retina included) are as follows:

I [ $\mu\text{A}$ ]	V <sub>1</sub> [V]	V <sub>0</sub> [V]	V <sub>tissue</sub> [V] (V <sub>0</sub> -V <sub>1</sub> )	R <sub>tissue</sub> [k $\Omega$ ] ( $\Delta V / I$ )
0	0	0	0	-
0.3	0.136	0.2	0.064	213
1.4	0.229	0.6	0.371	265
2.6	0.269	1	0.731	281
5.7	0.303	2	1.697	298
15.2	0.339	5	4.661	307
31	0.363	10	9.637	311
63	0.384	20	19.616	311
126	0.405	40	39.595	314

Table C.1: Overpotential (V<sub>1</sub>), voltage across tissue (V<sub>tissue</sub>) and tissue resistance (R<sub>tissue</sub>) based on the applied electrode voltage (V<sub>0</sub>). Above values are for quasi-static simulation incorporating the electrode interface equations for 50  $\mu\text{m}$  diameter disc electrode at 1 kHz.

From Table C.1, a relation between the overpotential and the current through the charge transfer resistance, I<sub>ct</sub>, can be plotted as shown in Figure C.2. We observe that the effective voltage across the tissue is reduced by V<sub>0</sub>. For currents above 2  $\mu\text{A}$ , the tissue voltage is reduced by 0.3-0.4 V as shown in Figure C.3.

To reach a threshold current value of  $\sim 38 \mu\text{A}$  for subretinal scheme of stimulation based on computations from our simulation framework, it is necessary to apply approximately 12 V on the electrode. The voltage across the interface impedance is negligible in comparison to the applied voltage and therefore interface impedance can be ignored in our simulation framework.

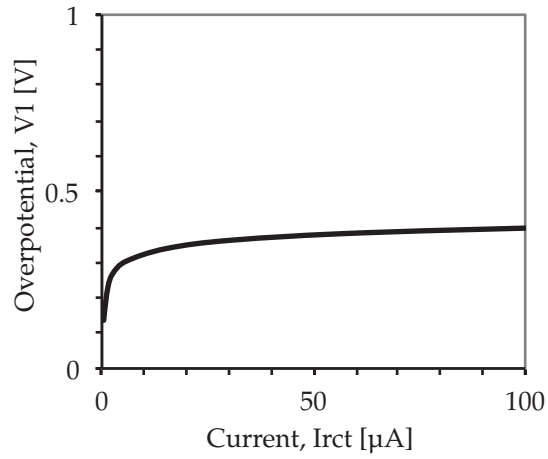


Figure C.2: Overpotential versus current through the charge transfer resistance. Above  $2\ \mu\text{A}$ , the voltage drop across the interface (overpotential) reaches  $0.3\ \text{V}$ , and then slowly increases.

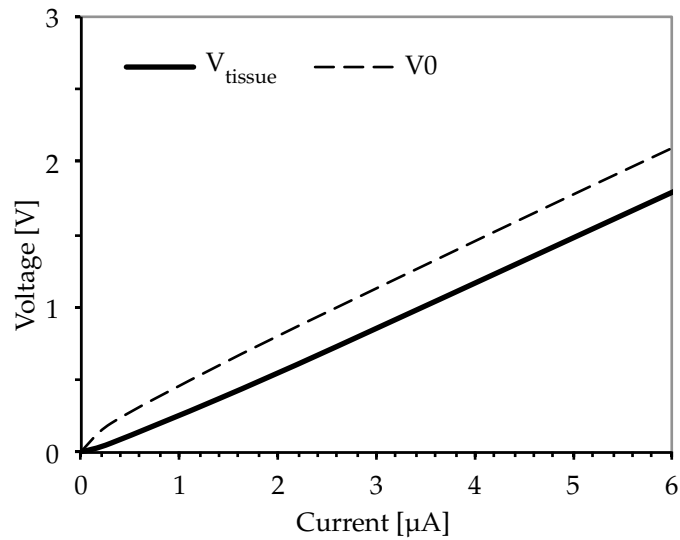


Figure C.3: Tissue voltage ( $V_{\text{tissue}}$ ) and overpotential ( $V_0$ ) for all values of applied electrode voltage. The effective voltage across in the tissue is reduced by  $V_0$  for all ranges of applied electrode voltages. For currents above  $2\ \mu\text{A}$ , the tissue voltage has a constant reduction by  $0.3\text{--}0.4\ \text{V}$ .

## C.2 VALIDATION FOR NEGLECTING CAPACITIVE TISSUE IMPEDANCE

### C.2.1 Model

Consider a Cole electrical equivalent of the computational model as shown in Figure C.4.

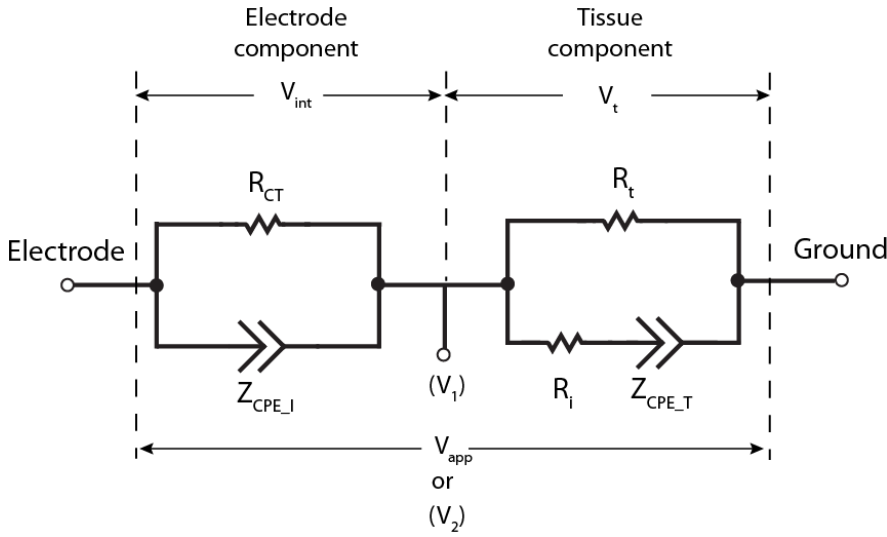


Figure C.4: Circuit equivalent (Cole model) of the simulation model between the electrode and the ground. The various components are: Charge transfer resistance ( $R_{CT}$ ), Constant phase element (CPE) impedance of the electrode ( $Z_{CPE\_I}$ ), tissue resistance ( $R_t$ ), intracellular bulk resistance ( $R_i$ ) and CPE impedance of the tissue ( $Z_{CPE\_T}$ ). Voltage across the electrode interface ( $V_{int}$ ), voltage across tissue ( $V_t$  or  $V_1$ ), applied voltage ( $V_{app}$  or  $V_2$ )

### C.2.2 Calculations

A  $50\mu\text{m}$  recessed disc electrode is considered for all calculations. The  $200\mu\text{m}$  thick retina model is considered in contact with the electrode.

Using quasi-static computations, at 1 kHz, we have:

$$V_t \text{ or } V_1|_{V_2=10} = 9.79V [9.77 + i(0.28)]$$

Considering negligible influence of intracellular conductivity over extracellular medium conductivity, the spread resistance can be computed with conductivity of physiological saline as:

$$R_i|_{\text{@high frequencies}} = \frac{\rho}{4r} \times 1.6 = 24\text{ k}\Omega$$

(resistivity of physiological medium,  $\rho = 1.5\Omega \cdot m$ )

This is the equation for a disc electrode in a uniform homogeneous medium [Newman 1966] – factor of 1.6 to account for recess (determined by computations).

Current ( $I$ ) flowing in the circuit can be computed as indicated in Chapter 4.

$$I|_{V_2=10} = 30.96\mu A [30.9 + i(2.56 \times 10^{-6})]$$

Now,

$$\frac{V_1}{I} = R_t || R_i + Z_{CPE\_T} \quad (C.3)$$

Considering the tissue impedance to be represented by a CPE component  $Z_{CPE\_T}$ , with the following equation:

$$Z_{CPE\_T} = |K_T \cdot (i\omega)^{-\alpha_t}|$$

and assuming  $\alpha_t = 0.75$  [Lempka *et al.* 2009], equation C.3 with two variables can be substituted with  $\alpha_t$  at 10 kHz also.

As a consequence, two equations are formed. Solving the two linear simultaneous equations, values of the variables are obtained as:

$$R_t = 316 \text{ k}\Omega$$

$$@ 1 \text{ kHz} \quad Z_{CPE\_T} = 76 \text{ M}\Omega$$

$$@ 10 \text{ kHz} \quad Z_{CPE\_T} = 14 \text{ M}\Omega$$

It can be inferred that the capacitive impedance of the tissue is more than one order of magnitude compared to the tissue resistance.

## BIBLIOGRAPHY

---

- Ahuja, A.K., Behrend, M.R., Kuroda, M., Humayun, M.S. and Weiland, J.D. (2008). "An in vitro model of a retinal prosthesis." *IEEE transactions on bio-medical engineering* 55(6): 1744–1753, URL <http://www.ncbi.nlm.nih.gov/pubmed/18714839>. (Cited on pages 29 and 52.)
- Ahuja, A.K., Dorn, J.D., Caspi, A., McMahon, M.J., Dagnelie, G., Dacruz, L., Stanga, P., Humayun, M.S. and Greenberg, R.J. (2010). "Blind subjects implanted with the Argus II retinal prosthesis are able to improve performance in a spatial-motor task." *The British journal of ophthalmology* URL <http://www.ncbi.nlm.nih.gov/pubmed/20881025>. (Cited on page 19.)
- Airan, R.D., Thompson, K.R., Fenno, L.E., Bernstein, H. and Deisseroth, K. (2009). "Temporally precise in vivo control of intracellular signalling." *Nature* 458(7241): 1025–1029, URL <http://www.ncbi.nlm.nih.gov/pubmed/19295515>. (Cited on page 23.)
- Ameri, H., Weiland, J. and Humayun, M. (2008). *Biological considerations for an intraocular retinal prosthesis*, Springer, chapter 1. pages 1–29, URL <http://www.springerlink.com/index/v0wj612741557278.pdf>. (Cited on page 7.)
- AREDS Study Research Group (2001). "A randomized, placebo-controlled, clinical trial of high-dose supplementation with vitamins C and E, beta carotene, and zinc for age-related macular degeneration and vision loss". *Archives of ophthalmology* 119(10): 1417–1436, URL <http://www.ncbi.nlm.nih.gov/pmc/articles/PMC1462955/?tool=pmcentrez&report=abstract>. (Cited on page 3.)
- Banghart, M., Borges, K., Isacoff, E., Trauner, D. and Kramer, R.H. (2004). "Light-activated ion channels for remote control of neuronal firing." *Nature neuroscience* 7(12): 1381–1386, URL <http://www.ncbi.nlm.nih.gov/pmc/articles/PMC1447674/?tool=pmcentrez&report=abstract>. (Cited on page 6.)
- Behrend, M.R., Ahuja, A.K., Humayun, M.S., Weiland, J.D. and Chow, R.H. (2009). "Selective labeling of retinal ganglion cells with calcium indicators by retrograde loading in vitro." *Journal of neuroscience methods* 179(2): 166–172, URL <http://www.ncbi.nlm.nih.gov/pubmed/19428523>. (Cited on pages 52 and 79.)
- Berndt, A., Yizhar, O., Gunaydin, L.A., Hegemann, P. and Deisseroth, K. (2009). "Bi-stable neural state switches." *Nature neuroscience* 12(2): 229–234, URL <http://www.ncbi.nlm.nih.gov/pubmed/19079251>. (Cited on page 23.)
- Besch, D., Sachs, H., Szurman, P., Gülicher, D., Wilke, R., Reinert, S., Zrenner, E., Bartz-Schmidt, K.U. and Gekeler, F. (2008). "Extraocular surgery for implantation of an active subretinal visual prosthesis with external connections: feasibility and outcome in seven patients." *The British journal of ophthalmology* 92(10): 1361–1368, URL <http://www.ncbi.nlm.nih.gov/pubmed/18662916>. (Cited on page 14.)
- Bi, A., Cui, J., Ma, Y.P., Olshevskaya, E., Pu, M., Dizhoor, A.M. and Pan, Z.H. (2006). "Ectopic expression of a microbial-type rhodopsin restores visual responses in mice with photoreceptor degeneration". *Neuron* 50(1): 23–33, URL <http://www.ncbi.nlm.nih.gov/pubmed/16600853>. (Cited on page 6.)
- Boinagrov, D., Loudin, J. and Palanker, D. (2010). "Strength-duration relationship for extracellular neural stimulation: numerical and analytical models." *Journal of neurophysiology* 104(4): 2236–2248, URL <http://www.pubmedcentral.nih.gov/articlerender.fcgi?artid=2957463&tool=pmcentrez&rendertype=abstract>. (Cited on pages 10, 31, 32, 79, 80, 81, and 88.)
- Bonanomi, M.T.B.C., Nicoletti, A.G.B., Carricondo, P.C., Buzalaf, F., Kara-José, N., Gomes, A.M.V. and Nakashima, Y. (2006). "Retinal thickness assessed by optical coherence tomography (OCT) in pseudophakic macular edema." *Arquivos brasileiros de oftalmologia* 69(4): 539–44, URL <http://www.ncbi.nlm.nih.gov/pubmed/17119727>. (Cited on page 78.)
- Boughman, J.A., Conneally, P.M. and Nance, W.E. (1980). "Population genetic studies of retinitis pigmentosa". *American journal of human genetics* 32(2): 223–235, URL <http://www.ncbi.nlm.nih.gov/pubmed/7386458>. (Cited on page 3.)
- Boyden, E.S., Zhang, F., Bamberg, E., Nagel, G. and Deisseroth, K. (2005). "Millisecond-timescale, genetically targeted optical control of neural activity." *Nature neuroscience* 8(9): 1263–1268, URL <http://www.ncbi.nlm.nih.gov/pubmed/16116447>. (Cited on page 23.)
- Brindley, G.S. (1973). "Sensory effects of electrical stimulation of the visual and paraviscual cortex in man". *Handbook of Sensory Physiology. Central Processing of Visual Information, Part B VII*(3): 583–594. (Cited on page 6.)
- Brindley, G.S. and Lewin, W.S. (1968a). "The sensations produced by electrical stimulation of the visual cortex." *The Journal of physiology* 196(2): 479–493, URL <http://www.ncbi.nlm.nih.gov/pubmed/4871047>. (Cited on page 6.)
- Brindley, G.S. and Lewin, W.S. (1968b). "The visual sensations produced by electrical stimulation of the medial occipital cortex." *The Journal of physiology* 194(2): 54–5P, URL <http://www.ncbi.nlm.nih.gov/>

- [pubmed/5639368](#). (Cited on page 6.)
- Brighurst, R. and Marks, H.. (2002). *The elements of typographic style*. Hartley & Marks, ISBN 0881791326, 350 pages. (Cited on page 145.)
- Brummer, S.B. and Turner, M.J. (1977). "Electrochemical considerations for safe electrical stimulation of the nervous system with platinum electrodes." *IEEE transactions on bio-medical engineering* 24(1): 59–63, URL <http://www.ncbi.nlm.nih.gov/pubmed/851475>. (Cited on pages 90 and 103.)
- Busskamp, V., Duebel, J., Balya, D., Fradot, M., Viney, T.J., Siegert, S., Groner, A.C., Cabuy, E., Forster, V., Seeliger, M., Biel, M., Humphries, P., Paques, M., Mohand-Said, S., Trono, D., Deisseroth, K., Sahel, J.a., Picaud, S. and Roska, B. (2010). "Genetic reactivation of cone photoreceptors restores visual responses in retinitis pigmentosa." *Science (New York, N.Y.)* 329(5990): 413–417, URL <http://www.ncbi.nlm.nih.gov/pubmed/20576849>. (Cited on page 23.)
- Butterwick, A., Vankov, A., Huie, P., Freyvert, Y. and Palanker, D. (2007). "Tissue damage by pulsed electrical stimulation." *IEEE transactions on bio-medical engineering* 54(12): 2261–2267, URL <http://www.ncbi.nlm.nih.gov/pubmed/18075042>. (Cited on page 51.)
- Cai, C.F., Liang, P.J. and Zhang, P.M. (2007). *A Simulation Study on the Encoding Mechanism of Retinal Ganglion Cell*, Springer Berlin Heidelberg, Berlin, Heidelberg, volume 4689 of *Lecture Notes in Computer Science*. ISBN 978-3-540-74770-3, pages 470–479, URL <http://www.springerlink.com/content/8112h285306m8257/>. (Cited on page 26.)
- Cantrell, D.R., Inayat, S., Taflove, A., Ruoff, R.S. and Troy, J.B. (2008). "Incorporation of the electrode-electrolyte interface into finite-element models of metal microelectrodes." *Journal of neural engineering* 5(1): 54–67, URL <http://www.ncbi.nlm.nih.gov/pubmed/18310811>. (Cited on pages 82, 121, 125, 126, and 127.)
- Cardin, J.A., Carlén, M., Meletis, K., Knoblich, U., Zhang, F., Deisseroth, K., Tsai, L.H. and Moore, C.I. (2009). "Driving fast-spiking cells induces gamma rhythm and controls sensory responses." *Nature* 459(7247): 663–667, URL <http://www.ncbi.nlm.nih.gov/pubmed/19396156>. (Cited on page 23.)
- Chader, G.J., Weiland, J. and Humayun, M.S. (2009). "Artificial vision: needs, functioning, and testing of a retinal electronic prosthesis." *Progress in brain research* 175(09): 317–332, URL <http://www.ncbi.nlm.nih.gov/pubmed/19660665>. (Cited on pages 7 and 16.)
- Chen, B. and Cepko, C.L. (2009). "HDAC4 regulates neuronal survival in normal and diseased retinas." *Science (New York, N.Y.)* 323(5911): 256–259, URL <http://www.ncbi.nlm.nih.gov/pubmed/19131628>. (Cited on page 24.)
- Chow, A.Y., Chow, V.Y., Packo, K.H., Pollack, J.S., Peyman, G.A. and Schuchard, R. (2004). "The artificial silicon retina microchip for the treatment of vision loss from retinitis pigmentosa." *Archives of ophthalmology* 122(4): 460–469, URL <http://www.ncbi.nlm.nih.gov/pubmed/15078662>. (Cited on pages 14, 16, and 17.)
- Chow, A.Y., Pardue, M.T., Chow, V.Y., Peyman, G.A., Liang, C., Perlman, J.I. and Peachey, N.S. (2001). "Implantation of silicon chip microphotodiode arrays into the cat subretinal space." *IEEE transactions on neural systems and rehabilitation engineering : a publication of the IEEE Engineering in Medicine and Biology Society* 9(1): 86–95, URL <http://www.ncbi.nlm.nih.gov/pubmed/11482368>. (Cited on pages 78 and 108.)
- Ciulla, T.A., Danis, R.P. and Harris, A. (1998). "Age-related macular degeneration: a review of experimental treatments". *Survey of ophthalmology* 43(2): 134–46, URL <http://www.ncbi.nlm.nih.gov/pubmed/9763138>. (Cited on page 4.)
- Clausen, J. (1955). "Visual sensations (phosphenes) produced by AC sine wave stimulation." *Acta psychiatrica et neurologica Scandinavica. Supplementum* 94: 1–101, URL <http://www.ncbi.nlm.nih.gov/pubmed/13258326>. (Cited on page 5.)
- Coburn, B. (1989). "Neural modeling in electrical stimulation". *Critical reviews in biomedical engineering* 17(2): 133–78, URL <http://www.ncbi.nlm.nih.gov/pubmed/2663351>. (Cited on page 99.)
- Cohen, E.D. (2007). "Prosthetic interfaces with the visual system: biological issues." *Journal of neural engineering* 4(2): R14–R31, URL <http://www.ncbi.nlm.nih.gov/pubmed/17409473>. (Cited on page 39.)
- Cole, K.S. (1940). "Permeability and impermeability of cell membranes for ions". *Cold Spring Harbor Symposia on Quantitative Biology* 8: 110–122, URL <http://symposium.cshlp.org/content/8/110.short>. (Cited on page 58.)
- Colodetti, L., Weiland, J.D., Colodetti, S., Ray, A., Seiler, M.J., Hinton, D.R. and Humayun, M.S. (2007). "Pathology of damaging electrical stimulation in the retina." *Experimental eye research* 85(1): 23–33, URL <http://www.ncbi.nlm.nih.gov/pubmed/17531974>. (Cited on page 51.)
- Congdon, N., O'Colmain, B., Klaver, C.C.W., Klein, R., Muñoz, B., Friedman, D.S., Kempen, J., Taylor, H.R. and Mitchell, P. (2004). "Causes and prevalence of visual impairment among adults in the United States." *Archives of ophthalmology* 122(4): 477–485, URL <http://www.ncbi.nlm.nih.gov/pubmed/15078664>. (Cited on page 3.)
- Congdon, N.G., Friedman, D.S. and Lietman, T. (2003). "Important causes of visual impairment in the world today". *JAMA : the journal of the American Medical Association* 290(15): 2057–60, URL <http://www.ncbi.nlm.nih.gov/pubmed/14559961>. (Cited on page 3.)



- Cottaris, N.P. and Elfar, S.D. (2005). "How the retinal network reacts to epiretinal stimulation to form the prosthetic visual input to the cortex." *Journal of neural engineering* 2(1): S74–90, URL <http://www.ncbi.nlm.nih.gov/pubmed/15876658>. (Cited on pages 26, 34, 35, and 52.)
- Dagnelie, G. (2008). "Psychophysical evaluation for visual prosthesis." *Annual review of biomedical engineering* 10: 339–368, URL <http://www.ncbi.nlm.nih.gov/pubmed/18429703>. (Cited on page 6.)
- Dagnelie, G. (2011). *Visual prosthetics*. Springer, 1st edition, ISBN 978-1-4419-0753-0, 453 pages, URL <http://www.ingentaconnect.com/content/ftd/erd/2006/00000003/00000003/art00008>. (Cited on pages 49, 51, and 97.)
- de Balthasar, C., Patel, S., Roy, A., Freda, R., Greenwald, S., Horsager, A., Mahadevappa, M., Yanai, D., McMahon, M.J., Humayun, M.S., Greenberg, R.J., Weiland, J.D. and Fine, I. (2008). "Factors affecting perceptual thresholds in epiretinal prostheses." *Investigative ophthalmology & visual science* 49(6): 2303–2314, URL <http://www.ncbi.nlm.nih.gov/pubmed/18515576>. (Cited on pages 9, 12, 87, 88, 89, 91, 93, 94, 97, 100, 104, 108, and 109.)
- Dobelle, W.H. (2000). "Artificial vision for the blind by connecting a television camera to the visual cortex." *ASAIO journal (American Society for Artificial Internal Organs : 1992)* 46(1): 3–9, URL <http://www.ncbi.nlm.nih.gov/pubmed/10667705>. (Cited on pages 6 and 7.)
- Dobelle, W.H. and Mladejovsky, M.G. (1974). "Phosphenes produced by electrical stimulation of human occipital cortex, and their application to the development of a prosthesis for the blind." *The Journal of physiology* 243(2): 553–576, URL <http://www.ncbi.nlm.nih.gov/pmc/articles/PMC1330721/?tool=pmcentrez&report=abstract>. (Cited on page 6.)
- Dobelle, W.H., Mladejovsky, M.G. and Girvin, J.P. (1974). "Artificial vision for the blind: electrical stimulation of visual cortex offers hope for a functional prosthesis." *Science (New York, N.Y.)* 183(123): 440–444, URL <http://www.ncbi.nlm.nih.gov/pubmed/4808973>. (Cited on page 6.)
- Doh, S.T., Hao, H., Loh, S.C., Patel, T., Tawil, H.Y., Chen, D.K., Pashkova, A., Shen, A., Wang, H. and Cai, L. (2010). "Analysis of retinal cell development in chick embryo by immunohistochemistry and in ovo electroporation techniques." *BMC developmental biology* 10(1): 8, URL <http://www.pubmedcentral.nih.gov/articlerender.fcgi?artid=2822752&tool=pmcentrez&rendertype=abstract>. (Cited on page 66.)
- Dokos, S., Suanning, G.J. and Lovell, N.H. (2005). "A bidomain model of epiretinal stimulation." *IEEE transactions on neural systems and rehabilitation engineering* 13(2): 137–146, URL <http://www.ncbi.nlm.nih.gov/pubmed/16003891>. (Cited on page 27.)
- Dommel, N.B., Wong, Y.T., Lehmann, T., Dodds, C.W., Lovell, N.H. and Suanning, G.J. (2009). "A CMOS retinal neurostimulator capable of focussed, simultaneous stimulation." *Journal of neural engineering* 6(3): 035,006 (10pp), URL <http://www.ncbi.nlm.nih.gov/pubmed/19458399>. (Cited on page 7.)
- Doroudchi, M.M., Greenberg, K.P., Liu, J., Silka, K.A., Boyden, E.S., Lockridge, J.A., Arman, A.C., Janani, R., Boye, S.E., Boye, S.L., Gordon, G.M., Matteo, B.C., Sampath, A.P., Hauswirth, W.W. and Horsager, A. (2011). "Virally delivered Channelrhodopsin-2 Safely and Effectively Restores Visual Function in Multiple Mouse Models of Blindness." *Molecular therapy : the journal of the American Society of Gene Therapy* URL <http://www.ncbi.nlm.nih.gov/pubmed/21505421>. (Cited on page 5.)
- Dowling, J. (2009). "Current and future prospects for optoelectronic retinal prostheses." *Eye (London, England)* 23(10): 1999–2005, URL <http://www.ncbi.nlm.nih.gov/pubmed/19098703>. (Cited on page 11.)
- Duan, Y.Y., Clark, G.M. and Cowan, R.S.C. (2004). "A study of intra-cochlear electrodes and tissue interface by electrochemical impedance methods in vivo." *Biomaterials* 25(17): 3813–28, URL <http://www.ncbi.nlm.nih.gov/pubmed/15020157>. (Cited on page 93.)
- Dufier, J.L. (2003). "[Early therapeutic trials for retinitis pigmentosa]." *Bulletin de l'Académie nationale de médecine* 187(9): 1685–1692; discussion 1692–1694, URL <http://www.ncbi.nlm.nih.gov/pubmed/15369238>. (Cited on page 4.)
- Durand, D.M. (2000). *Electric Stimulation of Excitable Tissue*, CRC Press, Boca Raton, FL, chapter 17. 2nd edition, ISBN 978-0-8493-8594-0, page 23. (Cited on page 43.)
- Eckhorn, R., Wilms, M., Schanze, T., Eger, M., Hesse, L., Eysel, U.T., Kisvárdy, Z.F., Zrenner, E., Gekeler, F., Schwahn, H., Shinoda, K., Sachs, H. and Walter, P. (2006). "Visual resolution with retinal implants estimated from recordings in cat visual cortex." *Vision research* 46(17): 2675–2690, URL <http://www.ncbi.nlm.nih.gov/pubmed/16571357>. (Cited on page 107.)
- Eckmiller, R., Becker, M. and Hunermann, R. (1999). *Towards a learning retina implant with epiretinal contacts*. IEEE, ISBN 0-7803-5731-0, 396–399 pages, URL <http://ieeexplore.ieee.org/lpdocs/epic03/wrapper.htm?arnumber=812435>. (Cited on pages 15 and 26.)
- Fariss, R.N., Li, Z.Y. and Milam, A.H. (2000). "Abnormalities in rod photoreceptors, amacrine cells, and horizontal cells in human retinas with retinitis pigmentosa." *American journal of ophthalmology* 129(2): 215–223, URL <http://www.ncbi.nlm.nih.gov/pubmed/10682975>. (Cited on page 6.)
- Feucht, M., Laube, T., Bornfeld, N., Walter, P., Velikay-Parel, M., Hornig, R. and Richard, G. (2005). "[Development of an epiretinal prosthesis for stimulation of the human retina]." *Der Ophthalmologe : Zeitschrift der Deutschen Ophthalmologischen Gesellschaft* 102(7): 688–691, URL <http://www.ncbi.nlm.nih.gov/pubmed/15770506>. (Cited on page 19.)

- Foerster, O. (1929). "Beiträge zur pathophysiologie der sehspäre". *J Psychol Neurol (Ppz)* **39**: 463–485. (Cited on page 6.)
- Fohlmeister, J.F., Coleman, P.A. and Miller, R.F. (1990). "Modeling the repetitive firing of retinal ganglion cells." *Brain research* **510**(2): 343–345, URL <http://www.ncbi.nlm.nih.gov/pubmed/2331606>. (Cited on page 79.)
- Fried, S., Kubow, T. and Werblin, F. (2004). "Complex synaptic activation of bipolar, amacrine and ganglion cells is elicited with biphasic electrical stimulation". *Neural Networks, 2004. Proceedings. 2004 IEEE International Joint Conference on* **1**, URL [http://ieeexplore.ieee.org/xpls/abs\\_all.jsp?arnumber=1379952](http://ieeexplore.ieee.org/xpls/abs_all.jsp?arnumber=1379952). (Cited on pages 52 and 99.)
- Fried, S.I., Hsueh, H.A. and Werblin, F.S. (2006). "A method for generating precise temporal patterns of retinal spiking using prosthetic stimulation." *Journal of neurophysiology* **95**(2): 970–978, URL <http://www.ncbi.nlm.nih.gov/pubmed/16236780>. (Cited on pages 47 and 79.)
- Fried, S.I., Lasker, A.C.W., Desai, N.J., Eddington, D.K. and Rizzo, J.F. (2009). "Axonal sodium-channel bands shape the response to electric stimulation in retinal ganglion cells." *Journal of neurophysiology* **101**(4): 1972–1987, URL <http://www.ncbi.nlm.nih.gov/pubmed/19193771>. (Cited on pages 40, 52, and 79.)
- Fujikado, T., Morimoto, T., Kanda, H., Kusaka, S., Nakauchi, K., Ozawa, M., Matsushita, K., Sakaguchi, H., Ikuno, Y., Kamei, M. and Tano, Y. (2007). "Evaluation of phosphenes elicited by extraocular stimulation in normals and by suprachoroidal-transretinal stimulation in patients with retinitis pigmentosa." *Graefes archive for clinical and experimental ophthalmology* **245**(10): 1411–1419, URL <http://www.ncbi.nlm.nih.gov/pubmed/17342502>. (Cited on page 7.)
- Geddes, L.A. (2004). "Accuracy limitations of chronaxie values." *IEEE transactions on bio-medical engineering* **51**(1): 176–181, URL <http://www.ncbi.nlm.nih.gov/pubmed/14723507>. (Cited on page 48.)
- Gerding, H. (2007). "A new approach towards a minimal invasive retina implant." *Journal of neural engineering* **4**(1): S30–S37, URL <http://www.ncbi.nlm.nih.gov/pubmed/17325414>. (Cited on page 7.)
- Gerding, H., Benner, F.P. and Taneri, S. (2007). "Experimental implantation of epiretinal retina implants (EPI-RET) with an IOL-type receiver unit." *Journal of neural engineering* **4**(1): S38–S49, URL <http://www.ncbi.nlm.nih.gov/pubmed/17325415>. (Cited on pages 7 and 19.)
- Gerhardt, M., Alderman, J. and Stett, A. (2010). "Electric field stimulation of bipolar cells in a degenerated retina—a theoretical study." *IEEE transactions on neural systems and rehabilitation engineering : a publication of the IEEE Engineering in Medicine and Biology Society* **18**(1): 1–10, URL <http://www.ncbi.nlm.nih.gov/pubmed/20071281>. (Cited on pages 30, 52, and 99.)
- Gosalia, K., Weiland, J., Humayun, M. and Lazzi, G. (2004). "Thermal elevation in the human eye and head due to the operation of a retinal prosthesis." *IEEE transactions on bio-medical engineering* **51**(8): 1469–77, URL <http://www.ncbi.nlm.nih.gov/pubmed/15311834>. (Cited on page 25.)
- Gradinaru, V., Thompson, K.R. and Deisseroth, K. (2008). "eNpHR: a Natronomonas halorhodopsin enhanced for optogenetic applications." *Brain cell biology* **36**(1-4): 129–139, URL <http://www.pubmedcentral.nih.gov/articlerender.fcgi?artid=2588488&tool=pmcentrez&rendertype=abstract>. (Cited on page 23.)
- Greenberg, R. (1998). *Analysis of Electrical Stimulation of the Vertebrate Retina: Work Towards a Retinal Prosthesis. - PhD Thesis*. Phd thesis, The Johns Hopkins University Baltimore. (Cited on page 47.)
- Greenberg, R., Neysmith, J., Talbot, N., Little, J., McClure, K., Mech, B., Dai, R., Zhou, D. and Nolan, G. (2008). "Return Electrode for a Flexible Circuit Electrode Array". URL <http://www.freepatentsonline.com/y2009/0118805.html>. (Cited on page 25.)
- Greenberg, R.J., Velte, T.J., Humayun, M.S., Scarlatis, G.N. and de Juan, E. (1999). "A computational model of electrical stimulation of the retinal ganglion cell." *IEEE transactions on bio-medical engineering* **46**(5): 505–514, URL <http://www.ncbi.nlm.nih.gov/pubmed/10230129>. (Cited on pages 24, 52, and 80.)
- Grimnes, S. and Martinsen, O.G. (2008). *Bioimpedance and Bioelectricity Basics (Second Edition)*. Academic Press, ISBN 0-12-374004-5, 488 pages. (Cited on pages 33 and 58.)
- Güven, D., Weiland, J.D., Fujii, G., Mech, B.V., Mahadevappa, M., Greenberg, R., Roizenblatt, R., Qiu, G., Labree, L., Wang, X., Hinton, D. and Humayun, M.S. (2005). "Long-term stimulation by active epiretinal implants in normal and RCD1 dogs." *Journal of neural engineering* **2**(1): S65–S73, URL <http://www.ncbi.nlm.nih.gov/pubmed/15876657>. (Cited on page 51.)
- Hagins, W.A., Penn, R.D. and Yoshikami, S. (1970). "Dark current and photocurrent in retinal rods." *Biophysical journal* **10**(5): 380–412, URL <http://www.ncbi.nlm.nih.gov/pubmed/5439318>. (Cited on pages 65, 66, and 67.)
- Haim, M. (2002). "Epidemiology of retinitis pigmentosa in Denmark." *Acta ophthalmologica Scandinavica. Supplement* (233): 1–34, URL <http://www.ncbi.nlm.nih.gov/pubmed/11921605>. (Cited on page 3.)
- Haim, M., Holm, N.V. and Rosenberg, T. (1992). "A population survey of retinitis pigmentosa and allied disorders in Denmark. Completeness of registration and quality of data." *Acta ophthalmologica* **70**(2): 165–177, URL <http://www.ncbi.nlm.nih.gov/pubmed/1609564>. (Cited on page 3.)



- Han, X. and Boyden, E.S. (2007). "Multiple-color optical activation, silencing, and desynchronization of neural activity, with single-spike temporal resolution." *PloS one* 2(3): e299, URL <http://www.ncbi.nlm.nih.gov/pubmed/17375185>. (Cited on page 23.)
- Harding, S. (2003). "Extracts from "concise clinical evidence". Diabetic retinopathy." *BMJ (Clinical research ed.)* 326(7397): 1023–1025, URL <http://www.ncbi.nlm.nih.gov/pmc/articles/PMC1125930/?tool=pmcentrez&report=abstract>. (Cited on page 4.)
- Heynen, H. and van Norren, D. (1985). "Origin of the electroretinogram in the intact macaque eye—II. Current source-density analysis." *Vision research* 25(5): 709–15, URL <http://www.ncbi.nlm.nih.gov/pubmed/4024471>. (Cited on pages 10, 55, 65, 66, 67, 77, and 100.)
- Hims, M.M., Diager, S.P. and Inglehearn, C.F. (2003). "Retinitis pigmentosa: genes, proteins and prospects". *Developments in ophthalmology* 37: 109–125, URL <http://www.scopus.com/scopus/inward/record.url?eid=2-s2.0-0042285484&partnerID=40&rel=R7.0.0>. (Cited on page 4.)
- Hines, M. (1993). "NEURON—a program for simulation of nerve equations". *Neural systems: Analysis and modeling*: 127–136 URL <http://citeseerx.ist.psu.edu/viewdoc/summary?doi=10.1.1.45.9006>. (Cited on page 24.)
- Hodgkin, A.L. and Huxley, A.F. (1952). "A quantitative description of membrane current and its application to conduction and excitation in nerve." *The Journal of physiology* 117(4): 500–544, URL <http://www.ncbi.nlm.nih.gov/pubmed/12991237>. (Cited on page 40.)
- Holsheimer, J. (2003). *Principles of neurostimulation*, Elsevier Science Health Science div, chapter 3. ISBN 0444512586, page 17. (Cited on page 41.)
- Hornig, R. and Eckmiller, R. (2001). *Optimizing stimulus parameters by modeling multi-electrode electrical stimulation for retina implants*. IEEE, Washington, DC, ISBN 0-7803-7044-9, 860–865 pages, URL <http://ieeexplore.ieee.org/lpdocs/epic03/wrapper.htm?arnumber=939472>. (Cited on page 26.)
- Hornig, R., Laube, T., Walter, P., Velikay-Parel, M., Bornfeld, N., Feucht, M., Akguel, H., Rössler, G., Altheld, N., Lütke Notarp, D., Wyatt, J. and Richard, G. (2005). "A method and technical equipment for an acute human trial to evaluate retinal implant technology." *Journal of neural engineering* 2(1): S129–S134, URL <http://www.ncbi.nlm.nih.gov/pubmed/15876648>. (Cited on page 7.)
- Horsager, A., Boynton, G.M., Greenberg, R.J. and Fine, I. (2011). "Temporal interactions during paired-electrode stimulation in two retinal prosthesis subjects." *Investigative ophthalmology & visual science* 52(1): 549–557, URL <http://www.ncbi.nlm.nih.gov/pubmed/20720224>. (Cited on page 34.)
- Horsager, A., Greenwald, S.H., Weiland, J.D., Humayun, M.S., Greenberg, R.J., McMahon, M.J., Boynton, G.M. and Fine, I. (2009). "Predicting visual sensitivity in retinal prosthesis patients." *Investigative ophthalmology & visual science* 50(4): 1483–1491, URL <http://www.ncbi.nlm.nih.gov/pubmed/19098313>. (Cited on pages 34 and 75.)
- Huang, Y., Cideciyan, A.V., Papastergiou, G.I., Banin, E., Milam, A.H., Semple-Rowland, S.L. and Jacobson, S.G. (1998). "Relation of optical coherence tomography to microanatomy in normal and rd chickens." *Investigative ophthalmology & visual science* 39(12): 2405–16, URL <http://www.ncbi.nlm.nih.gov/pubmed/9804149>. (Cited on pages 56 and 78.)
- Hughes, M.L., Vander Werff, K.R., Brown, C.J., Abbas, P.J., Kelsay, D.M., Teagle, H.F. and Lowder, M.W. (2001). "A longitudinal study of electrode impedance, the electrically evoked compound action potential, and behavioral measures in nucleus 24 cochlear implant users." *Ear and hearing* 22(6): 471–486, URL <http://www.ncbi.nlm.nih.gov/pubmed/11770670>. (Cited on page 93.)
- Humayun, M.S., de Juan, E., Dagnelie, G., Greenberg, R.J., Propst, R.H. and Phillips, D.H. (1996). "Visual perception elicited by electrical stimulation of retina in blind humans." *Archives of ophthalmology* 114(1): 40–6, URL <http://www.ncbi.nlm.nih.gov/pubmed/8540849>. (Cited on pages 7 and 28.)
- Humayun, M.S., de Juan, E., Weiland, J.D., Dagnelie, G., Katona, S., Greenberg, R. and Suzuki, S. (1999). "Pattern electrical stimulation of the human retina." *Vision research* 39(15): 2569–2576, URL <http://www.ncbi.nlm.nih.gov/pubmed/10396625>. (Cited on page 7.)
- Humayun, M.S., Weiland, J.D., Chader, G. and Greenbaum, E. (2007). *Artificial Sight*. Biological and Medical Physics, Biomedical Engineering, Springer New York, New York, NY, biological edition, ISBN 978-0-387-49329-9, URL <http://www.springerlink.com/index/10.1007/978-0-387-49331-2>. (Cited on pages 28 and 35.)
- Humayun, M.S., Weiland, J.D., Fujii, G.Y., Greenberg, R., Williamson, R., Little, J., Mech, B., Cimarusti, V., Van Boemel, G., Dagnelie, G. and de Juan, E. (2003). "Visual perception in a blind subject with a chronic microelectronic retinal prosthesis." *Vision research* 43(24): 2573–2581, URL <http://www.ncbi.nlm.nih.gov/pubmed/13129543>. (Cited on page 87.)
- Humphries, P., Kenna, P. and Farrar, G.J. (1992). "On the molecular genetics of retinitis pigmentosa". *Science (New York, N.Y.)* 256(5058): 804–808, URL <http://www.ncbi.nlm.nih.gov/pubmed/1589761>. (Cited on page 3.)
- Jacobs, P., Varlan, A. and Sansen, W. (1995). "Design optimisation of planar electrolytic conductivity sensors". *Medical & biological engineering & computing* 33(6): 802–10, URL <http://www.ncbi.nlm.nih.gov/pubmed/8558953>. (Cited on page 60.)

- Jensen, R. and Rizzo, J. (2008). "Activation of retinal ganglion cells in wild-type and rd1 mice through electrical stimulation of the retinal neural network". *Vision Research* 48(14): 1562–1568, URL <http://linkinghub.elsevier.com/retrieve/pii/S0042698908002277>. (Cited on page 100.)
- Jensen, R.J. and Rizzo, J.F. (2007). "Responses of ganglion cells to repetitive electrical stimulation of the retina." *Journal of neural engineering* 4(1): S1–S6, URL <http://www.ncbi.nlm.nih.gov/pubmed/17325407>. (Cited on pages 51 and 99.)
- Jensen, R.J., Rizzo, J.F., Ziv, O.R., Grumet, A. and Wyatt, J. (2003). "Thresholds for activation of rabbit retinal ganglion cells with an ultrafine, extracellular microelectrode." *Investigative ophthalmology & visual science* 44(8): 3533–3543, URL <http://www.ncbi.nlm.nih.gov/pubmed/12882804>. (Cited on pages 27, 51, 87, and 89.)
- Jensen, R.J., Ziv, O.R. and Rizzo, J.F. (2005a). "Responses of rabbit retinal ganglion cells to electrical stimulation with an epiretinal electrode." *Journal of neural engineering* 2(1): S16–S21, URL <http://www.ncbi.nlm.nih.gov/pubmed/15876650>. (Cited on page 99.)
- Jensen, R.J., Ziv, O.R. and Rizzo, J.F. (2005b). "Thresholds for activation of rabbit retinal ganglion cells with relatively large, extracellular microelectrodes." *Investigative ophthalmology & visual science* 46(4): 1486–1496, URL <http://www.ncbi.nlm.nih.gov/pubmed/15790920>. (Cited on pages 74, 80, and 91.)
- Johnson, L., Scribner, D., Skeath, P., Klein, R., Ilg, D., Perkins, K., Helfgott, M., Sanders, R. and Panigrahi, D. (2007). "Impedance-based retinal contact imaging as an aid for the placement of high resolution epiretinal prostheses." *Journal of neural engineering* 4(1): S17–S23, URL <http://www.ncbi.nlm.nih.gov/pubmed/17325412>. (Cited on pages 88 and 104.)
- Johnston, D. (2010). "Lab plays key role in Department of Energy's artificial retina project". URL <https://www.llnl.gov/news/newsreleases/2010/NR-10-02-03.html>. (Cited on page 20.)
- Kameneva, T., Meffin, H. and Burkitt, A.N. (2010). "Differential stimulation of ON and OFF retinal ganglion cells: A modeling study." *Conference proceedings : ... Annual International Conference of the IEEE Engineering in Medicine and Biology Society* 1: 4246–4249, URL <http://www.ncbi.nlm.nih.gov/pubmed/21096639>. (Cited on pages 30 and 52.)
- Karwoski, C.J., Frambach, D.A. and Proenza, L.M. (1985). "Laminar profile of resistivity in frog retina". *Journal of neurophysiology* 54(6): 1607–1619, URL <http://www.ncbi.nlm.nih.gov/pubmed/3878863>. (Cited on pages 29, 33, and 66.)
- Karwoski, C.J. and Xu, X. (1999). "Current source-density analysis of light-evoked field potentials in rabbit retina." *Visual neuroscience* 16(2): 369–377, URL <http://www.ncbi.nlm.nih.gov/pubmed/10367970>. (Cited on pages 55, 65, 66, and 67.)
- Karwoski, C.J., Xu, X. and Yu, H. (1996). "Current-source density analysis of the electroretinogram of the frog: methodological issues and origin of components." *Journal of the Optical Society of America. A, Optics, image science, and vision* 13(3): 549–556, URL <http://www.ncbi.nlm.nih.gov/pubmed/8627411>. (Cited on page 55.)
- Kern, W. (1993). *Handbook of Semiconductor Wafer Cleaning Technology - Science, Technology, and Applications*. Elsevier Science and Technology Books, ISBN 0-8155-1331-3, 623 pages. (Cited on page 61.)
- Klassen, H.J., Ng, T.F., Kurimoto, Y., Kirov, I., Shatos, M., Coffey, P. and Young, M.J. (2004). "Multipotent retinal progenitors express developmental markers, differentiate into retinal neurons, and preserve light-mediated behavior". *Investigative Ophthalmology & Visual Science* 45(11): 4167–4173. (Cited on page 5.)
- Klomp, G.F., Womack, M.V. and Dobbelle, W.H. (1977). "Fabrication of large arrays of cortical electrodes for use in man." *Journal of biomedical materials research* 11(3): 347–364, URL <http://www.ncbi.nlm.nih.gov/pubmed/853046>. (Cited on page 6.)
- Kolb, H. (1994). "The architecture of functional neural circuits in the vertebrate retina. The Proctor Lecture." *Investigative ophthalmology & visual science* 35(5): 2385–2404, URL <http://www.ncbi.nlm.nih.gov/pubmed/8163331>. (Cited on page 13.)
- Krause, F. (1924). "Die sehbahnen in chirurgischer beziehung und die faradische reizung des sehzentrum." *Klin Wochenschr* 3: 1260–1265. (Cited on page 6.)
- Kreatsoulas, J. (2010). "Retinal prosthesis technology". URL <http://bmctoday.net/retinatoday/2010/08/article.asp?f=retinal-prosthesis-technology>. (Cited on page 19.)
- Kuras, A., Baginskas, A. and Batuleviciene, V. (2004). "Suprathreshold excitation of frog tectal neurons by short spike trains of single retinal ganglion cell." *Experimental brain research. Experimentelle Hirnforschung. Expérimentation cérébrale* 159(4): 509–18, URL <http://www.ncbi.nlm.nih.gov/pubmed/15221171>. (Cited on page 52.)
- Lambert, V., Laloyaux, C., Schmitt, C., Gerard, B., Delbeke, J. and Veraart, C. (2003). "Localisation, Discrimination, and Grasping of Daily Life Objects with an Implanted Optic Nerve Prosthesis". *ARVO Meeting Abstracts* 44(5): 4208, URL <http://abstracts.iovs.org/cgi/content/abstract/44/5/4208>. (Cited on page 7.)
- Lapicque, L. (1907). "Recherches quantitatives sur l'excitation électrique des nerfs traitée comme une polarisation". *J. Physiol. Pathol. Gen* 9: 620–635. (Cited on page 46.)

- Leanne Chan (2009). *Electrical excitation of degenerate retina*. Phd dissertation. (Cited on pages 40, 41, and 43.)
- Lebherz, C., Maguire, A., Tang, W., Bennett, J. and Wilson, J.M. (2008). "Novel AAV serotypes for improved ocular gene transfer." *The journal of gene medicine* 10(4): 375–382, URL <http://www.pubmedcentral.nih.gov/articlerender.fcgi?artid=2842078&tool=pmcentrez&rendertype=abstract>. (Cited on page 23.)
- Lecchi, M., Linderholm, P., Pelizzone, M., Picaud, S., Renaud, P., Salzmann, J., Sommerhalder, J., Safran, A. and Bertrand, D. (2006). "What physiology tells us about electrical stimulation in retinal implants". In "Invest Ophthalmol Vis Sci - ARVO 2006", pages 4–4. (Cited on page 73.)
- Lee, D.C. and Grill, W.M. (2005). "Polarization of a spherical cell in a nonuniform extracellular electric field." *Annals of biomedical engineering* 33(5): 603–15, URL <http://www.ncbi.nlm.nih.gov/pubmed/15981861>. (Cited on pages 13, 33, and 55.)
- Lempka, S.F., Miocinovic, S., Johnson, M.D., Vitek, J.L. and McIntyre, C.C. (2009). "In vivo impedance spectroscopy of deep brain stimulation electrodes." *Journal of neural engineering* 6(4): 046,001, URL <http://www.ncbi.nlm.nih.gov/pubmed/19494421>. (Cited on page 130.)
- Léveillard, T. and Sahel, J.A. (2010). "Rod-derived cone viability factor for treating blinding diseases: from clinic to redox signaling." *Science translational medicine* 2(26): 26ps16, URL <http://www.pubmedcentral.nih.gov/articlerender.fcgi?artid=2896730&tool=pmcentrez&rendertype=abstract>. (Cited on page 24.)
- Lin, B., Masland, R.H. and Strettoi, E. (2009). "Remodeling of cone photoreceptor cells after rod degeneration in rd mice." *Experimental eye research* 88(3): 589–599, URL <http://www.pubmedcentral.nih.gov/articlerender.fcgi?artid=2656412&tool=pmcentrez&rendertype=abstract>. (Cited on page 23.)
- Linderholm, P. (2006). *Two-dimensional microimpedance imaging for cell culture monitoring*. Ph.D. thesis, EPFL. (Cited on pages 39, 56, and 57.)
- Livesey, F.J. and Cepko, C.L. (2001). "Vertebrate neural cell-fate determination: lessons from the retina." *Nature reviews. Neuroscience* 2(2): 109–118, URL <http://www.ncbi.nlm.nih.gov/pubmed/11252990>. (Cited on page 66.)
- Löwenstein, W.K. and Borchart, M. (1918). "Symptomatologie und elektrische Reizung bei einer Schubverletzung des Hinterhauptlappens". *Dtsch Z Nervenheilk* 58: 264–292. (Cited on page 6.)
- MacLaren, R.E., Pearson, R.A., MacNeil, a., Douglas, R.H., Salt, T.E., Akimoto, M., Swaroop, a., Sowden, J.C. and Ali, R.R. (2006). "Retinal repair by transplantation of photoreceptor precursors." *Nature* 444(7116): 203–7, URL <http://www.ncbi.nlm.nih.gov/pubmed/17093405>. (Cited on page 5.)
- Mahadevappa, M., Weiland, J.D., Yanai, D., Fine, I., Greenberg, R.J. and Humayun, M.S. (2005). "Perceptual thresholds and electrode impedance in three retinal prosthesis subjects". *IEEE transactions on neural systems and rehabilitation engineering : a publication of the IEEE Engineering in Medicine and Biology Society* 13(2): 201–206, URL <http://www.ncbi.nlm.nih.gov/pubmed/16003900>. (Cited on pages 93 and 97.)
- Majji, A.B., Humayun, M.S., Weiland, J.D., Suzuki, S., D'Anna, S.A. and de Juan, E. (1999). "Long-term histological and electrophysiological results of an inactive epiretinal electrode array implantation in dogs." *Investigative ophthalmology & visual science* 40(9): 2073–2081, URL <http://www.ncbi.nlm.nih.gov/pubmed/10440263>. (Cited on page 15.)
- Marc, R.E., Jones, B.W., Watt, C.B. and Strettoi, E. (2003). "Neural remodeling in retinal degeneration." *Progress in retinal and eye research* 22(5): 607–655, URL <http://www.ncbi.nlm.nih.gov/pubmed/12892644>. (Cited on pages 6 and 35.)
- Margalit, E. and Sada, S.R. (2003). "Retinal and optic nerve diseases." *Artificial organs* 27(11): 963–974, URL <http://www.ncbi.nlm.nih.gov/pubmed/17471327>. (Cited on page 3.)
- Maynard, E.M., Hatsopoulos, N.G., Ojakangas, C.L., Acuna, B.D., Sanes, J.N., Normann, R.A. and Donoghue, J.P. (1999). "Neuronal interactions improve cortical population coding of movement direction." *The Journal of neuroscience* 19(18): 8083–8093, URL <http://www.ncbi.nlm.nih.gov/pubmed/10479708>. (Cited on page 7.)
- McAdams, E., Lacknermeier, A., McLaughlin, J.A., Macken, D. and Jossinet, J. (1995). "The linear and non-linear electrical properties of the electrode-electrolyte interface". *Biosensors and Bioelectronics* 10(1-2): 67–74, URL <http://linkinghub.elsevier.com/retrieve/pii/095656639596795Z>. (Cited on pages 39 and 58.)
- McCreery, D. (2004). *Tissue reaction to electrodes: The problem of safe and effective stimulation of neural tissue*, World Scientific Publishing, River Edge, NJ. pages 592–607. (Cited on page 49.)
- McCreery, D.B., Agnew, W.F., Yuen, T.G. and Bullara, L. (1990). "Charge density and charge per phase as cofactors in neural injury induced by electrical stimulation". *IEEE transactions on bio-medical engineering* 37(10): 996–1001, URL <http://www.ncbi.nlm.nih.gov/pubmed/2249872>. (Cited on page 50.)
- McCreery, D.B., Agnew, W.F., Yuen, T.G. and Bullara, L.A. (1995). "Relationship between stimulus amplitude, stimulus frequency and neural damage during electrical stimulation of sciatic nerve of cat." *Medical & biological engineering & computing* 33(3 Spec No): 426–469, URL <http://www.ncbi.nlm.nih.gov/pubmed/7666690>. (Cited on page 50.)



- McFarland, T.J., Zhang, Y., Appukuttan, B. and Stout, J.T. (2004). "Gene therapy for proliferative ocular diseases". *Expert Opinion on Biological Therapy* 4(7): 1053–1058. (Cited on page 4.)
- McIntyre, C.C. and Grill, W.M. (2001). "Finite Element Analysis of the Current-Density and Electric Field Generated by Metal Microelectrodes". *Annals of Biomedical Engineering* 29(3): 227–235, URL <http://www.springerlink.com/openurl.asp?id=doi:10.1114/1.1352640>. (Cited on page 26.)
- McMahon, M.J., Fine, I., Greenwald, S.H., Horsager, A., Palmer, G., Mech, B.V., Greenberg, R.J. and Humayun, M.S. (2006). "Electrode impedance as a predictor of electrode-retina proximity and perceptual threshold in a retinal prosthesis". In "ARVO 2006 Annual Meeting", Fort Lauderdale, Florida, volume 47, pages 3184–B552, URL <http://abstracts.iovs.org/cgi/content/abstract/47/5/3184>. (Cited on pages 93 and 104.)
- Mercanzini, A., Colin, P., Bensadoun, J.C., Bertsch, A. and Renaud, P. (2009). "In vivo electrical impedance spectroscopy of tissue reaction to microelectrode arrays". *IEEE Transactions on Biomedical Engineering* 56(7): 1909–1918, URL <http://www.ncbi.nlm.nih.gov/pubmed/19362904>. (Cited on page 58.)
- Merrill, D.R., Bikson, M. and Jefferys, J.G.R. (2005). "Electrical stimulation of excitable tissue: design of efficacious and safe protocols." *Journal of neuroscience methods* 141(2): 171–198, URL <http://www.ncbi.nlm.nih.gov/pubmed/15661300>. (Cited on pages 39, 49, 90, and 92.)
- Metz, S., Bertsch, A., Bertrand, D. and Renaud, P. (2004). "Flexible polyimide probes with microelectrodes and embedded microfluidic channels for simultaneous drug delivery and multi-channel monitoring of bioelectric activity". *Biosensors & bioelectronics* 19(10): 1309–1318, URL <http://www.ncbi.nlm.nih.gov/pubmed/15046764>. (Cited on pages 57 and 73.)
- Miesenböck, G. (2009). "The optogenetic catechism." *Science (New York, N.Y.)* 326(5951): 395–399, URL <http://www.ncbi.nlm.nih.gov/pubmed/19833960>. (Cited on pages 21 and 22.)
- Miller, G. (2006). "Optogenetics. Shining new light on neural circuits." *Science (New York, N.Y.)* 314(5806): 1674–1676, URL <http://www.ncbi.nlm.nih.gov/pubmed/17170269>. (Cited on page 21.)
- Minnikanti, S., Cohen, E. and Peixoto, N. (2010). "Quasi-static Analysis of Electric Field Distributions by Disc Electrodes in a Rabbit Eye Model". In "26th Southern Biomedical Engineering Conference SBEC 2010 April 30-May 2, 2010 College Park, Maryland, USA, IFMBE Proceedings", Springer Verlag, volume 32, ISBN 3642149979, pages 385–388, URL <http://www.springerlink.com/content/m3kh23120t023147>. (Cited on pages 13, 31, and 33.)
- Miranda, P.C., Correia, L., Salvador, R. and Basser, P.J. (2007). "Tissue heterogeneity as a mechanism for localized neural stimulation by applied electric fields." *Physics in medicine and biology* 52(18): 5603–5617, URL <http://www.ncbi.nlm.nih.gov/pubmed/17804884>. (Cited on pages 13, 33, and 55.)
- Mohand-Said, S., Hicks, D., Dreyfus, H. and Sahel, J.A. (2000). "Selective transplantation of rods delays cone loss in a retinitis pigmentosa model". *Archives of Ophthalmology* 118(6): 807–811. (Cited on page 5.)
- Nagel, G., Szellas, T., Huhn, W., Kateriya, S., Adeishvili, N., Berthold, P., Ollig, D., Hegemann, P. and Bamberg, E. (2003). "Channelrhodopsin-2, a directly light-gated cation-selective membrane channel." *Proceedings of the National Academy of Sciences of the United States of America* 100(24): 13,940–13,945, URL <http://www.pubmedcentral.nih.gov/articlerender.fcgi?artid=283525&tool=pmcentrez&rendertype=abstract>. (Cited on page 23.)
- Nakauchi, K., Fujikado, T., Kanda, H., Kusaka, S., Ozawa, M., Sakaguchi, H., Ikuno, Y., Kamei, M. and Tano, Y. (2007). "Threshold suprachoroidal-transretinal stimulation current resulting in retinal damage in rabbits." *Journal of neural engineering* 4(1): S50–S57, URL <http://www.ncbi.nlm.nih.gov/pubmed/17325416>. (Cited on page 51.)
- Newman, J. (1966). "Resistance for Flow of Current to a Disk". *Journal of The Electrochemical Society* 113(5): 501, URL <http://link.aip.org/link/JES0AN/v113/i5/p501/s1&Agg=doi>. (Cited on page 129.)
- Nunez, P. (1981). *Electric fields of the brain: the neurophysics of EEG*, volume 35. Oxford University Press, England, Oxford, URL <http://scholar.google.com/scholar?hl=en&btnG=Search&q=intitle:Electric+Fields+of+the+Brain:+the+neurophysics+of+EEG#0>. (Cited on page 43.)
- Ogden, T.E. and Ito, H. (1971). "Avian retina. II. An evaluation of retinal electrical anisotropy." *Journal of neurophysiology* 34(3): 367–373, URL <http://www.ncbi.nlm.nih.gov/pubmed/5560038>. (Cited on pages 55, 65, 66, and 67.)
- Palanker, D., Vankov, A., Huie, P. and Baccus, S. (2005). "Design of a high-resolution optoelectronic retinal prosthesis." *Journal of neural engineering* 2(1): S105–S120, URL <http://www.ncbi.nlm.nih.gov/pubmed/15876646>. (Cited on pages 7, 8, 9, 11, 12, 28, 35, 81, 87, and 99.)
- Palanker, D., Vankov, A., Huie, P., Butterwick, A., Chan, I., Marmor, M. and Blumenkranz, M. (2007). *High-Resolution Opto-Electronic Retinal Prosthesis: Physical Limitations and Design*, Springer New York, New York, NY. Biological and Medical Physics, Biomedical Engineering, ISBN 978-0-387-49329-9, pages 255–277, URL <http://www.springerlink.com/index/10.1007/978-0-387-49331-2>. (Cited on pages 12 and 116.)
- Pauleikhoff, D. (2005). "Neovascular age-related macular degeneration: Natural History and Treatment Outcomes." *Retina (Philadelphia, Pa.)* 25(8): 1065–1084, URL <http://www.ncbi.nlm.nih.gov/pubmed/16340538>. (Cited on page 4.)

- Peachey, N.S. and Chow, A.Y. (1999). "Subretinal implantation of semiconductor-based photodiodes: progress and challenges." *Journal of rehabilitation research and development* 36(4): 371–376, URL <http://www.ncbi.nlm.nih.gov/pubmed/10678460>. (Cited on page 16.)
- Penfield, W. and Jasper, H. (1954). *Epilepsy and the functional anatomy of the human brain*. Churchill, London, 896 pages. (Cited on page 6.)
- Perez Fornos, A. (2006). *Minimum requirements for a retinal prosthesis to restore useful vision - PhD Thesis*. Phd thesis, University of Geneva. (Cited on pages 7, 8, and 78.)
- Peterman, M.C., Bloom, D.M., Lee, C., Bent, S.F., Marmor, M.F., Blumenkranz, M.S. and Fishman, H.A. (2003). "Localized neurotransmitter release for use in a prototype retinal interface." *Investigative ophthalmology & visual science* 44(7): 3144–3149, URL <http://www.ncbi.nlm.nih.gov/pubmed/12824264>. (Cited on page 6.)
- Petreanu, L., Mao, T., Sternson, S.M. and Svoboda, K. (2009). "The subcellular organization of neocortical excitatory connections." *Nature* 457(7233): 1142–1145, URL <http://www.pubmedcentral.nih.gov/articlerender.fcgi?artid=2745650&tool=pmcentrez&rendertype=abstract>. (Cited on page 23.)
- Plonsey, R. and Heppner, D.B. (1967). "Considerations of quasi-stationarity in electrophysiological systems." *The Bulletin of mathematical biophysics* 29(4): 657–664, URL <http://www.ncbi.nlm.nih.gov/pubmed/5582145>. (Cited on pages 42 and 81.)
- Ranck, J.B. (1975). "Which elements are excited in electrical stimulation of mammalian central nervous system: a review." *Brain research* 98(3): 417–440, URL <http://www.ncbi.nlm.nih.gov/pubmed/1102064>. (Cited on pages 41, 44, and 45.)
- Rattay, F. and Resatz, S. (2004). "Effective electrode configuration for selective stimulation with inner eye prostheses". *IEEE transactions on bio-medical engineering* 51(9): 1659–1664, URL <http://www.ncbi.nlm.nih.gov/pubmed/15376514>. (Cited on page 25.)
- Resatz, S. and Rattay, F. (2003). "Excitability of bipolar and ganglion cells with retinal prosthesis: a modeling study". In "Proceedings of the 25th Annual International Conference of the IEEE Engineering in Medicine and Biology Society", IEEE, ISBN 0-7803-7789-3, pages 2039–2042, URL <http://ieeexplore.ieee.org/lpdocs/epic03/wrapper.htm?arnumber=1280136>. (Cited on page 52.)
- Resatz, S. and Rattay, F. (2004). "A Model for the Electrically Stimulated Retina". *Mathematical and Computer Modelling of Dynamical Systems* 10(2): 93–106, URL <http://www.informaworld.com/smpp/content-db=all-content=a713682520~frm=abslink>. (Cited on pages 14, 24, 35, and 52.)
- Richardot, A. and McAdams, E.T. (2002). "Harmonic analysis of low-frequency bioelectrode behavior." *IEEE transactions on medical imaging* 21(6): 604–612, URL <http://www.ncbi.nlm.nih.gov/pubmed/12166856>. (Cited on page 125.)
- Rijkhoff, N.J., Holsheimer, J., Koldewijn, E.L., Struijk, J.J., van Kerrebroeck, P.E., Debruyne, F.M. and Wijkstra, H. (1994). "Selective stimulation of sacral nerve roots for bladder control: a study by computer modeling." *IEEE transactions on bio-medical engineering* 41(5): 413–424, URL <http://www.ncbi.nlm.nih.gov/pubmed/8070800>. (Cited on page 44.)
- Rizzo, J., Snebold, L. and Kenney, M. (2007). *Development of a visual prosthesis*, Springer, chapter 6. pages 71–93, URL <http://www.springerlink.com/index/j558627477nq8126.pdf>. (Cited on pages 15 and 18.)
- Rizzo, J.F., Wyatt, J., Loewenstein, J., Kelly, S. and Shire, D. (2003). "Perceptual efficacy of electrical stimulation of human retina with a microelectrode array during short-term surgical trials." *Investigative ophthalmology & visual science* 44(12): 5362–5369, URL <http://www.ncbi.nlm.nih.gov/pubmed/14638739>. (Cited on pages 7, 15, and 17.)
- Rodieck, R.W. (1973). *The Vertebrate Retina: Principles of Structure and Function*. W.H.Freeman & Co Ltd (October 24, 1974), ISBN 0716706962, 1044 pages. (Cited on pages 13 and 55.)
- Roessler, G., Laube, T., Brockmann, C., Kirschkamp, T., Mazinani, B., Goertz, M., Koch, C., Krisch, I., Sellhaus, B., Trieu, H.K., Weis, J., Bornfeld, N., Röthgen, H., Messner, A., Mokwa, W. and Walter, P. (2009). "Implantation and explantation of a wireless epiretinal retina implant device: observations during the EPIRET3 prospective clinical trial." *Investigative ophthalmology & visual science* 50(6): 3003–3008, URL <http://www.ncbi.nlm.nih.gov/pubmed/19420330>. (Cited on pages 15 and 19.)
- Rose, T.L. and Robblee, L.S. (1990). "Electrical stimulation with Pt electrodes VIII Electrochemically safe charge injection limits with 0.2 ms pulses". *IEEE transactions on bio-medical engineering* 37(11): 1118–1120, URL <http://www.ncbi.nlm.nih.gov/pubmed/2276759>. (Cited on page 90.)
- Ross, J. (2008). *Microstimulation and multicellular analysis: A neural interfacing system for spatiotemporal stimulation*. Ph.D. thesis, URL <http://smartech.gatech.edu/dspace/handle/1853/24684>. (Cited on page 26.)
- Roth, B.J. (1992). "How the anisotropy of the intracellular and extracellular conductivities influences stimulation of cardiac muscle." *Journal of mathematical biology* 30(6): 633–646, URL <http://www.ncbi.nlm.nih.gov/pubmed/1640183>. (Cited on page 27.)
- Rubinstein, J.T., Spelman, F.A., Soma, M. and Suesserman, M.F. (1987). "Current density profiles of surface mounted and recessed electrodes for neural prostheses." *IEEE transactions on bio-medical engineering* 34(11): 864–75, URL <http://www.ncbi.nlm.nih.gov/pubmed/3319885>. (Cited on page 73.)

- Saenz, A. (2010). "Argus III - The Artificial Retina is Near!" URL <http://singularityhub.com/2010/02/25/argus-iii-the-artificial-retina-is-near>. (Cited on page 19.)
- Saigo, Y. (2004). "Transplantation of Transduced Retinal Pigment Epithelium in Rats". *Investigative Ophthalmology & Visual Science* 45(6): 1996–2004, URL <http://www.iovs.org/cgi/doi/10.1167/iovs.03-0777>. (Cited on page 5.)
- Salzmann, J., Linderholm, O.P., Guyomard, J.L., Paques, M., Simonutti, M., Lecchi, M., Sommerhalder, J., Dubus, E., Pelizzone, M., Bertrand, D., Sahel, J., Renaud, P., Safran, A.B. and Picaud, S. (2006). "Subretinal electrode implantation in the P23H rat for chronic stimulations." *The British journal of ophthalmology* 90(9): 1183–1187, URL <http://www.ncbi.nlm.nih.gov/pubmed/16754649>. (Cited on pages 73, 74, 101, and 105.)
- Scanziani, M. and Häusser, M. (2009). "Electrophysiology in the age of light." *Nature* 461(7266): 930–939, URL <http://www.ncbi.nlm.nih.gov/pubmed/19829373>. (Cited on page 21.)
- Schiefer, M.A. and Grill, W.M. (2006). "Sites of neuronal excitation by epiretinal electrical stimulation." *IEEE transactions on neural systems and rehabilitation engineering* 14(1): 5–13, URL <http://www.ncbi.nlm.nih.gov/pubmed/16562626>. (Cited on pages 28, 52, and 79.)
- Schmidt, E.M., Bak, M.J., Hambrecht, F.T., Kufta, C.V., O'Rourke, D.K. and Vallabhanath, P. (1996). "Feasibility of a visual prosthesis for the blind based on intracortical microstimulation of the visual cortex." *Brain : a journal of neurology* 119 ( Pt 2: 507–522, URL <http://www.ncbi.nlm.nih.gov/pubmed/8800945>. (Cited on page 7.)
- Schmidt, S., Cela, C., Singh, V. and Weiland, J. (2008). "Computational Modeling of Electromagnetic and Thermal Effects for a Dual-Unit Retinal Prosthesis: Inductive Telemetry, Temperature Increase, and Current Densities". *Artificial Sight* : 279–305 URL <http://www.springerlink.com/index/m8655p2068w00wn3.pdf>. (Cited on pages 13, 26, 28, 31, 33, and 35.)
- Schuetzler, M., Franke, M., Krueger, T.B. and Stieglitz, T. (2008). "A voltage-controlled current source with regulated electrode bias-voltage for safe neural stimulation." *Journal of neuroscience methods* 171(2): 248–252, URL <http://www.ncbi.nlm.nih.gov/pubmed/18471890>. (Cited on page 46.)
- Sekirnjak, C., Hottowy, P., Sher, A., Dabrowski, W., Litke, A.M. and Chichilnisky, E. (2007). *Electrical Stimulation of Mammalian Retinal Ganglion Cells Using Dense Arrays of Small-Diameter Electrodes*, Springer New York, New York, NY. Biological and Medical Physics, Biomedical Engineering, ISBN 978-0-387-49329-9, URL <http://www.springerlink.com/index/10.1007/978-0-387-49331-2>. (Cited on page 52.)
- Sekirnjak, C., Hottowy, P., Sher, A., Dabrowski, W., Litke, A.M. and Chichilnisky, E.J. (2006). "Electrical stimulation of mammalian retinal ganglion cells with multielectrode arrays." *Journal of neurophysiology* 95(6): 3311–3327, URL <http://www.ncbi.nlm.nih.gov/pubmed/16436479>. (Cited on pages 47, 74, 87, 91, 99, and 107.)
- Sekirnjak, C., Hottowy, P., Sher, A., Dabrowski, W., Litke, A.M. and Chichilnisky, E.J. (2008). "High-resolution electrical stimulation of primate retina for epiretinal implant design." *The Journal of neuroscience* 28(17): 4446–4456, URL <http://www.ncbi.nlm.nih.gov/pubmed/18434523>. (Cited on page 52.)
- Sernagor, E., Eglén, S., Harris, B. and Wong, R. (2006). *Retinal development*. Cambridge Press, 400 pages. (Cited on page 77.)
- Shannon, R.V. (1992). "A model of safe levels for electrical stimulation." *IEEE transactions on bio-medical engineering* 39(4): 424–426, URL <http://www.ncbi.nlm.nih.gov/pubmed/1592409>. (Cited on page 50.)
- Shepherd, R.K., Murray, M.T., Houghton, M.E. and Clark, G.M. (1985). "Scanning electron microscopy of chronically stimulated platinum intracochlear electrodes." *Biomaterials* 6(4): 237–242, URL <http://www.ncbi.nlm.nih.gov/pubmed/3840392>. (Cited on page 73.)
- Sieving, P.A. and Steinberg, R.H. (1987). "Proximal retinal contribution to the intraretinal 8-Hz pattern ERG of cat." *Journal of neurophysiology* 57(1): 104–120, URL <http://www.ncbi.nlm.nih.gov/pubmed/3559667>. (Cited on page 66.)
- Simpson, J. and Ghovanloo, M. (2007). "An Experimental Study of Voltage, Current, and Charge Controlled Stimulation Front-End Circuitry". In "2007 IEEE International Symposium on Circuits and Systems", IEEE, ISBN 1-4244-0920-9, pages 325–328, URL <http://ieeexplore.ieee.org/lpdocs/epic03/wrapper.htm?arnumber=4252637>. (Cited on page 46.)
- Singh, V. (2009). *Implantable devices for a retinal prosthesis: Design and electromagnetic and thermal effects*. Ph.D. thesis, North Carolina State University. (Cited on page 29.)
- Smith, F.W., Neuhaus, H.J., Senturia, S.D., Feit, Z., Day, D.R. and Lewis, T.J. (1987). "Electrical conduction in polyimide between 20 and 350 Å° C". *Journal of Electronic Materials* 16(1): 93–106, URL <http://www.springerlink.com/index/10.1007/BF02667796>. (Cited on page 75.)
- Stett, A., Barth, W., Weiss, S., Haemmerle, H. and Zrenner, E. (2000). "Electrical multisite stimulation of the isolated chicken retina". *Vision research* 40(13): 1785–95, URL <http://www.ncbi.nlm.nih.gov/pubmed/10814763>. (Cited on pages 99 and 100.)
- Stone, J.L., Barlow, W.E., Humayun, M.S., de Juan, E. and Milam, A.H. (1992). "Morphometric analysis of macular photoreceptors and ganglion cells in retinas with retinitis pigmentosa." *Archives of ophthalmology* 110(11): 1634–1639, URL <http://www.ncbi.nlm.nih.gov/pubmed/1444925>. (Cited on page 6.)



- Suzuki, S., Humayun, M.S., Weiland, J.D., Chen, S.J., Margalit, E., Piyathaisere, D.V. and de Juan, E. (2004). "Comparison of electrical stimulation thresholds in normal and retinal degenerated mouse retina." *Japanese journal of ophthalmology* 48(4): 345–349, URL <http://www.ncbi.nlm.nih.gov/pubmed/15295659>. (Cited on page 51.)
- Szobota, S., Gorostiza, P., Del Bene, F., Wyart, C., Fortin, D.L., Kolstad, K.D., Tulyathan, O., Volgraf, M., Numano, R., Aaron, H.L., Scott, E.K., Kramer, R.H., Flannery, J., Baier, H., Trauner, D. and Isacoff, E.Y. (2007). "Remote control of neuronal activity with a light-gated glutamate receptor." *Neuron* 54(4): 535–545, URL <http://www.ncbi.nlm.nih.gov/pubmed/17521567>. (Cited on page 23.)
- Tassicker, G.E. (1956). "Preliminary report on a retinal stimulator." *The British journal of physiological optics* 13(2): 102–105, URL <http://www.ncbi.nlm.nih.gov/pubmed/13315967>. (Cited on page 6.)
- Thomas, B.B., Arai, S., Ikai, Y., Qiu, G., Chen, Z., Aramant, R.B., Sadda, S.R. and Seiler, M.J. (2006). "Retinal transplants evaluated by optical coherence tomography in photoreceptor degenerate rats." *Journal of neuroscience methods* 151(2): 186–93, URL <http://www.ncbi.nlm.nih.gov/pubmed/16129495>. (Cited on page 56.)
- Thylefors, B., Negrel, A.D. and Pararajasegaram, R. (1992). "Epidemiologic Aspects of Global Blindness Prevention". *Current Opinion in Ophthalmology* 3(6): 824–834. (Cited on page 3.)
- Tsai, D., Morley, J.W., Suaning, G.J. and Lovell, N.H. (2009a). "Direct activation and temporal response properties of rabbit retinal ganglion cells following subretinal stimulation." *Journal of neurophysiology* 102(5): 2982–2993, URL <http://www.ncbi.nlm.nih.gov/pubmed/19741103>. (Cited on pages 52, 81, 99, 100, and 107.)
- Tsai, H.C., Zhang, F., Adamantidis, A., Stuber, G.D., Bonci, A., de Lecea, L. and Deisseroth, K. (2009b). "Phasic firing in dopaminergic neurons is sufficient for behavioral conditioning." *Science (New York, N.Y.)* 324(5930): 1080–1084, URL <http://www.ncbi.nlm.nih.gov/pubmed/19389999>. (Cited on page 23.)
- Urban, H. (1937). "Zur Physiologie der Occipitalregion des Menschen". *Zeitschrift für die gesamte Neurologie und Psychiatrie* 158(1): 257–261, URL <http://www.springerlink.com/index/10.1007/BF02870737>. (Cited on page 6.)
- van Kuyck, K., Welkenhuysen, M., Arckens, L., Sciôt, R. and Nuttin, B. (2007). "Histological Alterations Induced by Electrode Implantation and Electrical Stimulation in the Human Brain: A Review". *Neuromodulation* 10(3): 244–261, URL <http://www.blackwell-synergy.com/doi/abs/10.1111/j.1525-1403.2007.00114.x>. (Cited on page 100.)
- Veraart, C., Raftopoulos, C., Mortimer, J.T., Delbeke, J., Pins, D., Michaux, G., Vanlierde, A., Parrini, S. and Wanet-Defalque, M.C. (1998). "Visual sensations produced by optic nerve stimulation using an implanted self-sizing spiral cuff electrode." *Brain research* 813(1): 181–186, URL <http://www.ncbi.nlm.nih.gov/pubmed/9824694>. (Cited on page 7.)
- Wee, A.S. (2001). "Anodal excitation of intact peripheral nerves in humans." *Electromyography and clinical neurophysiology* 41(2): 71–77, URL <http://www.ncbi.nlm.nih.gov/pubmed/11284058>. (Cited on page 44.)
- Wee, A.S., Leis, A.A., Kuhn, A.R. and Gilbert, R.W. (2000). "Anodal block: can this occur during routine nerve conduction studies?" *Electromyography and clinical neurophysiology* 40(7): 387–391, URL <http://www.ncbi.nlm.nih.gov/pubmed/11142109>. (Cited on page 44.)
- Weiland, J.D. and Humayun, M.S. (2005). "A biomimetic retinal stimulating array." *IEEE engineering in medicine and biology magazine : the quarterly magazine of the Engineering in Medicine & Biology Society* 24(5): 14–21, URL <http://www.ncbi.nlm.nih.gov/pubmed/16248113>. (Cited on page 24.)
- Weiland, J.D., Humayun, M.S., Dagnelie, G., de Juan, E., Greenberg, R.J. and Iliff, N.T. (1999). "Understanding the origin of visual percepts elicited by electrical stimulation of the human retina." *Graefes's archive for clinical and experimental ophthalmology* 237(12): 1007–1013, URL <http://www.ncbi.nlm.nih.gov/pubmed/10654170>. (Cited on page 7.)
- Weiss, G. (1901). "Sur la possibilite de rendre comparables entre eux les appareils servant a l'excitation electrique". *Arch. Ital. Biol.* 35: 413–446, URL <http://scholar.google.com/scholar?hl=en&btnG=Search&q=intitle:Sur+la+possibilite+de+rendre+comparables+entre+eux+les+appareils+servant+a+l'excitation+electrique#0>. (Cited on page 47.)
- West, A.C. (1991). "Current Distributions on Recessed Electrodes". *Journal of The Electrochemical Society* 138(6): 1620–1625, URL <http://link.aip.org/link/JES0AN/v138/i6/p1620/s1&Agg=doi>. (Cited on page 73.)
- Wiley, J.D. and Webster, J.G. (1982). "Analysis and control of the current distribution under circular dispersive electrodes". *IEEE transactions on bio-medical engineering* 29(5): 381–5, URL <http://www.ncbi.nlm.nih.gov/pubmed/7084970>. (Cited on pages 42 and 73.)
- Wilke, R., Greppmaier, U., Harscher, A., Benav, H. and Zrenner, E. (2010a). "Factors Affecting Perceptual Thresholds of Subretinal Electric Stimulation in Blind Volunteers". *ARVO Meeting Abstracts* 51(5): 2026, URL <http://abstracts.iovs.org/cgi/content/abstract/51/5/2026>. (Cited on pages 37, 74, 100, and 108.)
- Wilke, R.G.H., Moghaddam, G.K., Dokos, S., Suaning, G. and Lovell, N.H. (2010b). *Stimulation of the Retinal Network in Bionic Vision Devices: From Multi-Electrode Arrays to Pixelated Vision*, Springer Berlin

- / Heidelberg. pages 140–147, URL [http://dx.doi.org/10.1007/978-3-642-17537-4\\_18](http://dx.doi.org/10.1007/978-3-642-17537-4_18). (Cited on pages 9, 12, 30, and 115.)
- Woch, G., Aramant, R.B., Seiler, M.J., Sagdullaev, B.T. and McCall, M.a. (2001). "Retinal transplants restore visually evoked responses in rats with photoreceptor degeneration." *Investigative ophthalmology & visual science* 42(7): 1669–76, URL <http://www.ncbi.nlm.nih.gov/pubmed/11381076>. (Cited on page 5.)
- Wu, P., Mehenti, N., Leng, T., Marmor, M., Blumenkranz, M. and Fishman, H. (2003). "Cell Demographics from Full Thickness Retinal Explant Growth on Micropatterned Surfaces". *Investigative Ophthalmology and Visual Science* 44(5): 5008, URL <http://abstracts.iovs.org/cgi/content/abstract/44/5/5008>. (Cited on page 6.)
- Xu, X. and Karwoski, C.J. (1994). "Current source density (CSD) analysis of retinal field potentials. I. Methodological considerations and depth profiles." *Journal of neurophysiology* 72(1): 84–95, URL <http://www.ncbi.nlm.nih.gov/pubmed/7965035>. (Cited on pages 33 and 56.)
- Yagi, T., Kameda, S., Hayashida, Y. and Li, L. (1999). "An artificial retina with adaptive mechanisms and its application to retinal prosthesis". In "IEEE SMC'99 Conference Proceedings. 1999 IEEE International Conference on Systems, Man, and Cybernetics", IEEE, Kyushu Inst of Technology, Fukuoka, Jpn, volume 4 of *Proceedings of the IEEE International Conference on Systems, Man and Cybernetics*, ISBN 0-7803-5731-0, pages 418–423, URL <http://ieeexplore.ieee.org/lpdocs/epic03/wrapper.htm?arnumber=812440>. (Cited on page 6.)
- Yanai, D., Weiland, J.D., Mahadevappa, M., Greenberg, R.J., Fine, I. and Humayun, M.S. (2007). "Visual performance using a retinal prosthesis in three subjects with retinitis pigmentosa." *American journal of ophthalmology* 143(5): 820–827, URL <http://www.ncbi.nlm.nih.gov/pubmed/17362868>. (Cited on pages 7 and 20.)
- Yang, Y., Mohand-Said, S., Danan, A., Simonutti, M., Fontaine, V., Clerin, E., Picaud, S., L  veillard, T. and Sahel, J.A. (2009). "Functional cone rescue by RdCVF protein in a dominant model of retinitis pigmentosa." *Molecular therapy : the journal of the American Society of Gene Therapy* 17(5): 787–795, URL <http://www.pubmedcentral.nih.gov/articlerender.fcgi?artid=2835133&tool=pmcentrez&rendertype=abstract>. (Cited on page 24.)
- Ye, J.H. and Goo, Y.S. (2007). "Comparison of voltage parameters for the stimulation of normal and degenerate retina." *Annual International Conference of the IEEE Engineering in Medicine and Biology Society* 2007: 5783–5786, URL <http://www.ncbi.nlm.nih.gov/pubmed/18003327>. (Cited on page 51.)
- Yin, S., Lovell, N.H., Suanning, G.J. and Dokos, S. (2010). "A continuum model of the retinal network and its response to electrical stimulation." In "Annual International Conference of the IEEE Engineering in Medicine and Biology Society", volume 1, pages 2077–2080, URL <http://www.ncbi.nlm.nih.gov/pubmed/21095947>. (Cited on page 27.)
- Zahn, M. (2003). *Electromagnetic Field Theory: A Problem Solving Approach*. Krieger Publishing Company, second edition, ISBN 1575242354, 753 pages. (Cited on page 60.)
- Zeiss, C.J., Allore, H.G., Towle, V. and Tao, W. (2006). "CNTF induces dose-dependent alterations in retinal morphology in normal and rcd-1 canine retina." *Experimental eye research* 82(3): 395–404, URL <http://www.ncbi.nlm.nih.gov/pubmed/16143329>. (Cited on page 4.)
- Zhang, F., Prigge, M., Beyri  re, F., Tsunoda, S.P., Mattis, J., Yizhar, O., Hegemann, P. and Deisseroth, K. (2008). "Red-shifted optogenetic excitation: a tool for fast neural control derived from *Volvox carteri*." *Nature neuroscience* 11(6): 631–633, URL <http://www.pubmedcentral.nih.gov/articlerender.fcgi?artid=2692303&tool=pmcentrez&rendertype=abstract>. (Cited on page 23.)
- Zhang, F., Wang, L.P., Brauner, M., Liewald, J.F., Kay, K., Watzke, N., Wood, P.G., Bamberg, E., Nagel, G., Gottschalk, A. and Deisseroth, K. (2007). "Multimodal fast optical interrogation of neural circuitry." *Nature* 446(7136): 633–639, URL <http://www.ncbi.nlm.nih.gov/pubmed/17410168>. (Cited on page 23.)
- Zhou, D. and Greenberg, R. (2009). *Implantable Neural Prostheses 1 - Devices and Applications*. Springer, 1–42 pages, URL <http://www.springerlink.com/index/t5l7g263u75nm530.pdf>. (Cited on pages 8 and 20.)
- Zhou, J.A., Woo, S.J., Park, S.I., Kim, E.T., Seo, J.M., Chung, H. and Kim, S.J. (2008). "A suprachoroidal electrical retinal stimulator design for long-term animal experiments and in vivo assessment of its feasibility and biocompatibility in rabbits." *Journal of biomedicine & biotechnology* 2008: 547,428, URL <http://www.ncbi.nlm.nih.gov/pmc/articles/PMC2246081/?tool=pmcentrez&report=abstract>. (Cited on page 7.)
- Zibek, S., Hagmeyer, B., Stett, A. and Stelzle, M. (2010). "Chemical stimulation of adherent cells by localized application of acetylcholine from a microfluidic system." *Frontiers in neuroengineering* 3: 113, URL <http://www.pubmedcentral.nih.gov/articlerender.fcgi?artid=2999818&tool=pmcentrez&rendertype=abstract>. (Cited on page 6.)
- Ziv, O.R., Rizzo, J.F. and Jensen, R.J. (2005). "In vitro activation of retinal cells: estimating location of stimulated cell by using a mathematical model." *Journal of neural engineering* 2(1): S5–S15, URL <http://www.ncbi.nlm.nih.gov/pubmed/15876655>. (Cited on page 27.)
- Zrenner, E. (2002). "The subretinal implant: can microphotodiode arrays replace degenerated retinal photoreceptors to restore vision?" *Ophthalmologica* 216 Suppl: 8–20; discussion 52–3, URL <http://www>.



[ncbi.nlm.nih.gov/pubmed/12207119](http://ncbi.nlm.nih.gov/pubmed/12207119). (Cited on page 26.)

Zrenner, E., Bartz-Schmidt, K.U., Benav, H., Besch, D., Bruckmann, A., Gabel, V.P., Gekeler, F., Greppmaier, U., Harscher, A., Kibbel, S., Koch, J., Kusnyerik, A., Peters, T., Stingl, K., Sachs, H., Stett, A., Szurman, P., Wilhelm, B. and Wilke, R. (2010). "Subretinal electronic chips allow blind patients to read letters and combine them to words". *Proceedings of the Royal Society B: Biological Sciences* URL <http://rsbp.royalsocietypublishing.org/cgi/doi/10.1098/rspb.2010.1747>. (Cited on pages 7, 15, 17, and 18.)



## COLOPHON

This thesis was typeset with  $\text{\LaTeX} 2_{\epsilon}$  using Hermann Zapf's *Palatino* and *Euler* type faces (Type 1 PostScript fonts *URW Palladio L* and *FPL* were used).

The typographic style was inspired by [Bringhurst and Marks](#)'s genius as presented in *The Elements of Typographic Style* [[Bringhurst and Marks 2002](#)]. It is available for  $\text{\LaTeX}$  via CTAN as "[classicthesis](#)".



# Curriculum Vitae

Harsha Kasi

---

## EDUCATION

---

**Doctor of Philosophy, Microtechnology and Microsystems** **2006 – 2011**

**Swiss Federal Institute of Technology (EPF Lausanne)**

**Lausanne, Switzerland**

- Research Assistant in the Microsystems Laboratory (advisor: Prof. Philippe Renaud)
- Thesis title: Analysis of factors affecting the performance of retinal prostheses using finite element modelling and simulation of electric field distribution in the retina

**Master of Science, Micro and Nano Technology** **October 2004 – February 2006**

**Institute of Microtechnology (EPF Lausanne)**

**Neuchâtel, Switzerland**

- Master Thesis: Microfabrication and characterisation of a novel DNA hybridisation reaction chamber
- Semester Project 1: Electrical characterisation of cell membrane support chips
- Semester Project 2: Optical demultiplexer using diffractive lens – Theoretical analysis

## PROFESSIONAL EXPERIENCE

---

**Software Intern**

**July 2005 – September 2005**

**EM Microelectronic (a Swatch Group Ltd. company)**

**Marin, Switzerland**

- Developed a customised interactive Result Viewing Environment (RVE) in TCL/TK
- The tool was deployed at the EM offices in Czech Republic and USA

**Software Engineer****February 2003 – June 2004****SoCrates Software India Pvt. Ltd. (A Toshiba Group Company)****Bengaluru, India**

- Led two members of the product validation team, who were supervised and guided in daily tasks

**Associate Software Engineer****August 2002 – February 2003****SoCrates Software India Pvt. Ltd. (A Toshiba Group Company)****Bengaluru, India**

- Implemented a Sub-band coding standard for Audio in C language

**SKILLS**

---

**Microfabrication & laboratory techniques** : Polyimide-based flexible implants, impedance spectroscopy, MEMS characterisation, basic dissection (retina extraction) Programming

Languages : TCL/TK, C/C++, Scripting in Linux, Perl, Java

**Simulation/analysis Software** : Matlab® & Simulink®, Mathematica®, PSpice®, MapleTM, Origin®, Comsol Multiphysics® (FEMLAB)

**Design (CAD) Software** : Solidworks®, Clewin

**Operating Systems** : Macintosh OSX, Linux, Solaris®, MS Windows®

**Spoken Languages** : English (Fluent), French (Advanced), German (Beginner), Hindi (Fluent)

**CERTIFICATIONS**

---

**Swiss Animal Experimentation Certificate****May 2007 - July 2008****French Language Participation Certificate****July 2004 - September 2004****SCHOLARSHIPS AND AWARDS**

---

**Doctoral research scholarship****November 2006 – December 2010**

Jointly by Swiss National Science Foundation and Swiss Federal Institute of Technology (EPF/ETH Lausanne)

**Top 10 finalists****July 2010****IEEE Change the World Competition****Graduate research scholarship****Oct. 2004 – Dec. 2005**

Jointly by IMT and University of Neuchâtel to pursue master studies at Neuchâtel

**Ranked fourth in the University**

**2003**

Bachelor studies, amongst more than 100 colleges and at least 4000 students

**Award for Best Achiever and Academic Excellence**

**2001 - 2002**

During Bachelor studies at M. S. Ramaiah Institute of Technology

## PUBLICATIONS/CONFERENCES

---

### Publications

1. Simulation of epiretinal prostheses – Evaluation of geometrical factors affecting stimulation thresholds - Kasi H. et al., Accepted by the Journal of NeuroEngineering and Rehabilitation, 2011
2. Simulations to study spatial extent of stimulation and effect of electrode–tissue gap in subretinal implants - Kasi H. et al., Medical Engineering & Physics, 2011 (in Press)
3. Direct localised measurement of electrical resistivity profile in rat and embryonic chick retinas using a microprobe - Kasi H. *et al.* , Journal of Electrical Bioimpedance, 2010
4. Distinguishing drug-induced minor morphological changes from major cellular damage via label-free impedimetric toxicity screening - Meissner R., Eker B., Kasi H. *et al.* , Lab Chip, 2011

### Conference Proceedings

1. A new flexible microfabricated polyimide-based platinum electrodes for stimulation of rat retinal tissue in vitro and recording using a multi-electrode array - Kasi H. et al., Proceedings of the 12th International Conference on Miniaturised Systems for Chemistry and Life Sciences, San Diego, 2008
2. Modelling and microfabrication of a polyimide-based 3D tissue coupled electrodes for electrical stimulation in the chick retina - Kasi H. et al., USGEB, Lausanne, 2008
3. Retinal Prosthesis: Testing Prototypes on a Dystrophic Rat Retina, Salzmann J., Guyomard J.-L., Linderholm P., Kolomiets B., H. Kasi et al., European Conference on Circuit Theory and Design, 2007